GEOCHEMISTRY AND PETROGENESIS OF THE ALKALINE LAVAS AND THEIR ASSOCIATED XENOLITHS, MOUNT OVERLORD, NORTHERN VICTORIA LAND, ANTARCTICA.

by

Mark Richard Noll

Submitted in Partial Fulfillment
of the Requirements for the Degree of
Master of Science in Geology

New Mexico Institute of Mining and Technology

Socorro, New Mexico

August, 1984

This thesis is accepted on behalf of the faculty of

New Mexico Institute of Mining and Technology

by the following committee:

Philip R. Kyle

Adviser

30 April 1985

Date

ABSTRACT

Mount Overlord (3396m, 73 10'S, 164 50'E) is a 7 Ma old, mainly ice and snow covered stratovolcano capped by an 800m wide caldera. It is part of the Late Cenozoic McMurdo Volcanic Group in Northern Victoria Land, Antarctica.

The lavas are all alkaline in nature and range widely in composition from basanite to comendite. Essexite, anorthosite, and sodalite syenite cognate xenoliths are common. Two distinct suites are recognized, a weakly undersaturated suite (WUS) with normative nepheline less than 10% and in some cases normative quartz, and a strongly undersaturated suite (SUS) with greater than 10% normative nepheline. On major element and trace element variation diagrams, the SUS shows a well-defined, tightly constrained evolutionary trend from basanite through ne-hawaiite, ne-mugearite, ne-benmoreite to phonolite. The WUS lavas show no clearly defined trend except from alkali basalt to mugearite. From mugearite through benmoreite, trachyte, quartz trachyte to comendite, the WUS suite develops along numerous trends. Least squares mass balance models suggest that the SUS evolved by the fractional crystallization dominated by kaersutite with lesser olivine, clinopyroxene, plagioclase, apatite, and opaque oxides. The WUS lavas evolved by fractionation of similiar species except feldspar

was the dominant phase and kaersutite was absent. The cumulates calculated from the mass balance models are grossly similiar to the cognate xenoliths. Trace element analyses evaluated by the Rayleigh equation generally agree with the fractional crystallization models.

Evolution of the lavas took place in a high level subvolcanic magma chamber. For the WUS, evolution was a complex process involving a number of small apophyses which evolved separately under varying conditions. The SUS evolved under more tightly constrained conditions resulting in a single evolutionary trend.

ACKNOWLEDGEMENTS

I would like to take this oppurtunity to thank those people which were involved in this research project. Dr. Philip R. Kyle for providing this unique oppurtunity for study, and along with Dr. Kent C. Condie and Mr. Robert Osburn for their critical review of this manuscript. My special thanks go to my parents, family, former professors, and many friends for their continued support and assistance. This project was funded by National Science Foundation grant DPP-8218493.

TABLE OF CONTENTS

LIST OF FIGURES

LIST OF TABLES

1 INTRODUCTION

1.1 Introduction

Alkali volcanism has been widespread in Antarctica during the Late Cenozoic, occurring in three broad regions (Fig. 1.1). The McMurdo Volcanic Group (MVG) comprises all the volcanic rocks of Late Cenozoic age in the western Ross Sea, the Balleny and Scott Islands (Harrington, 1958). Kyle and Cole (1974) have divided the McMurdo Volcanics into four provinces, Erebus, Melbourne, Hallett, and Balleny (Fig. 1.2).

The Melbourne volcanic province includes the Late Cenozoic volcanics of Northern Victoria Land forming an arcuate belt inland from Mt Melbourne and including Mt Overlord and The Pleiades (Fig. 1.3). On its northern and eastern extremities, the Melbourne volcanic province borders on the Hallett volcanic province. The Melbourne volcanic province comprises the only major group of the MVG which lie within the main structure of the Transantarctic Mountains.

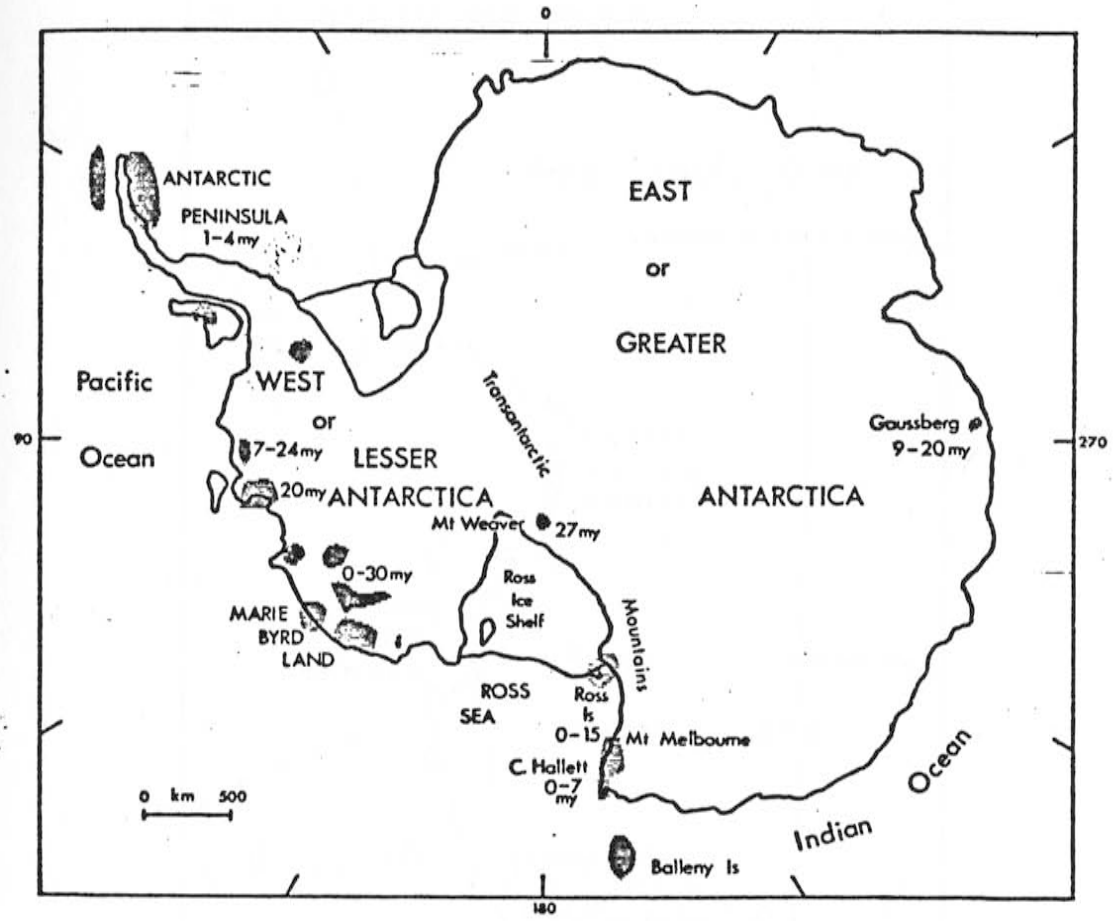

FIGURE 1.1 Distribution of Late Cenozoic rocks in Antarctica and selected radiometric age determinations. All rocks of this age are alkali volcanics. (after Kyle 1976).

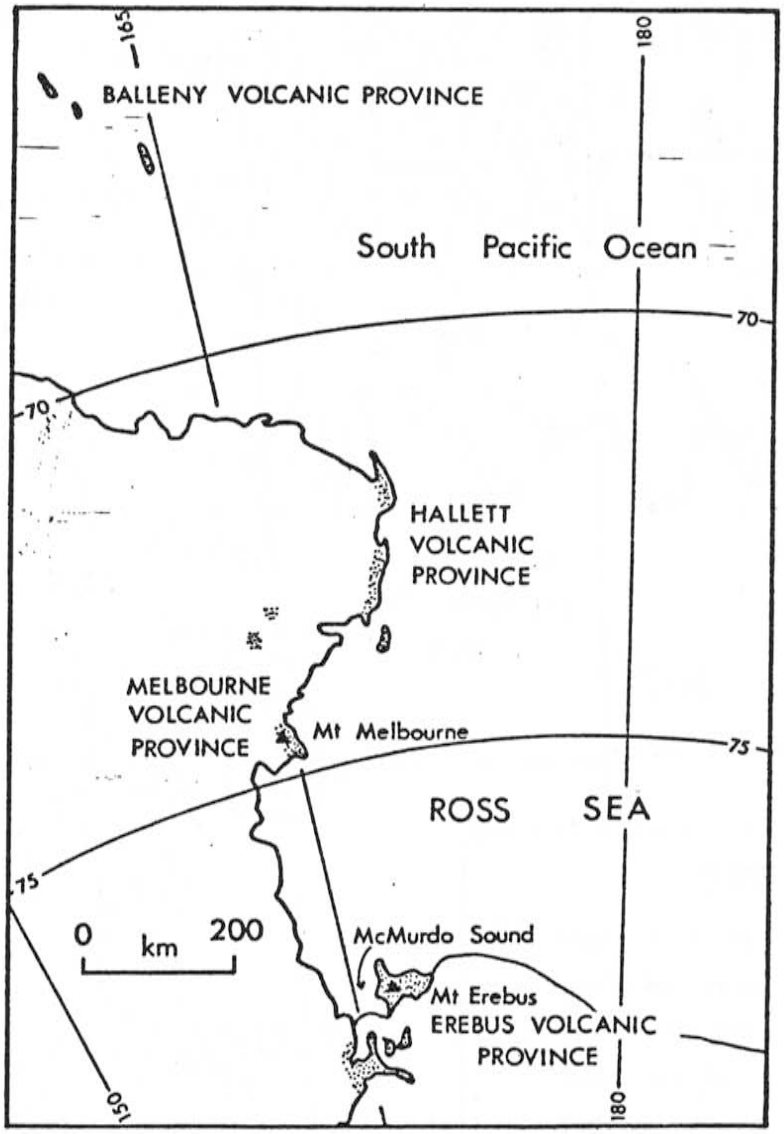

FIGURE 1.2 Distribution of the McMurdo Volcanic Group in Victoria Land, the Balleny Islands and islands in the western Ross Sea (after Kyle, 1976).

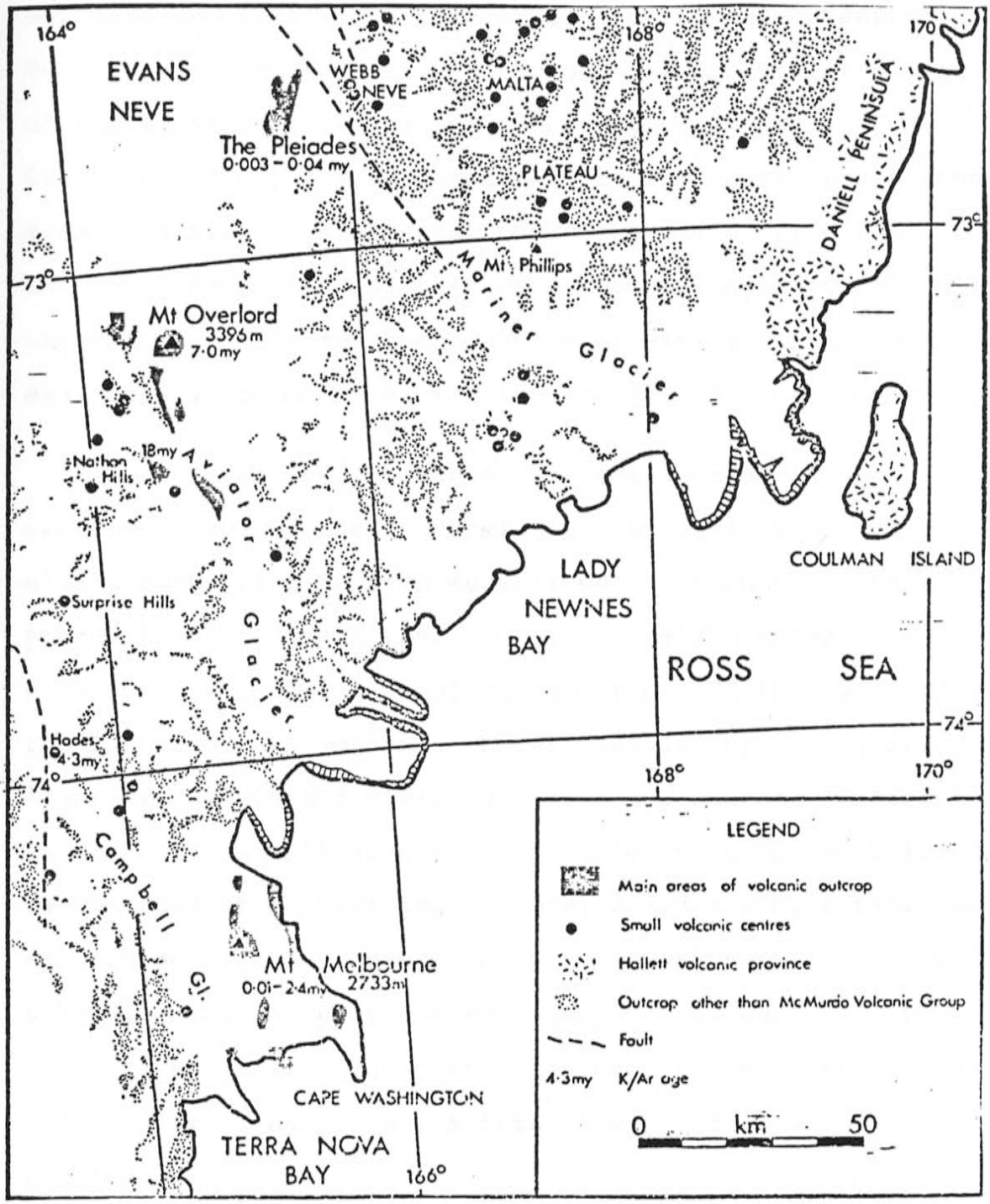

FIGURE 1.3 Location map of the Melbourne volcanic province, showing the distribution of volcanic centers and age determinations of major volcanoes (after Kyle 1976).

Nathan and Schulte (1968) have divided the Melbourne volcanic province rocks into a Local Suite and a Central Suite. The Central Suite is the more extensive and consists of the large stratovolcanoes of Mt Melbourne (2733m), Mt Overlord (3396m) and the cones of The Pleiades. Lavas range from basanites to trachytes, phonolites, and comendites. The Local Suite includes all other occurrences not part of the Central Suite and are almost exclusively olivine-bearing basanites which occur as small outcrops and cinder cones.

Mount Overlord, the object of this study, is a stratovolcano composed predominantly of differentiated alkali rocks ranging from mugearites to trachytes with some phonolites and comendites. Younger basaltic cones containing ultramafic xenoliths occur around the base and on the flanks of the volcano. Mount Overlord has a 800 meter diameter caldera and a very youthful appearance. Exposures in the caldera wall show that the upper part of the volcano is composed of alternating benmoreite and trachyte flows and associated pyroclastics. One of the final eruptions carried a large number of plutonic xenoliths to the surface. Some are derived from the granitic basement, but most are cognate and consist of essexites, anorthosites, and sodalite syenites.

1.2 Purpose of Study

In order to better understand the geologic history and petrogenesis of Mount Overlord, and its relationship to other MVG rocks, a detailed geochemical and petrographic study was made on samples collected during the 1981-82 field season. The study includes; 1) chemical analysis of major, trace, and rare earth elements; 2) petrographic analysis of thin sections; 3) classification of the lava suites and related cognate inclusions and; 4) development of petrogenetic models for the evolution of the Mount Overlord rocks.

1.3 Previous Work

Mount Overlord has only been visited on three previous occasions, by the New Zealand Geologic Survey Antarctic Expedition Northern Party, 1962-63, lead by H. S. Gair, the Southern New Zealand Geologic Survey Expediton, 1966-67, with geologists Simon Nathan and F. J. Schulte, and a brief visit by P. R. Kyle in 1972 with the Victoria University of Wellington Antarctic Expedition.

Gair (1967) described the rocks of Mount Overlord as consisting of trachybasalts, trachyandesites, and trachytoid phonolites lavas, and peralkaline rhyolitic ignimbrites. He

also describes cognate xenoliths of essexitic gabbros and sodalite-bearing syenites. The volcano was believed to be very young due to its undissected nature and Gair believed that eruptions may have taken place in the last few hundred years.

Nathan and Schulte (1968) also investigated the rocks of Mount Overlord, coming to the same conclusions as Gair on their classification. They however, recognized an older age and described the caldera as a collapse feature rather than an erosional feature. A ridge on the north-east side was believed to be the remnant of an older cone, but exposure was not good enough to be certain.

Kyle visited Mount Overlord briefly while doing work at The Pleiades. Three samples were collected and found to be a hawaiite and two tristanites (Kyle, 1976).

2 GENERAL GEOLOGY

2.1 Field Investigations

Field investigations as part of this study were conducted from December 17, 1981 to January 15, 1982 of the 1981-82 Austral summer field season. Work was conducted out of the North Victoria Land (NVL) field camp using skidoos and sledges and helicopter support. Seven days were spent at Mount Overlord examining the geology from a tent camp ENE of the caldera. Field work on Mount Overlord consisted of reconnaissance mapping, measurement and sampling of stratigraphic sections along the east and west rims where the caldera wall is well exposed, and the collection of samples, plotting their locations on aerial photographs. 91 representative samples were collected from flow units, measured sections, xenoliths, and float material (Fig. 2.1). Several areas were not visited due to inaccessibility and/or lack of exposure.

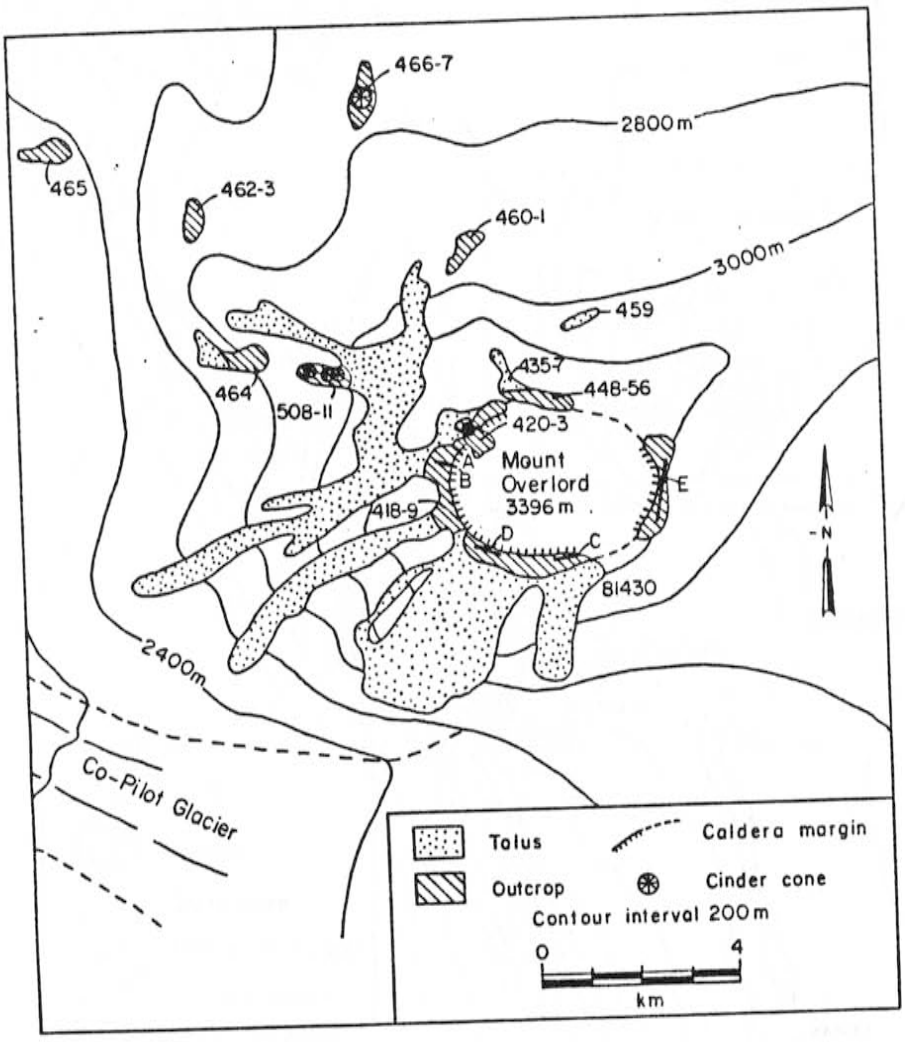

FIGURE 2.1 Simplified geologic sketch map of Mount Overlord and the surrounding area with sample locations. Letters indicate the locations of short measured sections. A) 81424-26,38-41,57,58; B) 81442-44; C) 81427,32-34 ; D)81428,29,31; E) 81414-17.

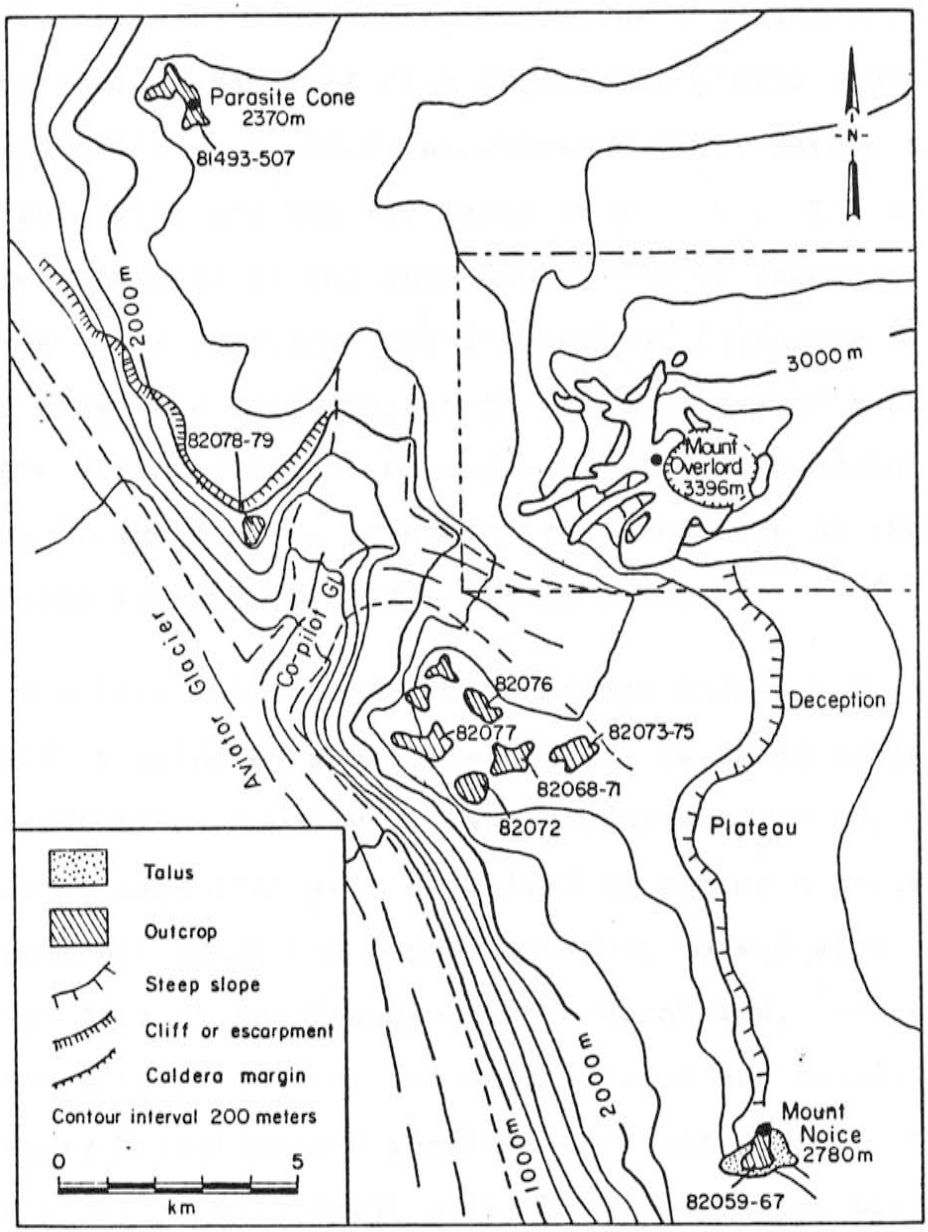

FIGURE 2.1 (cont.) Location of samples along the flanks of Mount Overlord, at Parasite Cone, and Mount Noice.

2.2 Regional Geology

The Aviator Glacier region of the Transantarctic Mountains is made up of five major rock groups (Gunn and Warren, 1962; Gair, 1967; Harrington, 1967; Nathan and Schulte, 1968; and Nathan, 1971) (Fig. 2.2). The basement complex consists of the Ross Supergroup of Precambrian age, and the lower Paleozoic Granite Harbour Intrusive Group. Above these are the Devonian to Triassic Beacon Supergroup and the Jurassic Ferrar Supergroup. The most recent rocks belong to the McMurdo Volcanic Group and make up the Melbourne volcanic province (Table 2.1).

The late Precambrian rocks of the Ross Supergroup are defined by Grindley and Warren (1964) as those sediments and metasediments, probably of late Proterozoic or early Paleozoic age, that were deposited in one or a series of geosynclinal basins of deposition that formed along the present site of the Transantarctic Mountains. In the Aviator Glacier region, two subdivisions are found, the Priestley Formation and the Retreat Hills Schist. These units occur in only small areas between granite plutons as they have been otherwise removed by erosion (Nathan, 1971).

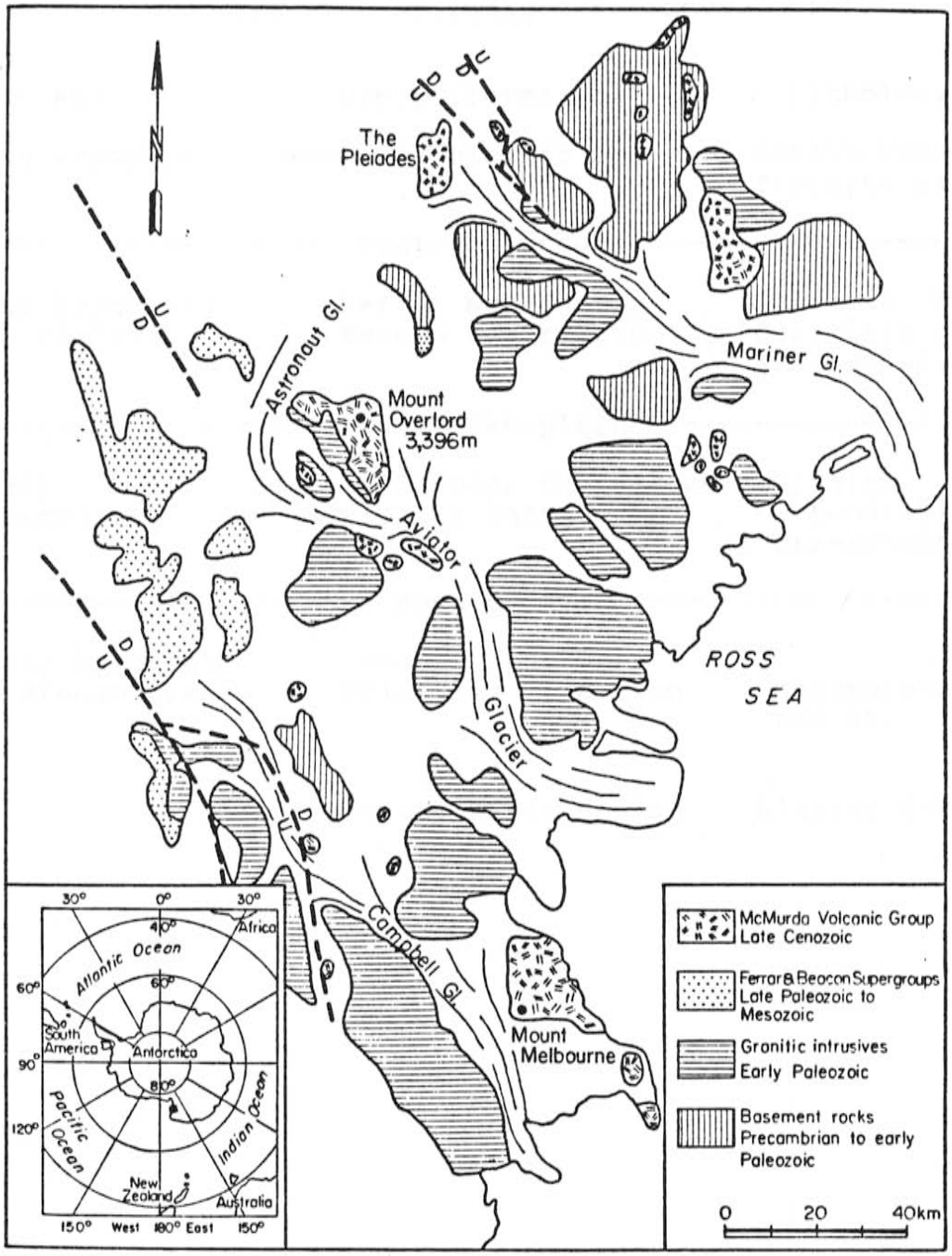

FIGURE 2.2 Regional geologic map of the Aviator Glacier region, Transantarctic Mountains, Northern Victoria Land.

TABLE 2.1 STRATIGRAFIC UNITS

Modified from Riddolls and Hancox (1968)

Age	Group (Formation)	Lithology
Late Cenozoic	McMurdo Volcanic Group	Basalt-Phonolite-Trachyte assoc.
---------- Victoria Orogeny ----------		
Late Paleozoic to Mesozoic	Ferrar Supergroup Beacon Supergroup	Dolerite, Basalt Quarzitic to Arkosic ss.
---------- Kukri Peneplain ----------		
Early Paleozoic	Granite Harbour Intrusives Admiralty Intrusives	Granite, Granodiorite, Qtz-Monzonite
---------- Ross Orogeny ----------		
Early Paleozoic to Precambrian	Ross Supergroup Priestley Formation	Metamorphosed ss. and sh.
	Retreat Hills Schist	Biotite Schist

The Priestley Formation (Ricker, 1964) is characterized by dark colored, variably metamorphosed, sandstones and shales, with rare volcanics and calcareous horizons. The Retreat Hills Schist is a uniform biotite schist and is thought to be formed by the metamorphism of the Robertson Bay Group during the emplacement of granitic rocks during the Ross Orogeny (Riddols and Hancox, 1964).

The granitic rocks in the area are included in the early Paleozoic Granite Harbour Intrusive Group (Gunn and Warren, 1962). Around Mount Overlord, this group is represented by the Aviator Granodiorite (Nathan, 1971), a coarse grained, white to light gray, unfoliated and very uniform biotite granodiorite. An average modal analysis by Nathan (1971) gives 35% quartz, 47% plagioclase, 5% potash feldspar, 11% biotite, and 2% accessory minerals. The Aviator Granodiorite outcrops and forms the basement at Navigator Nunatak and the lower portion of the cliffs on the eastern side of the Aviator Glacier below Mount Overlord.

During the middle and late Paleozoic, the basement complex was deeply eroded to form the Kukri peneplain surface (Gunn and Warren, 1962). This is best developed in the area between the Aviator and Mariner glaciers.

Cropping out to the west of Overlord are the flat lying, late Paleozoic to Mesozoic Beacon and Ferrar Supergroups. The Ferrar Supergroup consists of a thick

sequence of flood basalts and dolerite intrusives of Jurassic age (Kyle et al, 1982). The Beacon is a series of quartzitic to arkosic sandstones of possible Devonian to Triassic age (Walker, 1983; Collinson and Kemp, 1983).

Following the Jurassic, no continental volcanics or sediments were formed until the Late Cenozoic and the eruption of the MVG. The Melbourne volcanic province forms a definite curvilinear trend (Nathan and Schulte, 1968) along the Cambell-Aviator Divide. Kyle and Cole (1974) have suggested that Mount Overlord and Mount Melbourne are associated with the N to NW trending faults which are part of the Rennick Graben, a possible extension of the Tasman Fracture Zone (Hayes and Conolly, 1972). Rocks of the Local Suite may be formed along local structures.

2.3 Mount Overlord

Mount Overlord (3396m) forms an asymmetrical cone on the NW corner of the Deception Plateau overlooking the Aviator Glacier (Fig. 2.3). A well-defined caldera, over 800m across, is surrounded by a largely undissected rim with reasonable exposures on the western half of the cone. The caldera is breached to the south and northeast. Parasitic cones are found along the northern and western flanks where exposure is best. On the whole, snow and ice cover limits

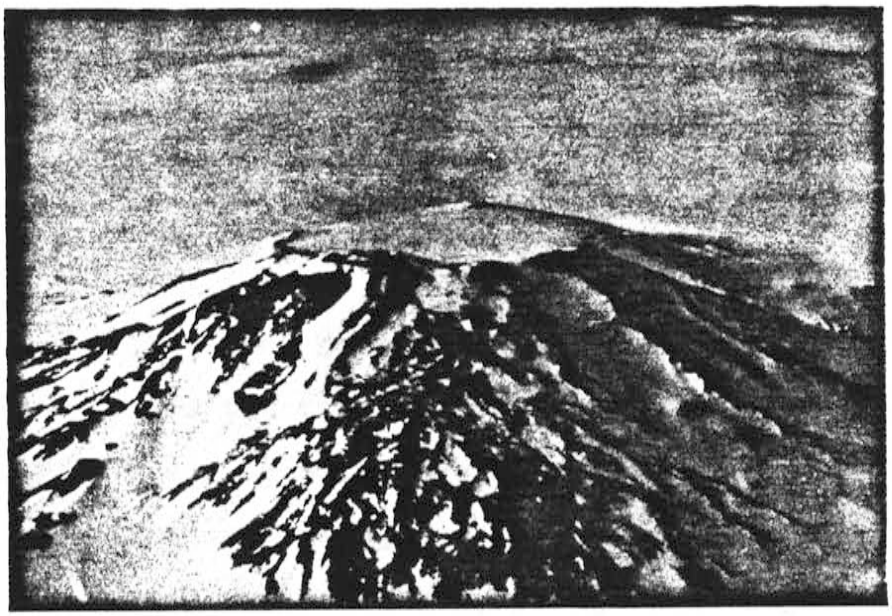

FIGURE 2.3 Photographs of Mount Overlord; a) oblique aerial photo looking east; b) as seen from Parasite Cone, looking south.

much of the exposure.

Nathan and Schulte (1968) have suggested that the assymmetrical nature of Mount Overlord is due possibly to more than one vent, and the preferential flow of lava away from the Deception Plateau (Fig. 2.3).

The undissected nature of the cone, and the preservation of the rim, suggest that the caldera is a collapse feature rather than an erosional one. This would also suggest a very young age for Overlord. Gair (1967) considered Overlord to be very young with eruptions in the last 300 years. K-Ar dating of three samples by Armstrong (1978) however, have a mean age of 7.4 my. (Table 2.2). If these dates are correct, they indicate that erosional rates have been very slow.

Scoriaceous parasitic cones are found on the northern and western flanks. One of the larger of these cone is located on the rim just north of the summit and has flows which travel down the flank of the volcanoe as well as into the caldera.

Sample No.	Rock Type/Location	Source	Age (my.)
35412	Trachyandesite, Mount Overlord	N	6.8+0.14
35413	Trachyandesite, Mount Overlord	N	8.1+1.7
37085a	Trachybasalt, Mount Overlord	N	7.2+0.14
81501	Alkali basalt, Parasite Cone	K	14.67+0.30
81512b	Alkali basalt, Mount Overlord	K	7.5+0.14

N - samples from S. Nathan, dates by R. Armstrong (1978).
K - Kyle, unpublished data.

TABLE 2.2 K-Ar dates for Mount Overlord and Parasite Cone from Armstrong (1978) and Kyle (1983 personal communication).

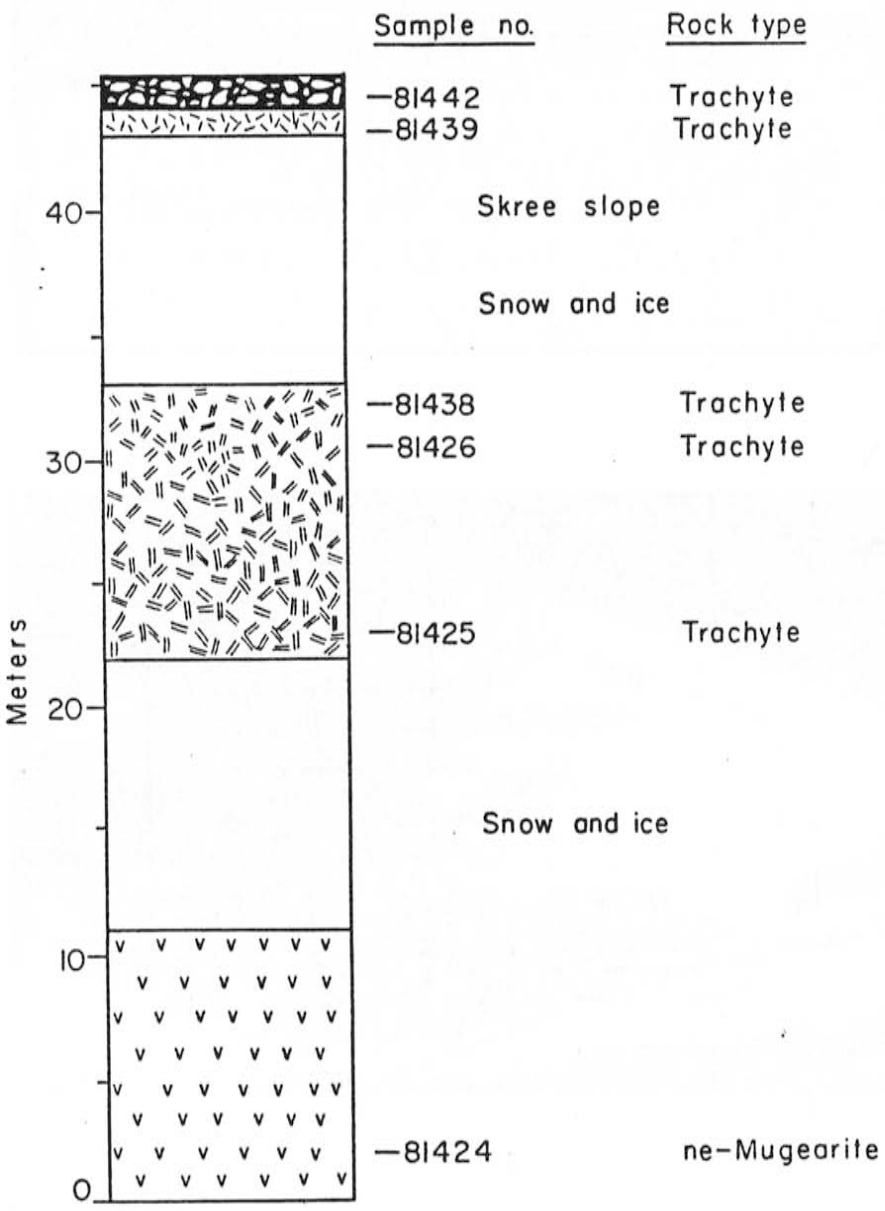

FIGURE 2.4 Measured stratigraphic section of the exposed inner wall of the western caldera rim.

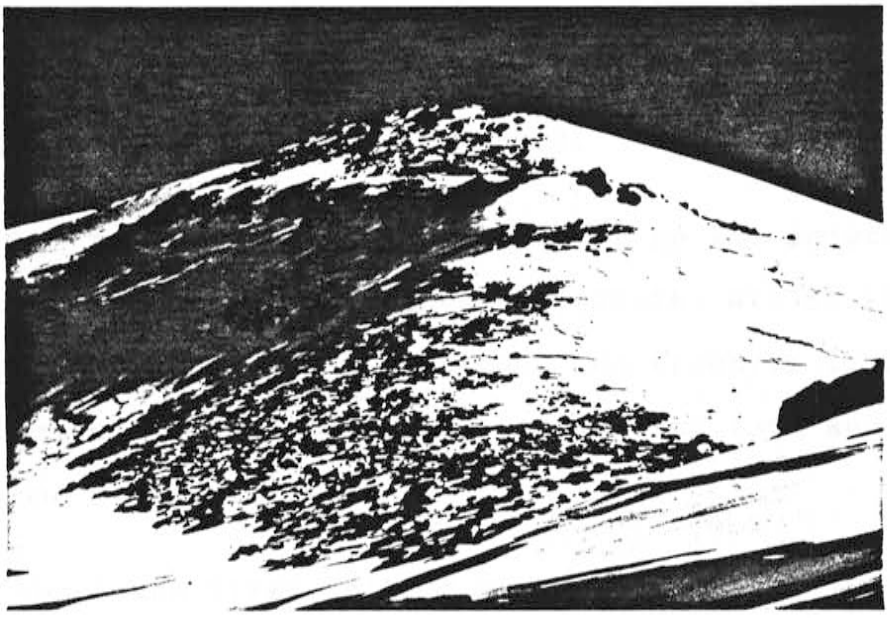

FIGURE 2.5 Photos of caldera wall section; A) from eastern edge of caldera looking west; B) from directly north of the measured section (left half of photo, cliff extending from the base of the slope to summit).

2.3.1 CALDERA WALL SECTION

Two stratigraphic sections were measured (using tape and compass) and sampled on the western rim of the caldera just north of the summit. The two sections combined (Fig. 2.4) consist of approximately 15m of ice and snow cover, 10m of scree, and 25m of outcrop. The rocks in this section range from a ne-mugearite at the base to a series of differentiated trachytes near the summit.

The Ne-mugearite (81424) is a vesicular, dark gray flow rock characterized by large pyroxene phenocrysts up to 10mm and plagioclase feldspar laths up to 3mm. At the base of the section, it makes up the first 11m and is overlain by an equal amount of snow and ice cover.

The following unit is made up of an 11m sequence of light gray, pumiceous trachyte (81425-26, 81438) showing varying degrees of flow banding. The trachyte is dominated by plagioclase phenocrysts up to 5mm, but lack any visible pyroxene or amphibole.

Above the first unit of trachytes is a scree slope covered with a basaltic float material which may be derived from a nearby parasitic cinder cone. On top of the scree slope is a 4m ice cliff.

The next exposure is a 1m thick sequence of a porphyritic, holocrystalline, blue-gray trachyte (81439) with plagioclase phenocrysts up to 15mm and pyroxenes to 3mm.

The sequence is capped by a 1.5m unit of a dark brown to black, glassy, flow banded trachyte (81442) which contains up to approximately 25% cumulate cognate and basement xenoliths. This unit forms the summit of Mount Overlord and extends over a wide area around the summit. A small isolated outcrop of benmoreite (81444) appears to be interbedded with this unit just south of the summit. This could either be an isolated flow or a very shallow dike like intrusion, the exposure was too poor to differentiate which was more likely.

2.3.2 RIM GEOLOGY

The rim of Mount Overlord is largely intact with small breaches to the northeast and southeast. Sample locations can be divided into four areas corresponding to compass directions (Fig. 2.1).

To the east, and isolated from the rest of the rim, is a three unit sequence consisting of a benmoreite (81414) at the base, and two comendite units (81415-17) above. The benmoreite is a dark gray, vesicular, porphyritic, and flow

banded with phenocrysts of plagioclase and clinopyroxene. The second unit is a comenditic welded tuff (81415) which is moderately welded with large fiamme structures common throughout. The top unit is also a comendite in which devitrification has destroyed the primary structures in thin section. Its location on the rim and dense welding suggests an air-fall tuff and not an ash-flow tuff ignimbrite.

The remainder of the rim is intact. On the south and southwest portion is a series of up to nine distinct flows consisting of seven ne-benmoreites and benmoreites (81418,19,27,29-32,34), one phonolite (81428) and one mugearite (81433). The benmoreites are dominately light gray, porphyritic rocks with large phenocrysts of plagioclase up to 15mm. A few of the benmoreites are dark gray to black and slightly vesicular, these may represent the tops of flows. The phonolite does not differ in appearence from the majority of benmoreites in hand specimen or thin section.

The western portion of the rim is capped by a dark brown to black, xenolith-rich trachyte (81442,46), and is described in the previous section (Fig. 2.6).

The northern rim area is composed of a xenolith rich, reddish brown unit (81437) which may be an altered equivalent to the summit flow (81442), and a small trachyte (81436) flow. Comenditic welded tuff float is also found.

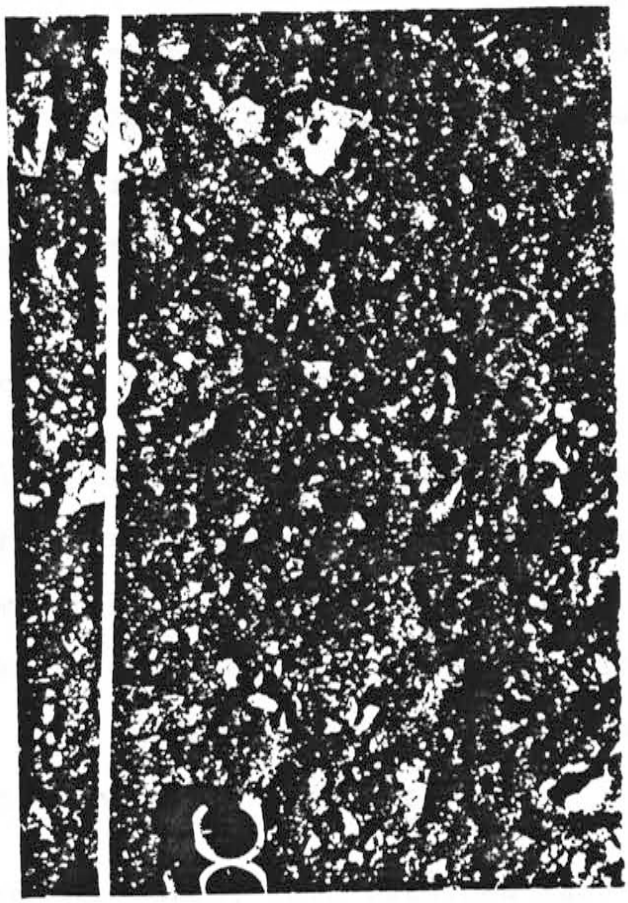

FIGURE 2.5 Xenolith rich trachyte which caps the western rim. The scale of the photo is approximately 1 meter in length

2.3.3 PARASITIC CONES AND VENTS

Two types of parasitic cones exist around Mount Overlord. These two types consist of relatively older cones which are roughly circular craters of basaltic material near the base of the mountain, and apparently younger cones farther up the flanks which have retained more of their original structures. The rocks from all the cones range from a basanite to mugearite, but are dominately hawaiites. They are scoriaceous, dark brown to black on fresh surfaces, and oxidize to a reddish brown color.

The older cones (81460-65) were thought by Nathan and Schulte (1968) to be the remains of an older shield volcano on top of which Mount Overlord was built. This may not be the case as the older and younger cones have similiar chemistry. The difference in preservaton may be due to greater erosional rates near the base.

The younger cones, have retained much of their original character and are easily recognized on aerial photographs. One of the cones is located on the rim and flows both into and away from the caldera. This shows a post collapse age for that cone and possibly the others.

Ultramafic xenoliths are abundant in many of the cones. The xenoliths are dunites and spinel lherzolites which occur in rounded chunks up to fist size and show some crude layering.

2.3.4 XENOLITHS

Many cognate cumulate xenoliths were collected from around the rim. Those looked at in detail were from the main volcanic rocks which make up Mount Overlord, and not from the parasitic cones. Also sparse xenoliths of probable basement material were collected but not studied in detail.

The cumulates are divided into three groups by petrography and chemistry. There are essexites, anorthosites, and sodalite syenites.

2.4 Parasite Cone

Parasite Cone (2340m), located 12km northwest of Mount Overlord, is composed of a hawaiite hyaloclastite presumably formed as a sub-glacial eruption. The rock is light to medium brown in color, contains fragments of congealed lava and some basement material, mainly sedimentary rock fragments of the Beacon Supergroup, which occur in a scoured channel (Fig. 2.7).

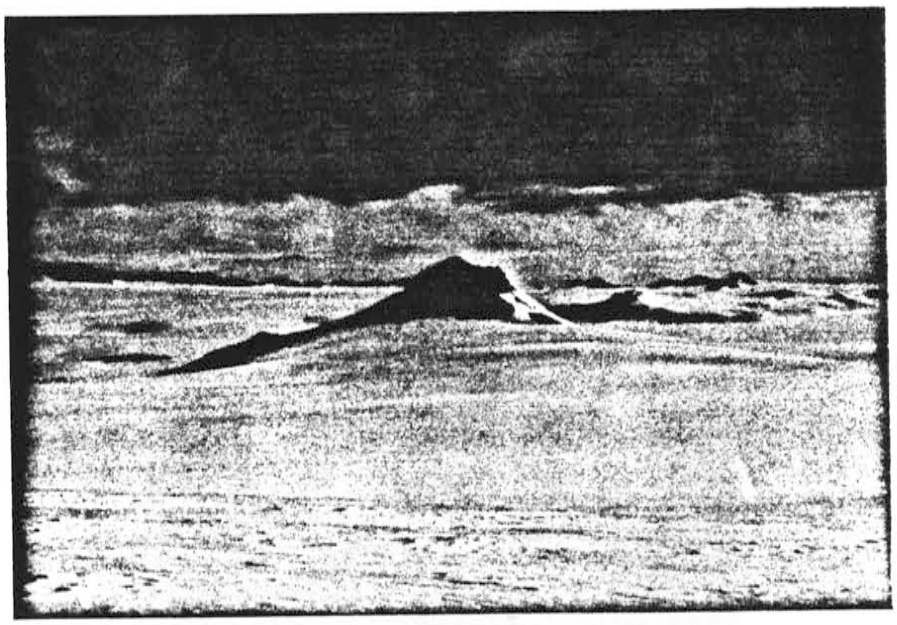

FIGURE 2.7 Photos of Parasite Cone: A) Parasite cone looking north from Mount Overlord, B) Basalt dyke intruding yellow palagonitized hyaloclastite on the south side of Parasite Cone.

FIGURE 2.7 (cont.) C) Hyaloclastite with scoured channel filled by more breccia with clasts of Beacon sandstone (white).

The hawaiite lava which forms the hyaloclastite also occurs as small dike-like intrusions into the hyaloclastite, and as clasts in the breccia. A basalt clast (81500) has a conventional K/Ar age determination of 14.67 my (table 2.2.)

If the hyaloclastite is a sub-glacial eruption, it shows that ice levels in the past were higher than at present

2.5 Mount Noice

Five samples (82059-62,65) from Mount Noice (2780m), located 5.5km south of Mount Overlord were analyzed for major elements. Four of the samples (82059-61,65) were in-situ flow rocks, the other sample (82062) was a massive float block of obsidian.

All rocks were found to be comendites. The four flow rocks correspond to comendites with 10% to 20% normative quartz. The obsidian corresponds to comendites with greater than 20% normative quartz, and is similiar to the comendites found on Overlord. No welded tuffs were observed, however the outcrop exposure was very limited.

The Deception Plateau, located between Mounts Overlord and Noice may be capped by welded tuff outflow sheets from both locations. The plateau shows very little relief.

Also, outcrops of welded tuff on the south flank of Mount Overlord suggest a flow on to the Deception Plataeu.

3 PETROGRAPHY

3.1 Introduction

Fourty-nine thin section samples representing 11 different rock types were examined petrographically. As most of the rocks are glassy or fine-grained, they were classified using their chemical compositions, rather than based on modal abundances. A summary of the classification is given in table 3.1 and discussed in more detail in chapter 4. In this chapter, each rock type is discussed separately and, when appropriate, broken down into different groups with similiar textures. A brief description for each group is given in table 3.2.

Rock Type	Classification Criteria
Basanite	An > 50%, Ne > 5%
Alkali Basalt	An > 50%, Ne < 5%
Hawaiites	An = 30-50%, DI < 65
Mugearites	An = 10-30%, DI < 65
Benmoreites	DI = 65-75
Phonolites	DI > 75, Ne > 10%
Trachytes	DI > 75, Ne < 10%
Qtz-Trachytes	DI > 75, Q > 0
Comendites*	DI > 75, Ac > 0

TABLE 3.1 Summary of nomenclature. A detailed description is found in chapter 4.
An, normative 100 An/An+Ab
Ne, normative nepheline
Q, normative quartz
DI, normative Q+Ab+Or+Ne+Lc
Hawaiites, mugearites, and benmoreites with Ne > 10% are prefixed with ne-.
*Comendites cannot be distinguised from trachytes using this classification scheme and are further classified by Macdonald (1974) (Fig. 4.4).

TABLE 3.2 SUMMARY OF THE PETROGRAPHIC CHARACTER OF EACH ROCK TYPE FORM MOUNT OVERLORD

		Mineralogy						
Rock Type	Texture	Ol	Cpx	Kaer	Fspr	Op	Ap	Groundmass
Basanite/ Alkali Basalt	p(30),v	r,c	p	p	p	p		h
Hawaiite	p(50),v		p	p	p	p		h
Mugearite	p(30),v	r,po	p	p	p	p		h
Benmoreite								
Gp1	p(40),v		p	p	p	p		h-i
Gp2	p(85)		p	p	p	p		h-i
Gp3	p(70)		p	p	p	p		h-i
Gp4	p,c		p	p	p	p		g
Gp5	mp(75)		p		p			i
Phonolite	p,mp,c		p		p	p		p,tr
Trachyte								
Gp1	p(60),v		p		p	p		h
Gp2	p(75),v		p		p	p		h-gl,tr
Gp3	p,c		p	r	p	p		mc,g,p,tr
Gp4	p,c		p		p	p		td
Qtz-trachyte	mp(20)		p		p	p		mc,h
Comendite								
Gp1,2	f		p		p			gl,2d
Gp3	f		p		p			mc,g,2d
Essexite	c,cu	r	p	p	p	p	p	
Anorthosite	c,cu	r,po	p	p	p	p	p	
Sodalite Syenite	c,cu		p	p	p	p		

Abbreviations:
Texture: p(10)-porphyritic (% phenocrysts to nearest 5%), mp(10)-microporphyritic phenocrysts average less than 1 mm, v-vesicular, c-holocrystalline, f-felsitic, cu-cumulates
Mineralogy: p-present, r-rare, c-cores, po-partially oxidized
Groundmass: gl-glassy, h-hyalopilitic, i-intersertal, p-pilotaxitic, g-intergranular, tr-trachytic, td-trachytoid mc-microcrystalline, 2d-secondary minerals

3.2 Alkali Basalts and Basanites

Three samples of alkali basalt (81508, 09, 11) and one of basanite (81510) are dominately fine grained, hypocrystalline, hypidiomorphic, porphyritic, scoriaceous flow rocks from cones on the flanks of Mount Overlord. The minerals present include plagioclase (10%), clinopyroxene (15%), with lesser amounts of kaersutite and opaque oxides (< 5%), and traces of olivine (< 2%). Plagioclase occurs as fine grained, euhedral to subhedral, prismatic phenocrysts, and as microlites and crystallites in a glassy groundmass. The phenocrysts average 1mm, show normal zoning, and have inclusions of clinopyroxene and opaque oxides. Clinopyroxene occurs as fine grained, euhedral to anhedral, equant to prismatic phenocrysts and microlites in the glassy groundmass. Phenocrysts average 1 to 1.5mm and show some zonation. Opaque oxides are found as very fine grained, anhedral grains scattered throughout the groundmass, and as euhedral to subhedral grains as inclusions in clinopyroxene and plagioclase. Kaersutite occurs as an alteration product after pyroxene, but some grains may be primary. Olivine is found as small cores, no larger than 0.5mm, in some clinopyroxene grains.

3.3 Hawaiites

Five samples of hawaiite (81459, 61, 65, 66, 500) were found to be hypocrystalline to hypohyaline (81466), porphyritic, microcrystalline, fine grained rocks. 81466 is vesicular while the others are not. The dominant mineralogy includes phenocrysts of plagioclase (20-60%), clinopyroxene (5-30%), kaersutite (0-10%), and opaque oxides (5-10%). Plagioclase is found chiefly as euhedral to subhedral, prismatic to lath-shaped phenocrysts and microlites up to 3mm in length, the larger crystals being zoned and having poikilitic inclusions. Clinopyroxene occurs in euhedral to anhedral, prismatic to equant phenocrysts and microlites up to 2mm in length. Some of the larger crystals are zoned, have inclusions of opaque oxides, and have reaction rims of kaersutite. Kaersutite, when found, is subhedral to anhedral, equant to prismatic, and occurs as primary crystals and as an alteration product of clinopyroxene. The grains are strongly pleochroic and exhibit mesh texture as they alter to opaque oxides. Opaque oxides occur as subhedral to anhedral grains up to 0.5mm, is associated with phenocrysts and scattered throughout the groundmass.

3.4 Mugearites

Four samples of mugearites (81420, 22, 24, 33) are found to be fine to medium grained, hypohyaline, hyalopilitic, porphyritic, flow rocks. 81420 is the only sample that is not vesicular, having a dense aphanitic groundmass. The dominant mineralogy includes plagioclase (15%), clinopyroxene (5%), kaersutite (5%), and opaque oxides (5%), with rare olivine (81420) and lithic fragments. Plagioclase is found as euhedral to anhedral, broken and rounded, equant to prismatic grains ranging up to 4mm, and averaging 0.5mm. Most show zoning and have inclusions of ferromagnesian minerals. Clinopyroxene occurs as pale green, subhedral grains ranging from 0.1 to 1.5mm, with many crystals rimmed by kaersutite. Kaersutite occurs as euhedral to subhedral, prismatic to tabular, pleochroic crystals up to 4mm in length, and averaging 0.5mm. Opaque oxides occur as euhedral to subhedral grains, and anhedral patches up to 0.5mm and scattered throughout the groundmass. Olivine occurs as small, less than 0.2mm, anhedral grains, strongly reacted and altering to kaersutite. The lithic fragments found are composed of 75% or more fine grained, mosaic to pilitic plagioclase with lesser amounts of clinopyroxene, amphibole, and opaque oxides.

3.5 Benmoreites

Nine samples of benmoreites (81414, 18, 27, 29, 30, 32, 34, 44, 82077) may be divided into five distinct textural groups. All groups are similiar mineralogically, being dominated by plagioclase with lesser amounts of clinopyroxene, opaque oxides, kaersutite, and biotite.

The first group (81414) consists of a vesicular, porphyritic, hypocrystalline flow rock with a microcrystalline groundmass. The dominant mineralogy includes plagioclase (30%), opaque oxides (5%), and clinopyroxene and kaersutite (5%). Plagioclase is found as subhedral to anhedral, equant to prismatic, zoned phenocrysts up to 3mm in length, and as parallel to subparallel, acicular microlites in the groundmass. Clinopyroxene and kaersutite occur as subhedral to anhedral, equant to tabular, crystals averaging 0.3mm in length with included opaques and reaction rims. The opaque oxides are found as subhedral to euhedral, equant grains averaging 0.2mm, and usually associated with the ferromagnesian minerals.

The second group (81418, 27, 29, 34) consists of fine grained, hypocrystalline, porphyritic, rocks with phenocrysts of plagioclase (65%), clinopyroxene (5%), biotite (5%), kaersutite (5%), and opaques (5%).

Plagioclase occurs as euhedral to anhedral, equant to prismatic, zoned phenocrysts up to 5mm, and the groundmass includes acicular crystals and microlites up to 0.05mm. Clinopyroxene is found as euhedral to anhedral, equant to prismatic, light green to tan grains up to 1.5mm. Some crystals are zoned and all show varying degrees of alteration to opaques, biotite, and kaersutite. Biotite and kaersutite occur as alteration products of clinopyroxene and are themselves being oxidized to opaque oxides. The opaque oxides occur as euhedral to anhedral grains spread through the groundmass and associated with ferromagnesian minerals.

Group three (81430, 32) consists of fine grained to microcrystalline, porphyritic, subparallel, hypidiomorphic, hypocrystalline flow rocks with phenocrysts of plagioclase (40%), clinopyroxene (10%), opaque oxides (10%), kaersutite (5%), biotite (5%), and lithics (5%). Plagioclase occurs as euhedral to anhedral, equant to prismatic, zoned phenocrysts up to 3mm in length. Clinopyroxene occurs as euhedral to anhedral, equant to prismatic, light green to tan, faintly pleochroic phenocrysts up to 3mm with most showing alteration to kaersutite and biotite. Biotite occurs as subhedral to anhedral, tabular to lathlike phenocrysts up to 4mm and strongly altered to opaques. Kaersutite occurs primarily as an alteration product of clinopyroxene, but also assubhedral to anhedral, equant to prismatic phenocrysts up to 2mm. Opaque oxides occur as euheral to

anhedral grains up to 0.1mm scattered throughout and as inclusions and alteration products with phenocrysts.

Group four (81444) is a fine grained, porphyritic, holocrystalline flow rock or shallow dike composed of plagioclase (60%), clinopyroxene (15%), anorthoclase (10%), opaque oxides (10%), and a trace of kaersutite and hematite. The groundmass consists of fine grained, subhedral, intergrown, and sutured grains of plagioclase, clinopyroxene, and opaques up to 0.2mm. Phenocrysts of plagioclase are subhedral to anhedral, equant to prismatic, up to 4mm in length with some having been strongly altered. Clinopyroxene is found as subhedral to anhedral, equant to prismatic phenocrysts up to 3mm in length with minor reaction rims. Anorthoclase forms large anhedral to subhedral, equant to prismatic grains up to 6mm in length.

Group five (82077) is a fine grained to microcrystalline, hypocrystalline flow rock composed dominantly of plagioclase. The groundmass (25%) consists of microlites of plagioclase and clinopyroxene while the phenocrysts (75%) are almost exclusively euhedral to subhedral, acicular to lathlike plagioclase crystals up to 0.5mm in length.

3.6 Phonolites

Three samples of phonolite (81428, 64, 82072) were examined and occur in two textural forms but have similiar mineralogy. 82072 is a holocrystalline, fine grained, equigranular, porphyritic, hypidiomorphic rock showing trachytoid groundmass textures. 81428 and 81464 are holocrystalline, idiomorphic, porphyritic rocks with a fine grained groundmass of plagioclase laths and medium to coarse grained phenocrysts. Trachytoid texture is best developed in 81464, and weakly in 81428. The mineralogy consists of plagioclase (65%), clinopyroxene (15%), opaque oxides (5%) and minor amounts of hematite, biotite and olivine (81428,464), and chlorite (82072).

In 82072, the plagioclase occurs as fine grained, subhedral, fibrous to acicular crystals and microlites. The clinopyroxene occurs as deep green, very fine grained, subhedral to anhedral, acicular to prismatic microlites. Opaque oxides is found as very fine grained, subhedral crystals spread throughout the section. Hematite is found as an alteration product along fractures. Chlorite, or clay minerals, are also found in varying degrees along fractures as an alteration product.

In 81428 and 81464, plagioclase is found as euhedral to subhedral, tabular to prismatic phenocrysts which are zoned along the rims. They range from 0.5 to 10mm, average 2mm, and contain poikiliths of clinopyroxene and opaque oxides. Clinopyroxene occurs as euhedral to subhedral, equant to tabular crystals ranging up to 3mm, but averaging only 0.5mm. Opaque oxides occurs as fine grained, euhedral to subhedral grains ussually associated with ferromagnesian minerals. Biotite is found as dark brown, pleochroic, anhedral to subhedral grains up to 1.5mm, all showing strong alteration. Olivine occurs as rounded, anhedral grains averaging 0.05mm, included in clinopyroxenes and optically continuous. Hematite again is found as an alteration product along fractures.

3.7 Trachytes

Seven trachytes may be divided into four distinct petrographic groups. The first group (81425, 26) consists of a hypocrystalline, fine grained to microcrystalline, porphyritic, vesicular flow rock. The dominant mineralogy includes plagioclase (50%), clinopyroxene (5%), opaque oxides (5%), and a trace of hematite. Plagioclase is found as euhedral to subhedral, tabular to prismatic, zoned phenocrysts up to 1mm, and prismatic to acicular, diverse microlites. Clinopyroxene occurs as subhedral to anhedral,

equant grains averaging 0.5mm, and having reaction rims going to opaque oxides. Opaque oxides are found as euhedral to subhedral grains up to 0.1mm, associated with clinopyroxene, and smaller grains throughout the groundmass.

Group two (81442, 46) consists of a hypocrystalline, microcrystalline, porphyritic, trachytic, fluidal, and eutaxitic flow rock with fine to medium grained phenocrysts and abundant lithic fragments in hand specimen. The dominant mineralogy includes plagioclase (60%), clinopyroxene (5%), biotite (5%), and opaque oxides (5%). Plagioclase occurs as euhedral to subhedral, tabular to prismatic, broken phenocrysts up to 8mm in length having inclusions of clinopyroxene and opaque oxides. Clinopyroxene occurs as euhedral to anhedral, equant grains averaging 0.5mm with reaction rims of opaque oxides. Biotite is found as subhedral, prismatic crystals up to 0.6mm with reaction rims. The opaque oxides are scattered throughout the groundmass or associated with the ferromagnisian minerals.

Group three (81436, 39) is characterized by holocrystalline, porphyritic rocks with a fine grained to microcrystalline groundmass which varies from trachytic with acicular plagioclase laths, to plagioclase grains which are prismatic to tabular. The dominant mineralogy includes plagioclase (75%), clinopyroxene (15%), opaque oxides

(5-10%), and minor amounts of biotite and kaersutite. Plagioclase occurs as euhedral to subhedral, tabular to prismatic, zoned phenocrysts up to 8mm in length, groundmass crystals are acicular to tabular, ranging up to 0.5mm. Clinopyroxene is found as small (0.2mm) subhedral grains in the groundmass and as euhedral to subhedral, tabular to equant, faintly pleochroic phenocrysts up to 1mm. Opaque oxides are found as subhedral to anhedral grains less than 0.02mm in the groundmass, and as euhedral to subhedral grains up to 0.4mm associated with the ferromagnisian minerals. Biotite occurs as anhedral grains going to opaque oxides and kaersutite is found as an alteration product of clinopyroxene.

Group four (82069) is a medium to fine grained, hollocrystaline, trachytoid flow rock consisting of plagioclase (80%), clinopyroxene (10%), and opaques (10%). Plagioclase is found as subhedral, medium to fine grained, equant to acicular grains up to 1mm. Many of the crystals have sieve and resorption textures. Clinopyroxene occurs as medium to fine grained, subhedral to anhedral, equant to prismatic grains up to 0.5mm with some reaction rims. The opaque oxides are anhedral to euhedral, fine grained crystals spread throughout the groundmass and associated with the other phenocrysts.

3.8 Quartz Trachytes

One quartz trachyte (82075) was found to be a fine grained hypohyaline flow rock with a microcrystalline groundmass (80%) of radial to actinoid, prismatic to acicular plagioclase and clinopyroxene. The phenocrysts consist of plagioclase (10%), clinopyroxene (5%), and opaque oxides (5%). Plagioclase occurs as anhedral to euhedral, prismatic to acicular grains up to 1mm. Clinopyroxene occurs as anhedral to subhedral, prismatic to acicular grains up to 0.2mm. The opaque oxides occur as anhedral to euhedral grains spread throughout the groundmass.

3.9 Comendites

The comendites may be broken down into three textural groups. The first two groups have an obvious pyroclastic origin, but the third is unknown. Group one (81415, 35B) are hypohyaline, felsitic, moderately welded tuffs. They are composed of a felsitic groundmass (75%) and phenocrysts of sanidine (15%), clinopyroxene (5%), quartz (5%), and a few phenocrysts of plagioclase and some pumice fragments. The groundmass consists of fine grained glass shards up to 0.5 mm in length, fiamme structures up to 1 mm, and crystallites. The glass shards are moderately welded

throughout and locally densely welded around large phenocrysts. The fiamme structures are long bladed stringers of dark glass, probably from the compaction of pumice fragments. Sanidine is found as anhedral to broken euhedral, equant to prismatic grains up to 3.5 mm. The clinopyroxene present ranges from a pale green, weakly pleochroic augite to a strongly pleochroic dark green to yellow aegirine. All of the clinopyroxene occurs as anhedral to subhedral, equant to prismatic grains up to 1 mm. Quartz is found as broken, irregular, anhedral grains up to 0.5 mm. A few phenocrysts of plagioclase were found to be broken euhedral, prismatic grains up to 1 mm in length. The pumice fragments are small, up to 1mm in length, and appear to be fairly well compacted. The rocks in group two (81416, 17, 35A) are similiar to the group one rocks in composition. The only significant difference is in the groundmass which shows varying degrees of devitrification. The amount of devitrification ranges from moderate in 81416 with shard stuctures and outlines still very obvious to severe in 81435A where most of the pyroclastic textures have been destroyed. A significant feature in this group is the formation of vapor phase crystals in the groundmass and filling cavities. The crystals appear to be either aenigmatite, acmite, or a sodic amphibole. Group three (82078) is a holocrystalline rock with very few large phenocrysts. The rock is dominately

composed of fine grained, equant to acicular, interlocking to mosaic grains of sanidine (70%), clinopyroxene (20%), and minor amounts of quartz and zeolites. The sanidine crystals appear to be a result of recrystallization, some areas of microcrystalline feldspar resemble recrystallized pumice fragments. Much of the clinopyroxene, which ranges from aegirine to acmite, seems to be a result of vapor phase crystallization throughout the groundmass and filling cavities, the remainder are phenocrysts of augite and aegirine. Also occuring as vapor phase crystals are aenigmatite and possible sodic amphiboles, and zeolites. Although there is some evidence for a pyroclastic origin, it is weak, and impossible to positively determine.

3.10 Essexites

Four essexite samples (81469, 71, 72, 73) are dominately medium to fine grained, holocrystalline, hypidiomorphic, with an overall interlocking texture. The dominant mineral phases include plagioclase (40%), clinopyroxene and kaersutite (40%), opaque oxides (10%), and apatite (5-10%), with rare sulfides, hematite, and olivine. Plagioclase occurs as euhedral to subhedral, meso to adcumulate (Cox et al, 1980), zoned crystals ranging in size from 0.5 to 5mm. Clinopyroxene composes from 5% (81471) to 40% (81473) of the total rock. The clinopyroxene occurs as

subhedral, equant to tabular crystals from 1 to 5mm. It is found as individual grains and in clusters of intergrown grains with apatite and opaque oxides poikiliths. Kaersutite exhibits similiar texures as those found for the clinopyroxenes, occuring as primary crystals with typical amphibole cleavage, and as patches and smears of alteration on clinopyroxenes. Opaque oxides occurs as anhedral clusters up to 3mm and in single euhedral to subhedral grains averaging 0.2mm. Small round blebs of sulfides (pyrrhotite) are included in some of the opaque oxides grains. Apatite forms euhedral crystals ranging from 0.05 to over 1mm in length, and averaging 0.4mm. Apatite is found as poikilitic inclusions and as small clusters of crystals.

3.11 Anorthosites

This group of four (81476, 78, 79, 85) clinopyroxene, opaque oxides bearing anorthosites varies very little in composition and texture. The rocks are holocrystalline, hypidiomorphic, medium grained adcumulates, dominated by plagioclase (70-80%), clinopyroxene (10-15%), opaque oxides (5-10%), and minor amounts of amphibole, biotite, hematite, and olivine. Plagioclase forms euhedral to subhedral, lath-like adcumulate crystals averaging 2 to 3mm. Individual grains are interlocking with intergranular

ferromagnesian minerals and oxides, and show zoning especially in the adcumulate overgrowths. Clinopyroxene occurs as subhedral, equant to prismatic, pale green to tan, faintly pleochroic crystals averaging 1mm with most showing some alteration to amphibole, biotite, or hematite. Kaersutite is found primarily as an alteration product, but may also occur as primary crystals in a similiar fashion as clinopyroxene but in smaller grains. Biotite and hematite are secondary products as a result of the alteration of clinopyroxene and opaque oxides. The alteration may be late stage hydrothermal alteration caused by trapped liquids derived from the intercumulus melt. Olivine, when found, occurs as strongly altered grains less than 0.5mm.

3.12 Sodalite Syenites

The two samples of sodalite syenite (81480, 84) are dominated by anorthoclase (>75%), clinopyroxene, amphibole, and biotite (10-20%), and minor amounts of sodalite and plagioclase, with rare opaque oxides and zircon. The rocks are light colored, holocrystalline, hypidiomorphic, and medium grained. Anorthoclase, is found as irregular, anhedral to subhedral crystals averaging 2mm. Adjacent grains are interlocking with a sutured texture and contain pokilitic inclusions of kaersutite and biotite. Clinopyroxene is generally found as cores, going to

amphibole, or as small grains (<0.5mm) with reaction rims. Kaersutite, occurs as an alteration of clinopyroxene, and as fine grained (0.2mm) euhedral crystals. Biotite is found as subhedral, prismatic pleochroic grains, and as an alteration product. Opaque oxides occurs as very fine grained euhedral crystals associated with clusters of ferromagnesian minerals. Zircon was identified as an inclusion in biotite, and occurs as euhedral, hexagonal, microcrystalline grains. Sodalite occurs as euhedral inclusions in the anorthoclase, some of the crystals may be altered to analcime.

4 GEOCHEMISTRY

4.1 Introduction

Major element analysis using X-ray fluorescence were determined on 51 samples at New Mexico Tech. Trace elements were determined on 38 samples by X-ray fluorescence (XRF) and instrumental neutron activation analysis (INAA) also at New Mexico Tech. For INAA, samples were irradiated at Sandia National Laboratory, Albuquerque, New Mexico. Analytical procedures are discussed in Appendix 1.

4.2 Nomenclature

4.2.1 Volcanic Rocks

Due to the fine grained nature of the volcanic rocks, classification using modal composition is difficult and a chemical analysis is more reliable. The classification scheme of Coombs and Wilkinson (1969) is used here, it classifies rocks based on their major element composition,

differentiation index (Thornton and Tuttle, 1960), and CIPW normative mineralogy. Oversaturated peralkaline rocks are not distinguished from trachytes in the above scheme, but are further classified using the procedure of Macdonald (1974).

Initially, the volcanic rocks are divided into sodic or potassic series (Coombs and Wilkinson, 1969; Irvine and Baragar, 1971). The distinction in this thesis will be made using the Na2O/K2O ratio (Macdonald, 1960; Macdonald and Katsura, 1964). When the majority of the rocks in a suite have Na2O/K2O ratios of greater than two, then all the rocks are referred to the sodic series. For the rocks of Mount Overlord, the basic and intermediate rocks are sodic but trend into the potassic range with the more evolved rocks (Fig. 4.2). This is consistant with observations made by Coombs and Wilkinson, as a suite becomes more evolved, it also becomes more enriched in K2O. Also, when plotting the differentiation index (DI) against normative anorthite of Coombs and Wilkinson, most samples fall into the sodic field. Therefore, sodic nomenclature is used in all cases.

Individual rock names were determined using differentiation index (DI) and normative anorthite (Fig. 4.3). This divides the rocks into five groups;

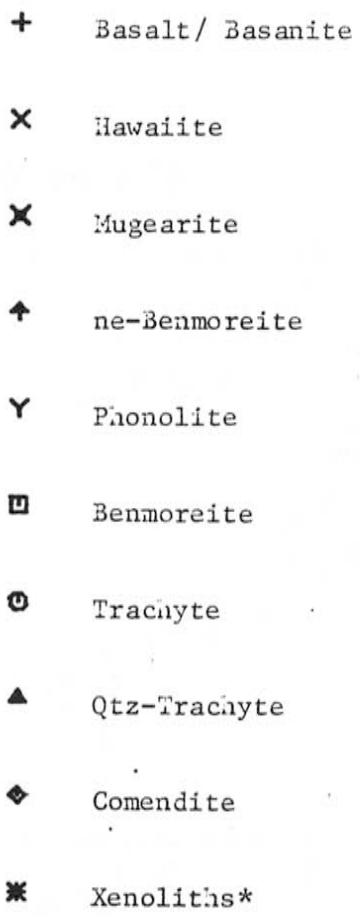

* xenoliths include essexites, anorthosites, and sodalite syenites.

FIGURE 4.1 Key to symbols used in variation diagrams. These symbols will be used for all diagrams throughout the text unless otherwise noted on the particular diagram. The symbols for rocks of the WUS and SUS have been separated to ease in the determination of the different suites.

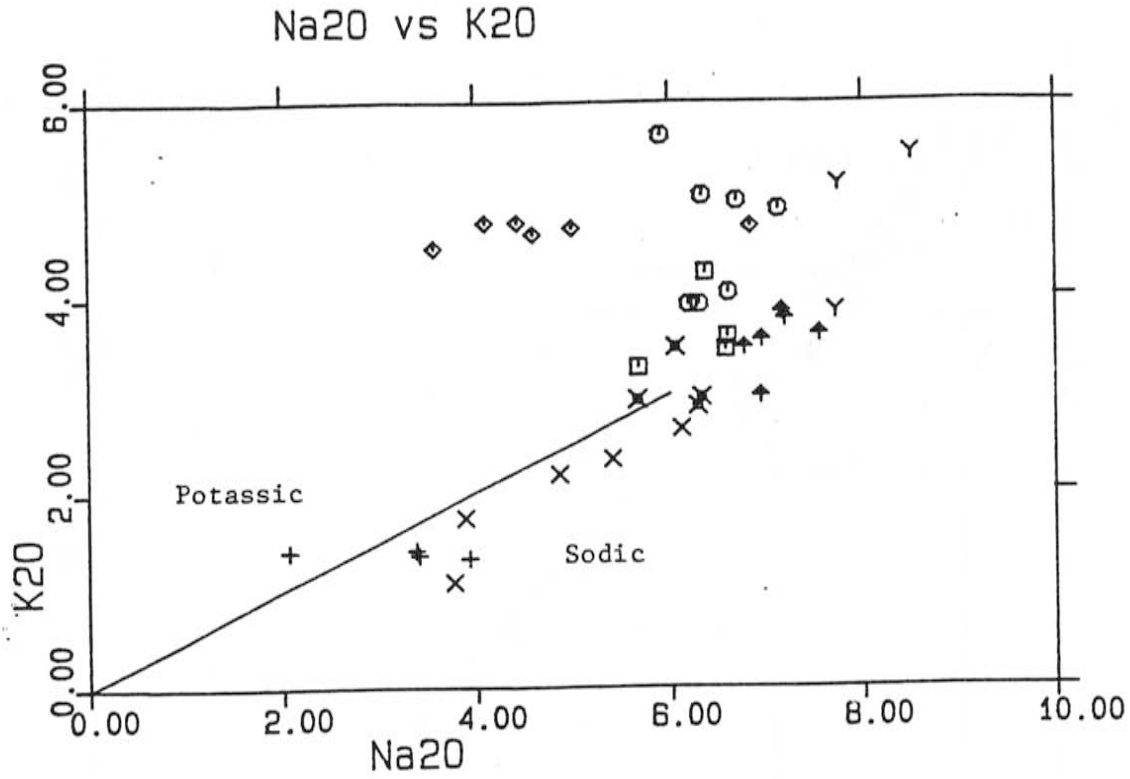

FIGURE 4.2 Plot of Na2O vs K2O (Macdonald, 1960). The line represents a Na2O/K2O ratio of 2 which separates the sodic and potassic series.

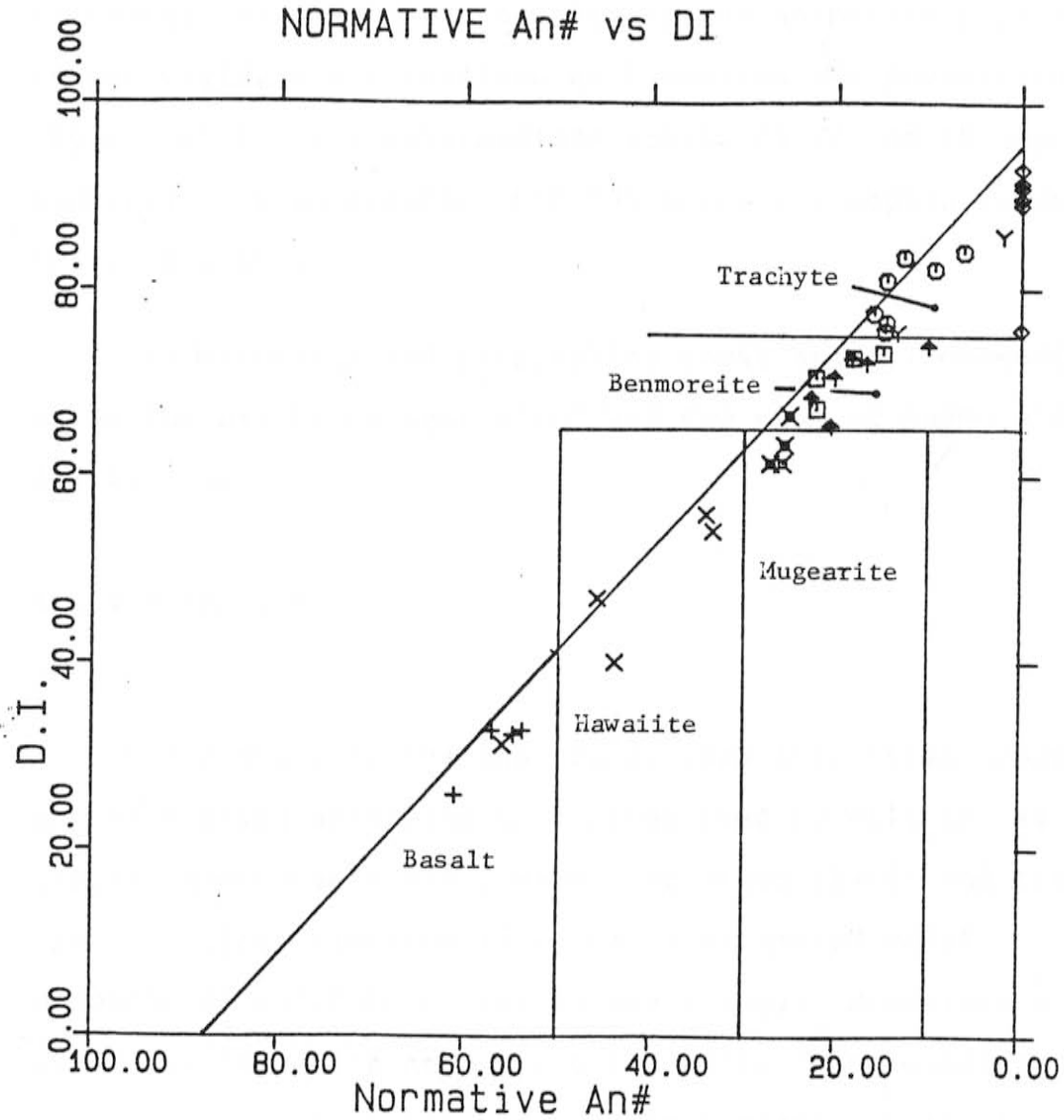

FIGURE 4.3 Plot of DI vs normative anorthite content. Classification scheme of Coombs and Wilkinson used to determine rock names.

basalts, An greater than 50; hawaiites, An 30 to An 50 and DI less than 65; mugearites, An 10 to An 30 and DI less than 65; benmoreites, DI from 65 to 75; trachytes, DI greater than 75. In addition to this, basalts and trachytes, with greater than 5% and 10% normative nepheline respectively, are classified as basanites and phonolites (Kyle, 1980). The intermediate rocks, hawaiites through benmoreites with greater than 10% normative nepheline are prefixed with ne-.

The oversaturated peralkaline rocks are all comendites using the weight percent Al2O3 and FeO plot of Macdonald (1974) (fig 4.4).

4.2.2 Xenoliths

The cognate inclusions are divided into three groups and classified according to schemes used by Williams et al (1954), Moorhouse (1959), Wager and Brown (1968) and Irvine (1982). Classification is based on estimated modal composition and CIPW normative mineralogy. Essexites are alkali gabbros with nearly equal amounts of plagioclase, titanaugite, and amphibole. Common accessory minerals include opaque oxides and apatite. The anorthosites contain at least 70% to 80% plagioclase and various other common ferromagnesian minerals. The sodalite syenites contain 60% or greater total feldspar (plagioclase, orthoclase, and

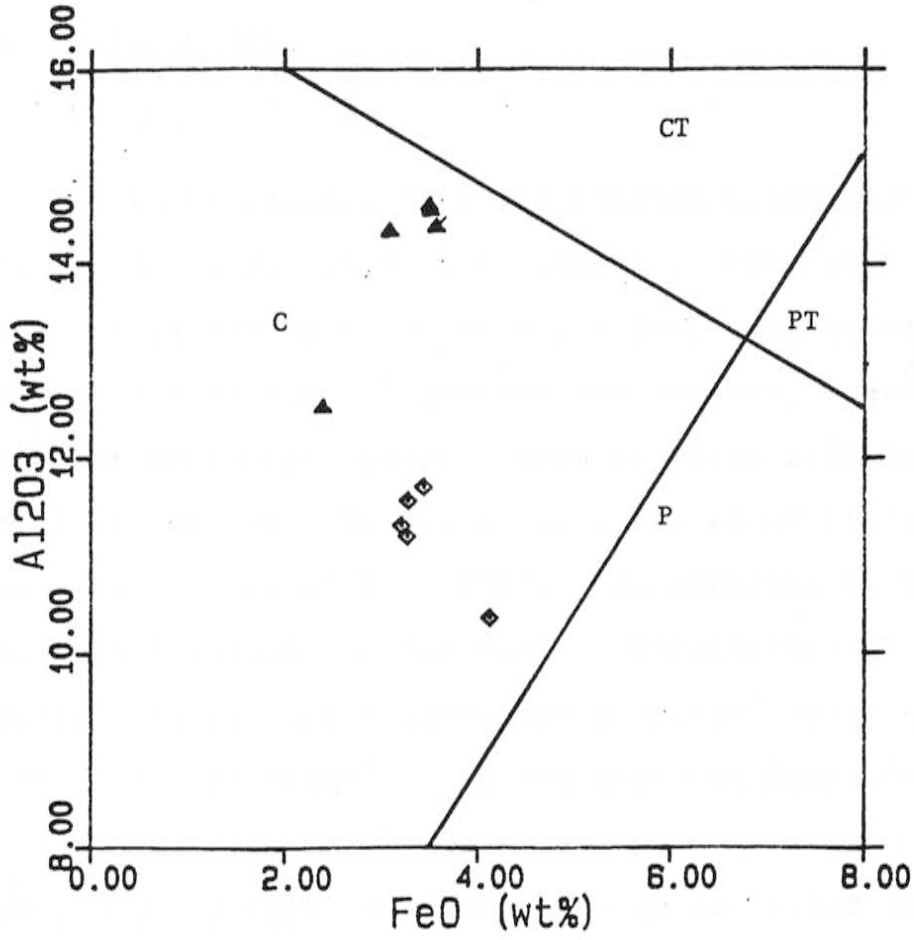

FIGURE 4.4 Classification of comendites using plot of Wt% Al2O3 and FeO (Macdonald 1974). C-comendites, CT- comenditic trachytes P-pantellerites, PT-pantelleritic trachytes

anorthoclase) along with ferromagnesian minerals and sodalite.

4.3 Major Element Chemistry

4.3.1 Introduction

The major element data are plotted using Harker variation diagrams (Fig. 4.5) (Harker, 1909) with SiO2 as the abscissa due to its wide variation. Harker variation diagrams are used to illustrate evolutionary trends in suites of cogenetic igneous rocks in which systematic variations may be interpreted as a result of crystal fractionaton (Cox et al., 1980). In addition to Harker variation diagrams, in the case of undersaturated rocks, plotting the DI versus normative nepheline (Fig. 4.6) further defines trends. For the rocks of Mount Overlord, two main suites are evident, a strongly undersaturated suite (SUS), and a weakly undersaturated to saturated suite (WUS). The basic end of both of these suites form parallel trends from basalt to mugearite on major element trends. For the remainder of the sequence, mugearite through phonolite and mugearite through trachyte, the two suites form distinctive trends on many diagrams: The SUS forming a generally tight trend, whereas the WUS sprays out into a number of possible

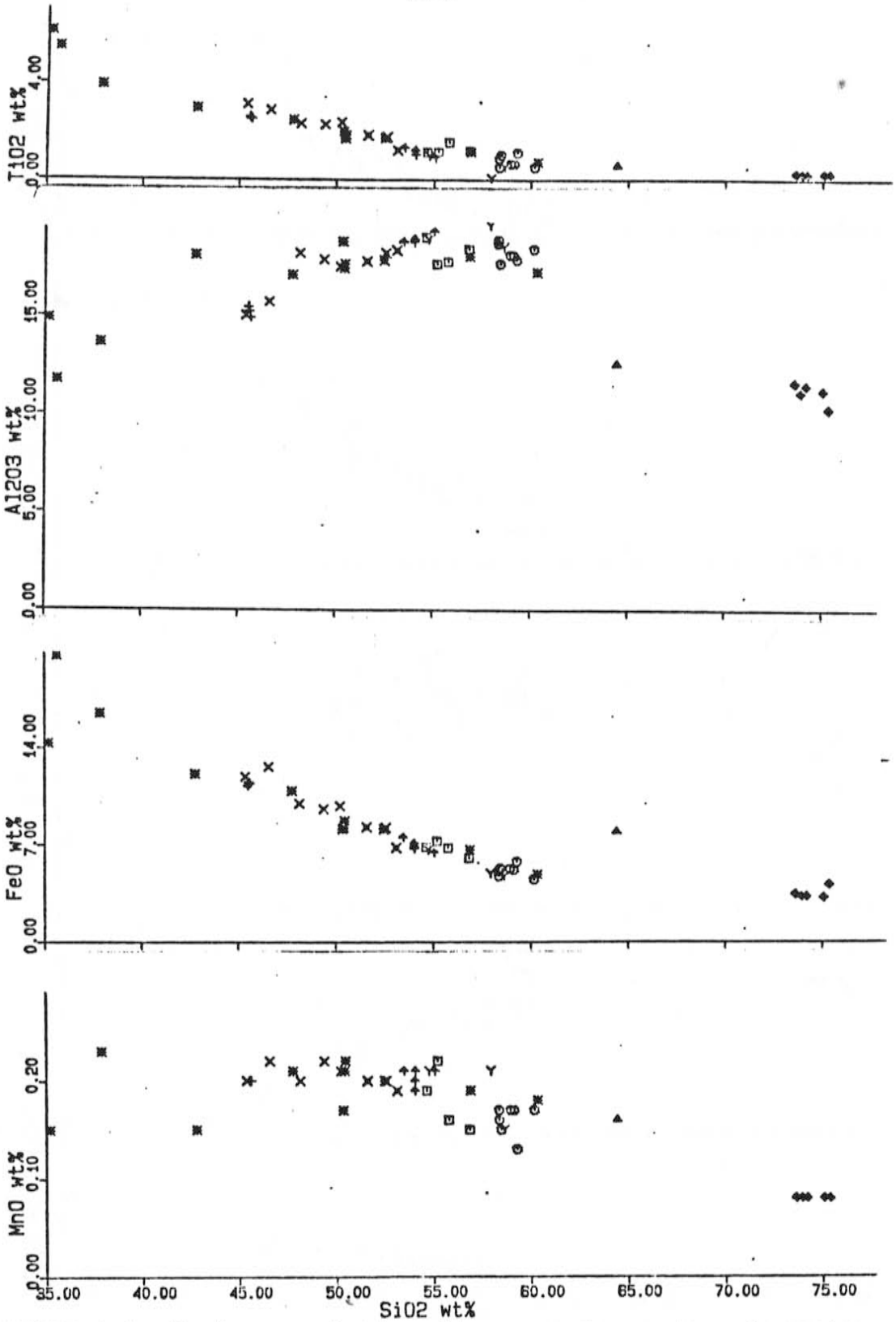

FIGURE 4.5 Harker variation diagrams for major elements vs silica.

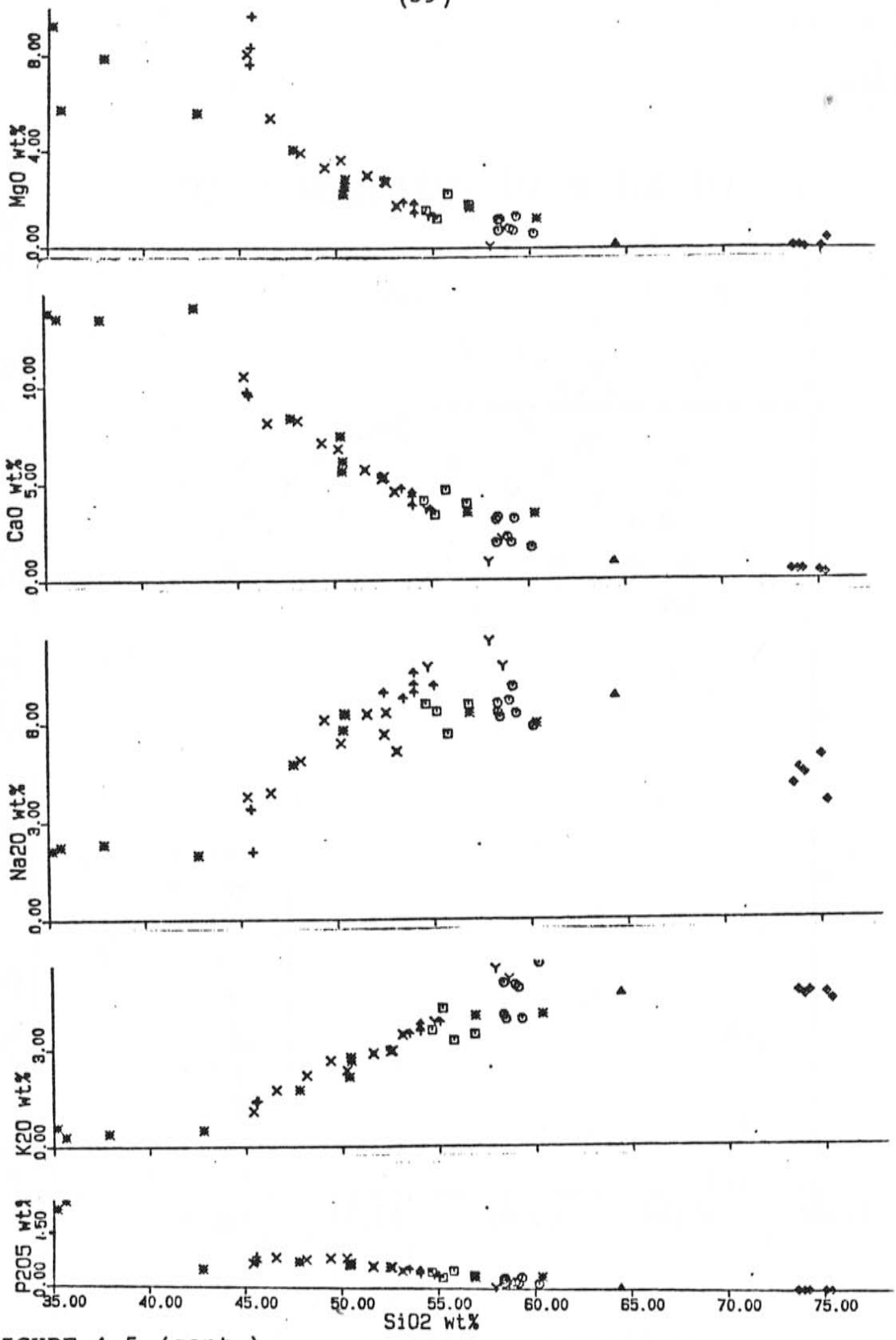

FIGURE 4.5 (cont.)

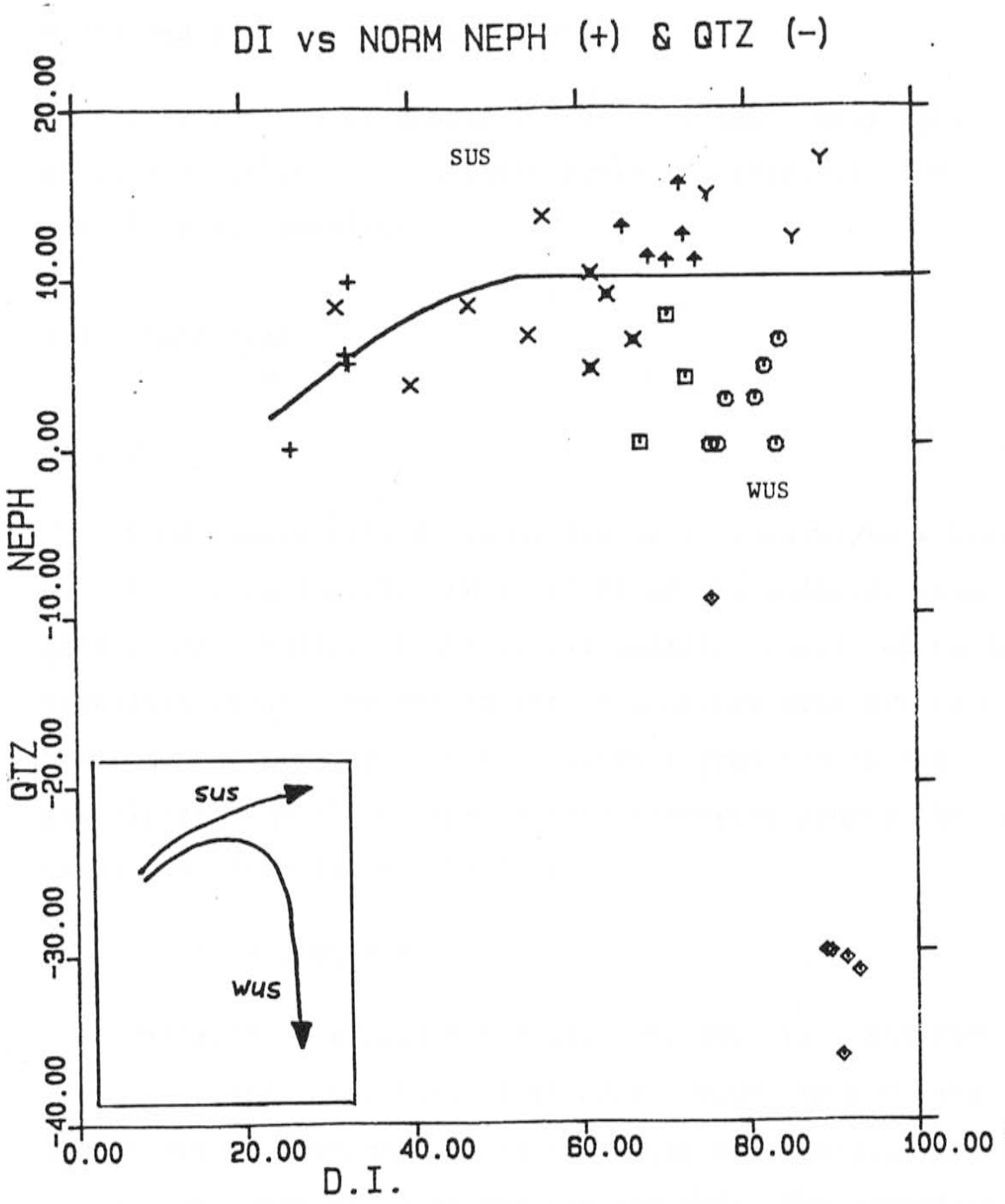

FIGURE 4.6 Plot of DI vs normative nepheline. Inset shows the paths of the WUS and SUS.

but related trends. There are also the strongly peralkaline comendites, including one qtz-trachyte, which will be discussed as a third separate group.

Data will be presented in two sections. They will cover the analysis of volcanic rocks (40 samples), and xenoliths (11 samples).

4.3.2 Volcanics

Silicon

SiO2 ranges from a low of 45% in a basanite to a high of 76% in a comendite. As a result of the classification scheme used, basanites and alkali basalts contain up to 46%, hawaiites range from 45% to 50%, mugearites from 51% to 53%, benmoreites from 52% to 57%, trachytes from 58% to 60%, phonolites from 55% to 59%, quartz trachytes around 65%, and comendites from 73% to 76% SiO2.

Ordinate Elements

Variation diagrams for TiO2, FeO, MgO, CaO, and P2O5 show a negative correlaton with SiO2. TiO2 and FeO have linear trends from basalts to trachytes and phonolites with no distinct separation of the SUS and WUS. The comendite group forms a separate group with low concentrations of these elements and does not fall on the main trend. CaO has

a similiar pattern to TiO2 and FeO however, there is slightly more scatter in the trachytes and phonolites with the WUS having slightly higher values of CaO. MgO has a curvilinear pattern but, like CaO, shows some scattering with higher silica. Values for P2O5 remain constant in the basalts and hawaiites. Following this, the pattern resembles those of TiO2 and FeO. In cases, where a separation of the SUS and WUS is suggested, the WUS has a greater scattering of points than the SUS.

Variation diagrams for Al2O3, Na2O, and K2O have complex patterns. Initially, they are positive then level off or decrease in the intermediate and highly evolved rocks. They all show good separation for the WUS and SUS with the SUS having generally higher values of all three oxides. Al2O3 increases slightly in the basalts and hawaiites. Beyond this, the SUS shows a continued, but slight increase through the phonolites, while concentrations in the WUS remain fairly constant. strongly peralkaline comendite group has the lowest values of Al2O3. Na2O is similiar to Al2O3 except for the comendite group, which does not have as great a depletion of Na2O. K2O shows a general enrichment through both trends. The comendite group has values of K2O similiar to those in the trachyte and phonolites. Again, the WUS has somewhat more scattering of points.

MnO shows a general decrease of values with increasing SiO2 but, the amount of scattering prevents the recognition of any distinct trends.

4.3.3 Xenoliths

Geochemically, as well as petrographically, the xenoliths define three groups, essexites, anorthosites, and sodalite syenites (Fig. 4.7). In all cases, except for MgO in essexites, the xenoliths fall on or very near the trends defined by the volcanic rocks. As these rocks are believed to be the products of the cumulation of fractionating phases, falling along trends for the volcanic rocks offers the mechanism for the enrichment or depletion in each trend.

4.4 Trace Element Chemistry

4.4.1 Volcanics

Variation diagrams for the trace elements may be divided into groups showing eight different patterns (Fig. 4.8). The patterns are characterized by Zr, Y, Rb, Sr, Ni, Sc, Ba, and Sb. Elements having a positive correlation with SiO2 are the Zr, Y, and Rb patterns,

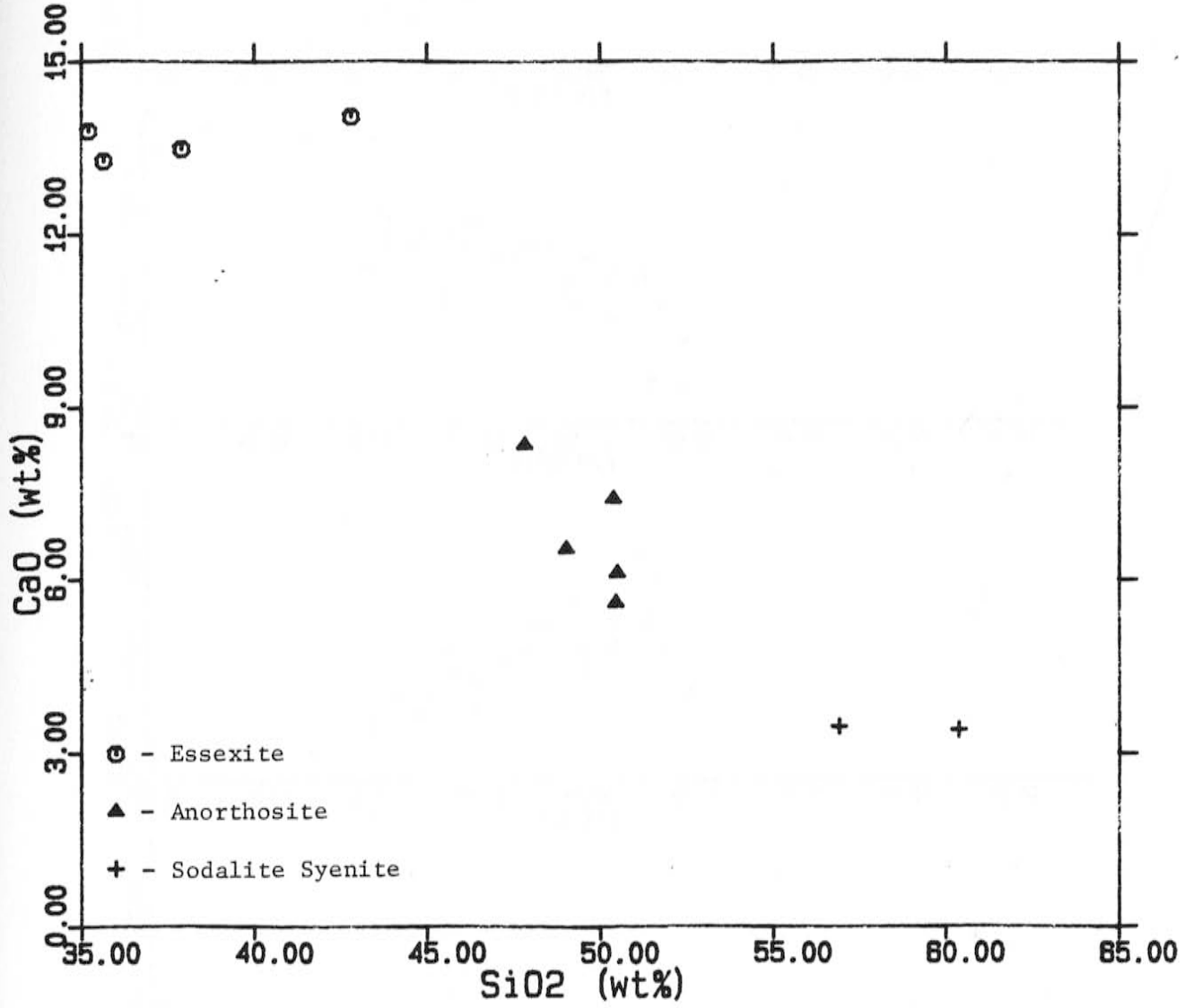

FIGURE 4.7 Harker variation diagram of CaO vs SiO2 showing the three different groupings of xenoliths.

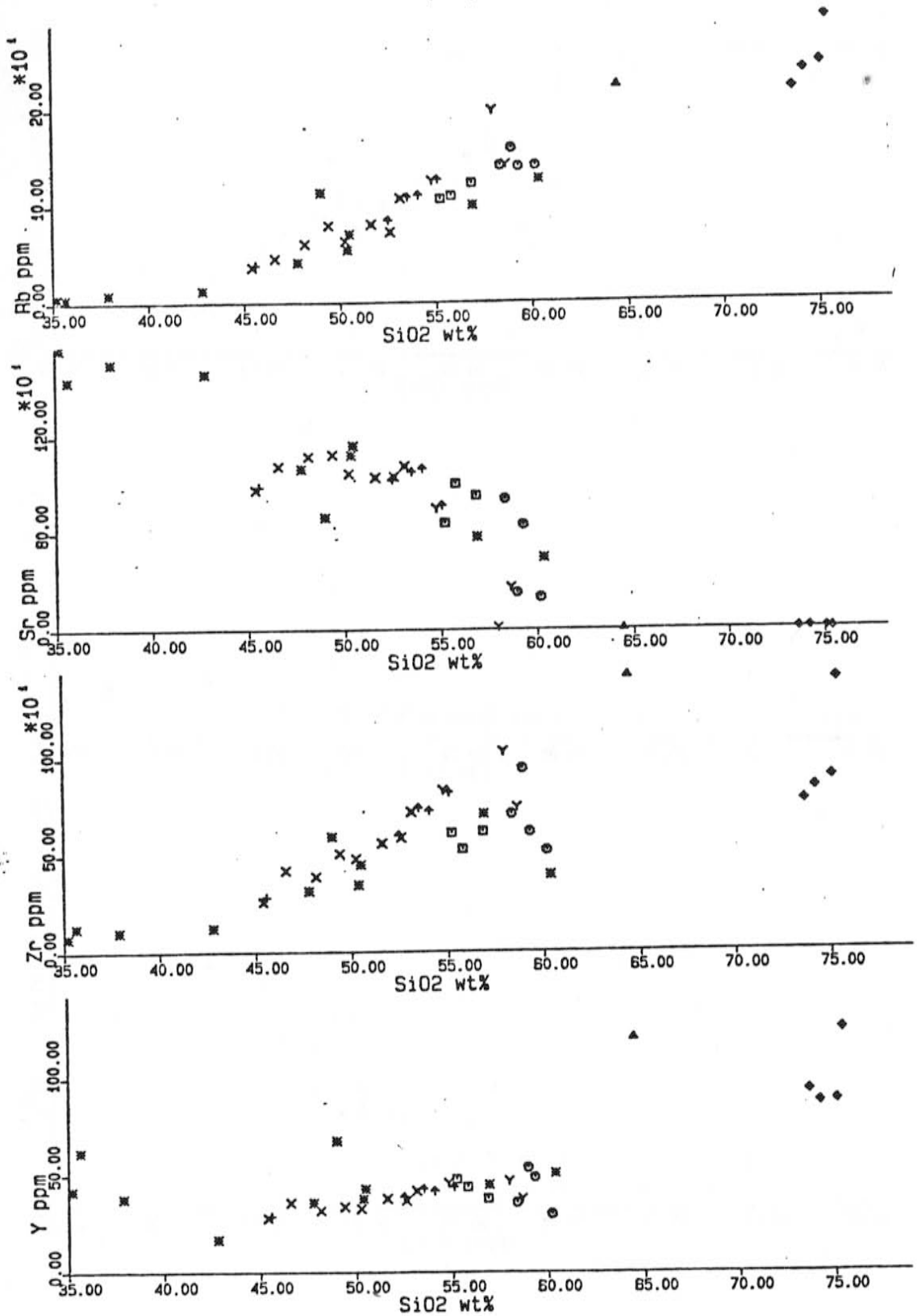

FIGURE 4.8 Harker variation diagrams for selected trace elements vs silica.

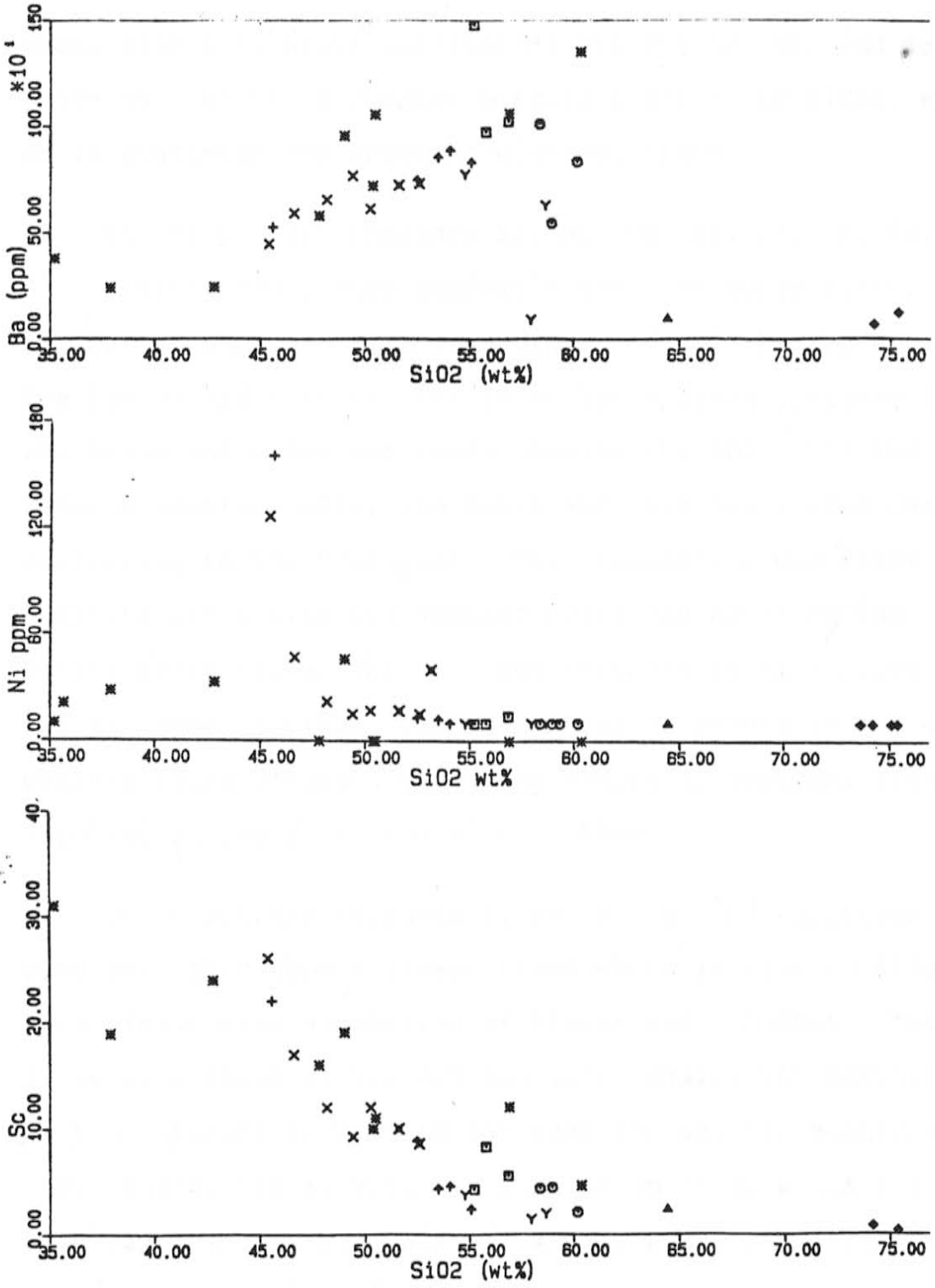

FIGURE 4.8 (cont.)

those with a negative correlation are the Sr, Ni, and Sc patterns. Ba has a complex pattern similiar to Al2O3, while Sb is scattered and shows no distinct trend.

The Zr pattern includes Zr, Nb, Cs, Hf, Ta, Th, Ga, and Se. Against SiO2, they exhibit a positive correlation, and all but Cs show at least some separation of the WUS and SUS. The typical pattern as seen in Zr has a linear pattern for the basic end which continues through the SUS. The WUS remains constant after the basic end, but has a good deal of scattering in the trachytes. The comendite group forms a separate group with two samples 82072 and 82075 having consistantly higher values. The elements in this group all act as incompatibles. The scattering of points in the more evolved rocks suggests a varying degree of residual liquid involved in the formation of each flow.

The Y pattern includes Y, Pb, and U. On variation diagrams, they show a linear trend which is flat to slightly curvilinear with scattering at higher SiO2 content. There is no separation of the WUS and SUS. Again, the comendites form a separate group with the same two samples mentioned above having higher values. This group of elements are slightly incompatible, but all may be partitioned into apatite, and Pb into feldspar.

Rb has its own distinct pattern which is positive and linear throughout the entire sequence, including the Comendite group. There is no distinction between the WUS and SUS. Rb is strictly incompatible and shows a steady increase throughout the entire sequence.

Sr also has its own unique pattern, showing a curvilinear negative trend against SiO2. At the basic end, the pattern is nearly flat but drops off sharply in the more evolved rocks. The WUS and SUS show some separation and the Comendite group again forms a separate group having very little Sr. Sr reflects the amount of feldspar fractionation. Initially, at the basic end, feldspar fractionation is not important, in benmoreites, trachytes, and phonolites it becomes a dominant fractionating phase.

The Ni pattern includes Cr, Ni, and Cu. In the basalts and hawaiites, the concentrations of these elements are very high. After this, they drop off rapidly and have a flat to slightly decreasing linear pattern for the rest of the sequence. All of the elements in this group are highly compatible, especially in mafic phases like olivine, pyroxene, and spinel.

The Sc pattern includes Sc and Co. This pattern is also curvilinear and resembles the pattern for MgO. Initially, there is a strong depletion at the basic end which gradually flattens out. Again, these elements are

compatible and are partitioned into pyroxenes and other mafic phases.

Ba has a pattern which is similiar in appearance to Al2O3. It has a positive correlation with SiO2 from the basic end through benmoreites. After this, there is a strong negative correlation in the trachytes and phonolites. The WUS and SUS show good separation and the Comendite group is again distinct. Ba is controlled by feldspar fractionation with anorthoclase and sanidine having the greatest partition coefficients.

Sb and Zn generally increases with SiO2, but there is a great deal of scattering and no distinct pattern can be recognized. These elements may be partially incompatible as they show a rough increase with increasing silica.

4.4.2 Xenoliths

As with the major elements, the xenoliths generally fall on or near the trace element trends. Noted exceptions to this are for Ni with the essexites usually having lower values than the basalts and hawaiites.

4.5 Rare Earth Element Chemistry

4.5.1 Introduction

The REE comprise the fourteen elements from lanthanum to lutetium. Seven REE were analyzed by INAA including; lanthanum (La), cerium (Ce), samarium (Sm), europium (Eu), terbium (Tb), ytterbium (Yb), and lutetium (Lu). Data is displayed on chondrite-normalized plots (Masuda, 1962; Coryell et al., 1963) and were normalized using Sun and Hanson (1976).

4.5.2 Volcanics

On chondrite-normalized plots all rock types (Figs. 4.9, 4.10) are REE enriched relative to chondrite. The light rare earth elements (LREE), La to Sm, are enriched relative to the heavy rare earth elements (HREE), Eu to Lu. Eu anomalies range from slightly positive in the mugearites,hawaiites and basanites to strongly negative in the comendites.

In the hawaiites and basanites, La ranges from 160 to 314 times chondrite. The HREE do not display as great an enrichment, Lu ranges from 10 to 17 times chondrite. The Eu/Eu* has a range of 1.15 to 1.22.

Mugearites have a similiar pattern to the hawaiites, fitting in to the upper end of the ranges of La and Lu. Eu/Eu* varies from 1.08 to 1.12.

La ranges from 290 to 376 times chondrite in the benmoreites , while Lu goes from 15 to 21 times chondrite. The Eu/Eu* goes from 0.96 to 1.10 except in sample 82077 which has an anomalous 1.25.

The trachytes have the greatest diversity of REE ranges. La varies from 274 to 598 times chondrite, and Lu from 12 to 44 times chondrite. Eu/Eu* varies from 0.60 to 1.03.

In the phonolites, La ranges from 329 to 426 times chondrite, and Lu from 19 to 22 times chondrite. Eu anomalies are stronger than those in the trachytes Eu/Eu* varies from 0.39 to 0.95.

The comendites have the greatest REE enrichment. La ranges from 330 to 676 times chondrite and Lu goes from 33 to 43 times chondrite. Eu anomalies are strongly negative with Eu/Eu* varying from 0.07 to 0.12.

The SUS shows a continuous enrichment relative to chondrite for all REE, and a enrichment of LREE over HREE. The middle REE (MREE) show a distinctive depletion as a result of kaersutite and clinopyroxene fractionation. A negative europium anomaly is not seen until the phonolites

when feldspar fractionation becomes more significant.

The WUS also shows continuous enrichment relative to chondrite and a LREE enriched pattern. The MREE do not show any depletion as kaersutite and clinopyroxene are not important fractionating phases. Strong Eu anomalies are seen as feldspar fractionation is very important in this sequence.

4.5.3 Xenoliths

On chondrite normalized plots (Fig. 4.11), essexites and anorthosites have positive Eu anomalies while the sodalite syenites have a negative anomaly. For the essexites, La ranges from 94 to 206 times chondrite, and Lu from 6 to 13 times chondrite. Anorthosites have a La range from 226 to 346 times chondrite, while Lu goes from 12 to 16 times chondrite. The sodalite syenites display La ranges from 365 to 378 times chondrite, and Lu varies from 17 to 20 times chondrite. Eu anomalies vary from 1.49 in the essexites to 0.70 in the sodalite syenites.

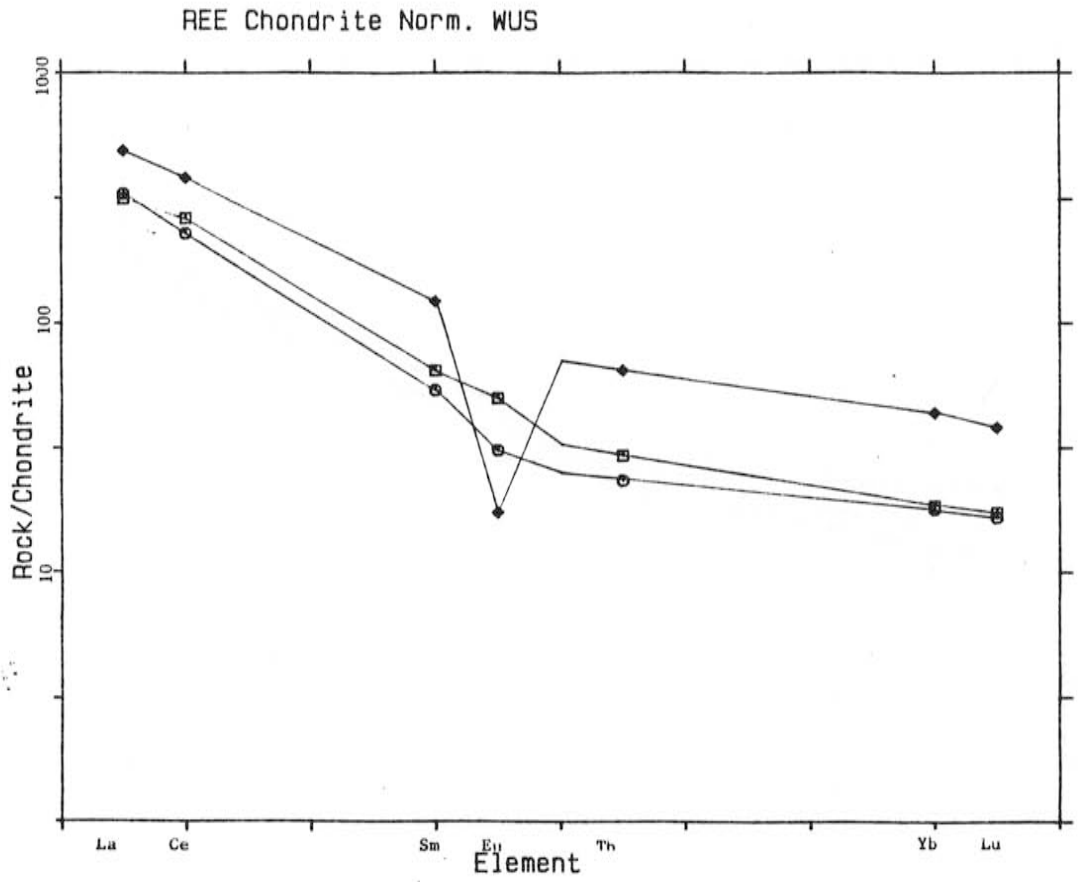

FIGURE 4.9 Chondrite normalized REE diagrams for each rock type in the SUS. Values are averages of all samples of each rock type.

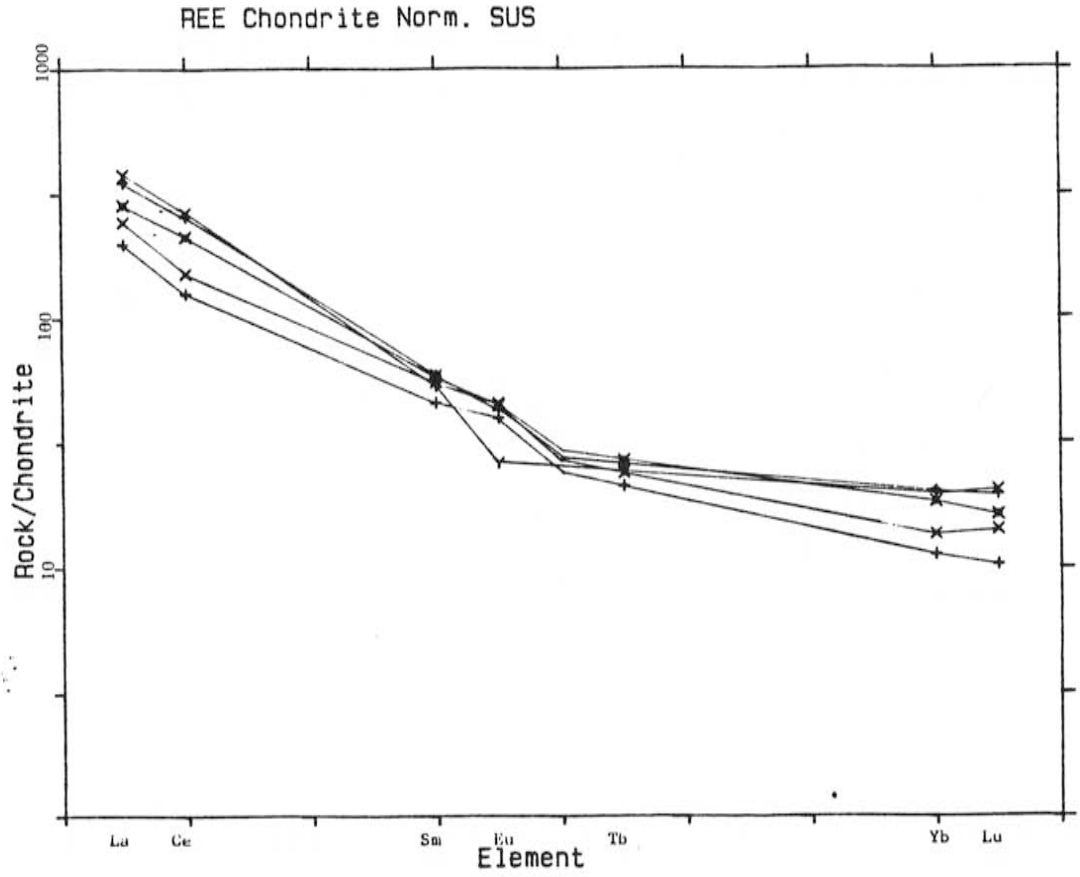

FIGURE 4.10 Chondrite normalized REE diagrams for each rock type of the WUS. Values are averages for all samples of each rock type.

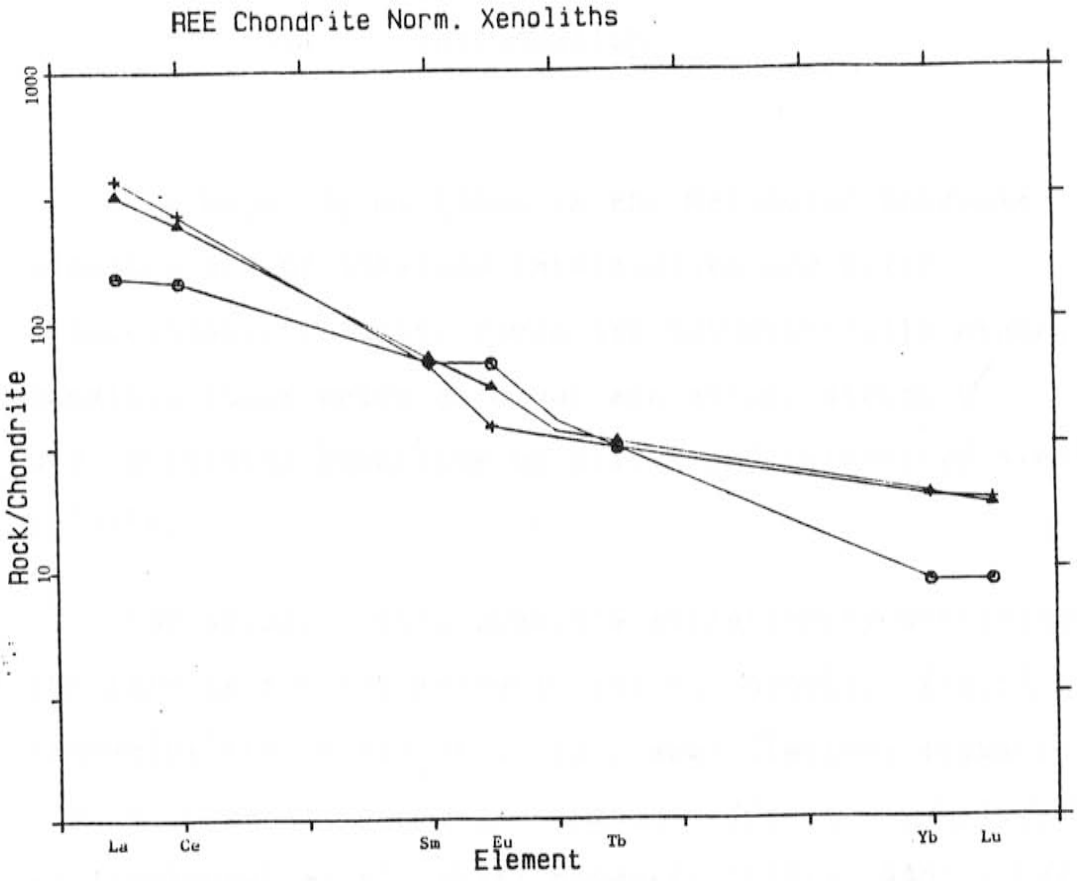

⊙ - Essexite

▲ - Anorthosite

\+ - Sodalite Syenite

FIGURE 4.11 Chondrite normalized REE diagrams for xenoliths. Values are averages of all samples of each type.

5 PETROGENESIS

5.1 Introduction

The majority of lavas in the Melbourne volcanic province are of alkaline intermediate and salic compositions, basaltic rocks are volumetrically minor. The basaltic rocks which do occur are either strongly undersaturated basanites or mildly undersaturated alkali basalts.

For alkali rocks, possible evolutionary mechanisms are the same as for all magmatic suites, namely; liquid immiscibility, differentiation, assimilation, magmatic mixing, crustal and mantle anatexis (Sorensen, 1974, ch 6; Carmichael et al, 1974; Stewart, 1979). Additional mechanisms which are specifically applied to alkaline rocks are volatile enrichment, metasomatism, and resorption of silicate minerals (Sorensen, 1974, ch 6).

For the rocks of Mount Overlord, differentiation by fractional crystallization appears to be the most viable evolutionary mechanism. Major and trace element data

suggest two main suites consisting of a strongly undersaturated suite (SUS) with a probable basanite parent, and a weakly undersaturated to saturated suite (WUS) with an alkali basalt parent.

Other possible evolutionary mechanisms which may produce a similiar suite a rocks are magma mixing, crustal contamination and progressive partial melting. Magmatic mixing would produce a similiar sequence of rocks with variation diagrams showing linear patterns for elements between the end members. This is not the case with the Mount Overlord rocks. Although many elements have linear relationships, many, notably MgO, have curvilinear trends. Progressive partial melting is also not a plausible solution. As the degree of partial melting increased, the magma would lose its alkaline nature. In addition, melting of the crust will not produce a basalt and with no crustal component the more salicic rocks would not be produced. Crustal contamination may be ruled out by Sr isotopic evidence. Sr 87/86 values are similiar to (Walker and Jones, 1972) the mantle making any possible crustal component insignificant.

5.2 Parental Basaltic Magmas

Kay and Gast (1973) and Frey et al (1978) have combined major element and trace element data to develop models for the generation of alkali basalt and basanites. The overall consensus is 1% to 2% partial melting of a hydrous garnet peridotite source at the top of the asthenosphere with CO2 as a probable important fluid phase (Wyllie, 1979). Trace element data suggests that this is a plausible model if the source is a garnet lherzolite with REE 2-5x chondritic levels (Frey et al, 1978)

The basalts generated by this process will be nepheline normative with Mg numbers ranging from 68 to 72. Trace elements will be characterized by high values for Ni, Cr, and other highly compatible elements, and an overall enrichment of REE with a LREE enriched pattern.

The basaltic rocks found at Mount Overlord are basanites and alkali basalts with Mg numbers between 60 and 64. They closely resemble those found at The Pleiades, 40 km to the northeast (Kyle 1976). The lower Mg number indicates that they do not represent the initial primary melt formed in the mantle, but have evolved somewhat. The presence of xenoliths of possible upper mantle origin suggests the initial stage of evolution occurred in the mantle followed by rapid ascent to the surface.

5.3 Evolution of the Differentiated Sequences

Rocks of the SUS show a well defined linear or curvilinear trend on many variation diagrams, which suggests evoluton by a single process.

The WUS parallels the SUS to the mugearites. After this, on many variation diagrams, a distinctive split occurs with the WUS spraying out. The scatter of points makes it difficult to specifically define one mechanism or path of evolution.

The comendites generally form a separate group, not falling along any specific trend. The evolution of these peralkaline rocks is difficult to define and possible explanations will be discussed later.

Coombs (1963) and Coombs and Wikinson (1969) have shown that the fractional crystallization paths of alkaline basaltic magmas are dependent on the initial composition. Mildly alkaline magmas, with little normative nepheline or hypersthene, differentiate close to the critical plane of silica undersaturation (Yoder and Tilley, 1962) and produce a trachytic magma. Further fractionation of the trachytic melt may yield a variety of alkaline and peralkaline rhyolitic magmas. Basanites follow a more strongly undersaturated crystallization path and produce a phonolitic

magma. Wilkinson (1966) has shown that in the Tertiary basic magmas of New South Wales, differentiation of an alkali basalt produced a trachyte while a basanite yielded a phonolite. Wright (1963) and Saggerson and Williams (1964) have presumed two different fractionation paths for volcanics in southern Kenya and northern Tanzania. The one of significance to this study is the alkali basalt-trachyte-comendite sequence. Coombs and Wilkinson (1969) and Schwarzer and Rogers (1974) have shown that there is a continuous spectrum of lineages from basic to salic liquids. They distinguish a number of general series. The two found in the Mount Overlord rocks correspond to the WUS, alkali basalt- hawaiite- mugearite- benmoreite- trachyte- qtz trachyte- comendite and the SUS, basanite- ne-hawaiite- ne-mugearite- ne-benmoreite- phonolite series (Fig. 5.1).

The peralkaline trend, represented by the comendites, may be the result of a variety of processes. The dominant process for the production of a peralkaline residue from a trachytic fluid is by feldspar fractionation (Macdonald, 1974) resulting in the 'plagioclase effect' (Bowen, 1945). Bailey (1974) suggests that this is only a partial solution.

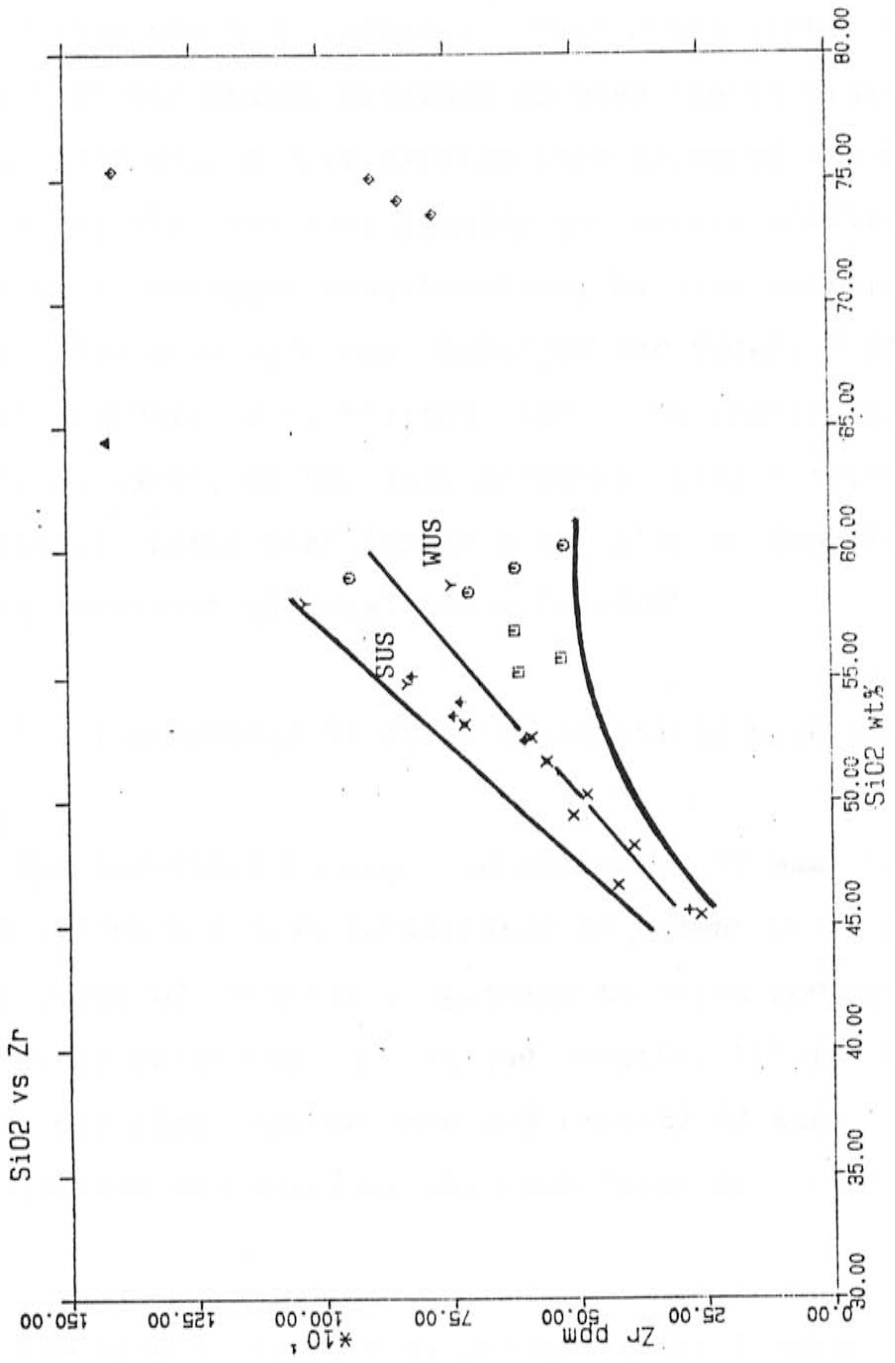

FIGURE 5.1 Variation diagram showing the trends of the SUS and WUS.

The plagioclase effect produces feldspars which are more calcic than the norm suggests. Carmichael (1964) found rocks from the Erebus province to have anorthoclase phenocrysts with higher calcium than expected and the rocks groundmass (the residual liquid) to contain acmite. In addition to feldspar fractionation, biotite (Carmichael, 1967), aluminous pyroxene (Schairer and Yoder, 1960), spinel, garnet, or Al-bearing iron oxide (Bailey and Schairer, 1966), or non-stoichiometric alkali feldspar (Luth and Tuttle, 1966) fractionation may play an important role in the formation of peralkaline liquids.

5.3.1 Modelling of the Differentiated Sequence

The modelling of magmatic processes by mass balance calculations has been facilitated in recent years with the development of computer programmes to solve complex least squares calculations (Wright and Doherty, 1970). Wright (1974) describes the methods and results of such calculations and outlines the procedures for their general use.

The Wright and Doherty procedure for fractional crystallization involves the summing of the compositions of the daughter liquid and the fractionated phases to produce the parent melt. The program calculates the percentage of each phase so as to reduce the difference between the

calculated and observed parent. The sum of the residuals squared is a measure of the accuracy of the model. A value less than 0.20 is considered a very good model, twice that is acceptable.

The compositions of the parent melt and the daughter liquid are the whole rock analyses for the respective rocks. The compositions for the fractionating mineral phases (Table 5.1) were taken mainly from microprobe data of phenocrysts from similiar rocks at The Pleiades (Kyle 1974). The remaining data is from analyses in Deer, Howie, and Zussman (1963).

Differentiating magmas may also be modelled using trace element abundances. In this case, trace elements are used as a check on the mass balance computer models. Assuming the simplest case, a closed system, crystal fractionation may be modelled using the Rayleigh fractionation equation $Cl/Co = FD-1$ (Cox et al, 1980). Co is the initial concentration of an element, Cl, the residual concentration, F, the fraction of liquid remaining, and D, the bulk distribution coefficient of the fractionated phases. D is calculated by summing the products of the mineral/melt partition coefficient of each fractionated phase and the percentage of fractionating material that each phase represents. Mineral/melt partition coefficients (Table 5.2) were taken from Kyle (1981).

Element	Mineral Phases				
	Ol 1	Ol 2	Cpx 1	Cpx 2	Cpx 3
SiO2	39.10	37.30	44.80	48.60	48.90
TiO2	0.03	-	2.97	1.81	1.33
Al2O3	0.04	-	10.10	2.48	3.85
FeO	19.40	29.60	8.73	8.76	12.10
MnO	0.27	0.57	0.15	0.21	0.41
MgO	40.50	33.10	10.70	14.30	11.70
CaO	0.27	0.25	0.91	0.00	19.60
Na2O	-	-	-	-	0.75
K2O	-	-	-	-	-
P2O5	-	-	-	-	-
Total	99.61	100.82	98.96	98.26	98.64
	Cpx 4	Cpx 5	Aegr*	Kaer 1	Kaer 2
SiO2	47.10	47.50	51.82	39.60	41.00
TiO2	1.99	0.63	0.77	6.34	4.77
Al2O3	7.70	0.25	1.85	13.30	9.95
FeO	10.05	26.70	29.06	12.10	12.27
MnO	0.13	1.59	-	0.19	0.19
MgO	14.80	1.48	-	11.60	12.80
CaO	19.20	19.80	-	11.60	11.60
Na2O	0.72	1.20	12.68	2.75	2.95
K2O	0.32	-	0.19	0.96	1.56
P2O5	-	-	-	-	-
Total	102.01	99.15	96.65	98.44	98.88
	Kaer 3	Plag 1*	Plag 2	Plag 3	Plag 4
SiO2	40.80	49.06	55.10	56.30	56.10
TiO2	6.43	-	-	-	-
Al2O3	12.55	32.14	26.70	26.30	26.40
FeO	12.30	0.24	0.40	0.55	0.70
MnO	0.19	-	-	-	-
MgO	12.80	0.20	-	-	-
CaO	11.60	15.38	10.90	10.50	9.70
Na2O	2.95	2.57	5.36	5.61	6.01
K2O	1.56	0.17	0.42	0.37	0.34
P2O5	-	-	-	-	-
Total	101.18	99.76	98.88	99.63	99.25

TABLE 5.1 Analyses of mineral phases used in the mass balance models. All analyses from Kyle (1976) except where noted. *Deer, Howie, and Zussman (1963)

Element	Mineral Phases				
	Plag 5	Anor 1*	Anor 2	Kspr*	
SiO2	56.60	64.30	65.20	65.58	
TiO2	-	0.08	-	-	
Al2O3	26.20	20.85	19.80	19.58	
FeO	-	0.34	0.16	0.19	
MnO	-	-	-	-	
MgO	-	0.07	-	0.12	
CaO	8.65	2.00	1.23	0.49	
Na2O	6.66	7.26	7.19	5.90	
K2O	0.44	4.77	5.41	7.88	
P2O5	-	-	-	-	
Total	98.86	99.67	98.99	99.74	
	Magn 1	Magn 2	Magn 3	Magn 4	Magn 5
SiO2	-	0.08	0.10	0.07	0.11
TiO2	15.00	16.70	19.40	22.40	18.70
Al2O3	0.06	1.59	2.88	2.15	6.33
FeO	76.20	72.60	71.70	70.50	65.30
MnO	0.52	1.80	0.69	1.91	0.36
MgO	1.37	0.54	1.90	0.97	6.24
CaO	-	-	-	-	-
Na2O	-	-	-	-	-
K2O	-	-	-	-	-
P2O5	-	-	-	-	-
Total	93.15	93.31	96.67	98.00	97.04
	Ilmn 1	Ilmn 2	Ilmn 3	Ilmn 4	
SiO2	-	0.05	-	0.05	
TIO2	51.70	51.70	51.50	49.40	
Al2O3	0.06	0.06	0.07	0.21	
FeO	43.74	43.80	43.90	45.50	
MnO	0.64	0.64	1.78	1.66	
MgO	3.40	3.40	3.37	2.36	
CaO	-	-	0.05	-	
Na2O	-	-	-	-	
K2O	-	-	-	-	
P2O5	-	-	-	-	
Total	99.54	99.65	100.67	99.18	

TABLE 5.1 (cont.)

Element	Mineral Phases		
	Apat 1	Apat 2	Apat 3
SiO2	0.20	0.24	0.20
TiO2	0.27	-	0.27
Al2O3	0.03	0.03	0.03
FeO	1.72	0.11	1.71
MnO	-	-	0.06
MgO	0.06	0.05	0.18
CaO	52.10	52.40	50.80
Na2O	0.16	0.09	0.15
K2O	-	-	-
P2O5	43.45	43.80	44.00
Total	97.99	96.72	97.40

TABLE 5.1 (cont.)

	Oliv.	Clinopyroxene		Kaer.	Apat.
La	(0.009)*	0.02	0.10	0.31	15.2
Ce	0.009	0.04	0.18	0.49	16.6
Sm	0.011	0.14	0.56	1.07	20.7
Eu	0.010	0.16	0.58	1.09	14.5
Tb	(0.013)	0.19	(0.73)	(1.12)	(19.8)
Yb	0.023	0.20	0.61	0.78	9.4
Sr	0.009	0.119	1.51	0.58	0.83
Ba	0.009	0.031	0.321	0.62	0.014

	Plagioclase		Anor.	Sanidine
	An 65	An 40		
La	(0.023)	(0.028)	0.219	(0.225)
Ce	0.023	0.215	0.173	0.223
Sm	0.024	0.135	0.139	0.221
Eu	0.232	1.10	1.72	2.35
Tb	(0.018)	(0.111)	(0.130)	(0.220)
Yb	0.030	0.062	0.116	0.227
Sr	1.36	4.62	5.57	3.08
Ba	0.15	1.47	5.04	3.20

TABLE 5.2 Mineral/melt partition coefficients (after Kyle, 1981).* Values in brackets determined by interpolaton and extrapolation

Data is sparse for partition coefficients for alkaline rocks and may have considerable variations due to composition, pressure, and temperature of formation. Kaersutite and clinopyroxene have large partition coefficients for the middle and heavy REE, plagioclase and anorthoclase have high values for Eu, Sr, and Ba, while apatite has extremely high values, all well above unity, for all of the REE (Table 5.2)

Apatite is very important in the trace element calculations. Apatite is the only mineral phase found in the Mount Overlord rocks which contains phosphorous, thus a deficit or excess of phosphorous may be easily corrected by changing the amount of apatite in the mass balance model. This does little to change the overall outcome of the mass balance model, but it does have a significant impact on the trace element calculation.

Even though apatite is only a minor constituent of the phases fractionated, it is the chief contributor to the bulk distribution coefficient for many elements. When the amount of apatite is adjusted to give agreement between the observed and calculated values of phosphorous in the mass balance model, there is a considerable change in D. In most cases, the correcting of phosphorous will improve the results of the trace element calculations, therefore, adjusted apatite contents have been used when calculating

the trace element compostions.

In comparing the calculated and observed data, coefficients of variation will determine the range of acceptable and marginal values. Good agreement will be considered to be within 10% of the observed value for the REE and 5% for the remaining trace elements. Marginal results will be within 25% and 15% respectively. If the calculated value is not within these limits, the are considered poor. For the model to be acceptable, over half of the trace elements should be in good agreement.

5.3.2 SUS

The phonolite trend of the SUS has been modelled using five separate steps, basanite to ne-hawaiite, ne-hawaiite to ne-mugearite, ne-mugearite to ne-benmoreite, ne-benmoreite to phonolite, and phonolite to phonolite (Fig. 5.2). Fractional crystallization models have been calculated for each of the steps and are described individually along with supporting trace element calculations.

5.3.2a Basanite to ne-hawaiite

Two models for the basanite to ne-hawaiite step have acceptable solutions for major elements. One model contains kaersutite and the other ilmenite in addition to various

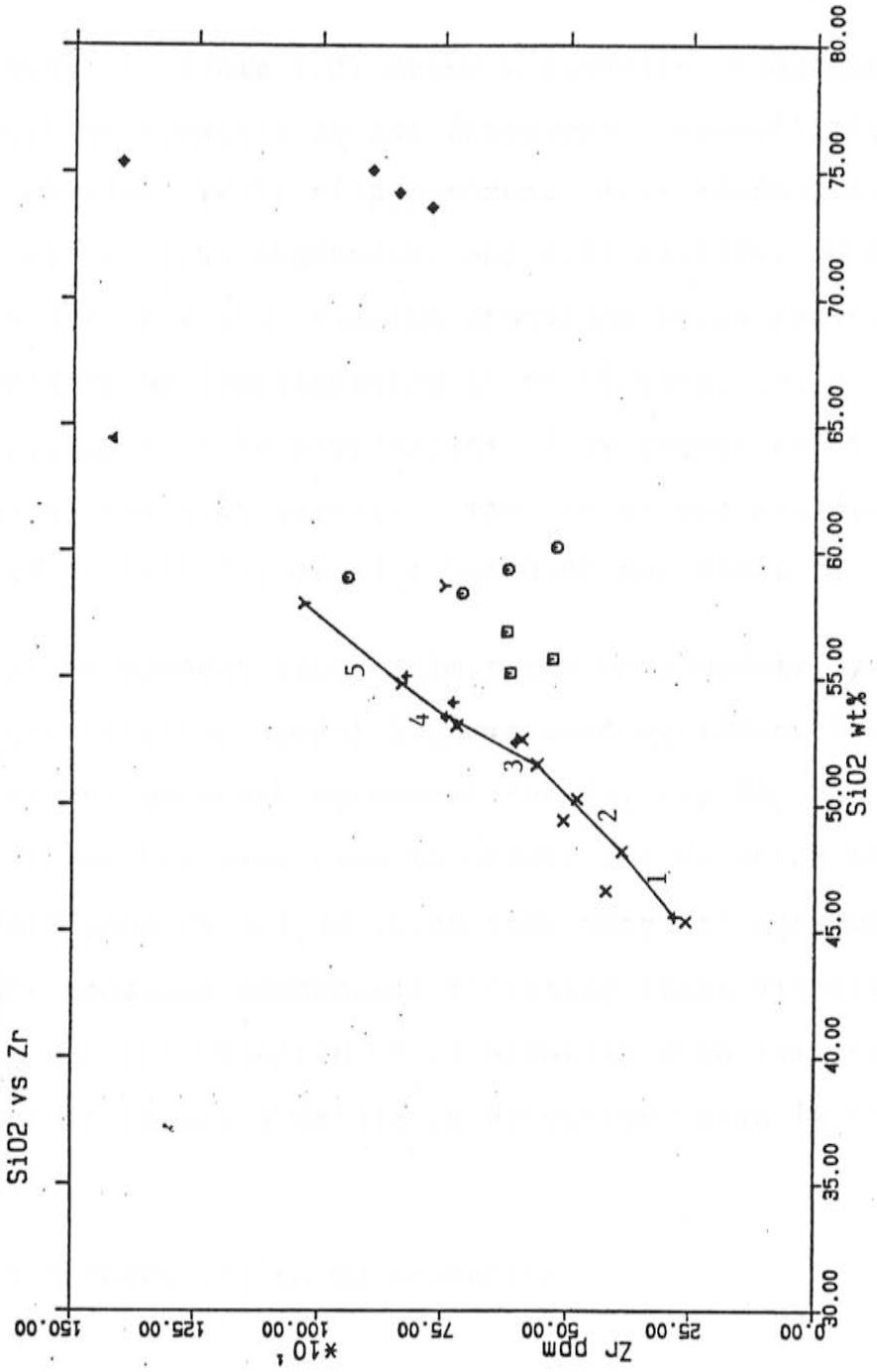

FIGURE 5.2 Variation diagram showing steps used in modelling the SUS; 1) basanite - hawaiite, 2) hawaiite - ne-mugearite, 3) ne-mugearite - ne-benmoreite, 4) ne-benmoreite - phonolite 1, 5) phonolite 1 - phonolite 2.

other phases.

Model 1 (Table 5.3) shows a basanite producing 58.6% residual ne-hawaiite by the fractional crystallization of 10.0% olivine, 16.9% clinopyroxene, 3.1% kaersutite, 8.4% plagioclase, 2.5% magnetite, and 0.5% apatite. Model 2 (Table 5.4) has the basanite producing 59.2% residual ne-hawaiite by fractionating 10.6% olivine, 17.7% clinopyroxene, 9.1% plagioclase, 2.3% magnetite, 0.5% ilmenite, and 0.6% apatite. The sum of the residuals squared is 0.11 for model 1 and 0.08 for model 2.

Trace element calculations for both models produce similiar results. Model 1 shows good agreement for Rb, Tb, and Yb, and marginal agreement for La, Ce, Sm, and Eu. Model 2 has the same results except for Eu which has good agreement,and Tb and Yb which show marginal agreement. With all the possible mechanisms affecting trace elements, the models for the basanite to ne-hawaiite step seem reasonable, however it is not possible to determine which is the most probable.

5.3.2b Ne-hawaiite to ne-mugearite

The model for the ne-hawaiite to ne-mugearite step (Table 5.5) is excellent with little difference between the calculated and observed ne-hawaiite parent, the sum of the residuals squared is 0.0007. Differentiation of the

Basanite to Hawaiite Model 1

Element	Basanite			Hawaiite +	Mineral phases	
	calc.	obs.	diff.			
SiO2	46.06	46.20	0.14	49.64	Ol 1	10.05%
TiO2	2.47	2.56	0.09	2.34	Cpx 1	16.88%
Al2O3	15.45	15.46	0.01	18.08	Kaer 1	3.06%
FeO	11.62	11.63	0.01	9.83	Plag 1	8.38%
MnO	0.20	0.20	0.00	0.21	Magn 1	2.46%
MgO	8.47	8.45	0.02	3.66	Apat 2	0.71%
CaO	9.83	9.78	0.05	7.42	*	0.52%
Na2O	3.68	3.42	0.26	5.50		
K2O	1.46	1.44	0.02	2.42		
P2O5	0.77	0.85	0.08	0.91		

residuals squared = 0.11 solution= 58.65%

Trace Element Calculations

	Co (ppm)	Cl (ppm)	
		calc.	obs.
La	63	91	78
Ce	125	172	152
Sm	8.8	11.6	10.2
Eu	2.8	3.8	3.2
Tb	1.0	1.3	1.2
Yb	2.3	3.3	2.8
Rb	40	68	68
Sr	887	1235	998
Ba	524	852	620
Zr	284	484	409
Y	29	49	32

TABLE 5.3 Model 1 basanite to ne-hawaiite and trace element calculations.
*Apatite not corrected for P difference.

Basanite to Hawaiite Model 2

Element	Basanite			Hawaiite +	Mineral	Phases
	calc.	obs.	diff.			
SiO2	46.04	46.20	0.16	49.64	Ol 1	10.64%
TiO2	2.55	2.56	0.01	2.34	Cpx 1	17.71%
Al2O3	15.45	15.46	0.01	18.08	Plag 1	9.11%
FeO	11.60	11.63	0.03	9.83	Magn 1	2.34%
MnO	0.20	0.20	0.00	0.21	Ilmn 1	0.50%
MgO	8.47	8.45	0.02	3.66	Apat 2	0.70%
CaO	9.81	9.78	0.03	7.42	*	0.55%
Na2O	3.65	3.42	0.23	5.50		
K2O	1.45	1.44	0.01	2.42		
P2O5	0.78	0.85	0.07	0.91		

residuals squared = 0.08 solution= 59.16%

Trace Element Calculatonsn

	Co (ppm)	Cl (ppm)	
		calc.	obs.
La	63	93	78
Ce	125	182	152
Sm	8.8	12.2	10.2
Eu	2.8	3.4	3.2
Tb	1.0	1.4	1.2
Yb	2.3	3.4	2.8
Rb	40	68	68
Sr	887	1235	998
Ba	524	863	620
Zr	284	480	409
Y	29	43	32

TABLE 5.4 Model 2 basanite to ne-hawaiite and trace element calculations.
*Apatite not corrected for P difference.

Hawaiite to ne-Mugearite

Element	Hawaiite			ne-Mugearite +	Mineral Phases	
	calc.	obs.	diff.			
SiO2	49.65	49.64	0.01	52.51	Ol 1	1.11%
TiO2	2.34	2.34	0.00	1.88	Cpx 1	4.00%
Al2O3	18.09	18.08	0.01	18.17	Kaer 1	1.93%
FeO	9.83	9.83	0.00	8.39	Plag 1	7.98%
MnO	0.19	0.21	0.02	0.20	Magn 1	2.57%
MgO	3.66	3.66	0.00	3.05	Ilmn 1	0.31%
CaO	7.42	7.42	0.00	5.79	Apat 2	0.78%
Na2O	5.50	5.50	0.00	6.40		
K2O	2.41	2.42	0.01	2.93		
P2O5	0.91	0.91	0.00	0.68		

residuals squared = 0.0007 solution= 81.33%

Trace Element Calculations

	Co (ppm)	Cl (ppm)	
		calc.	obs.
La	78	83	90
Ce	152	160	171
Sm	10.2	10.2	11.4
Eu	3.2	3.3	3.3
Tb	1.2	1.2	1.3
Yb	2.8	3.1	3.8
Rb	68	83	82
Sr	998	1061	943
Ba	620	740	723
Zr	409	503	559
Y	32	39	39

TABLE 5.5 Model of ne-hawaiite to ne-mugearite and trace element calculations.

ne-hawaiite can result in the production of 81.33% residual ne-mugearite with 1.1% olivine, 4.0% clinopyroxene, 1.9% kaersutite, 8.0% plagioclase, 2.6% magnetite, 0.3% ilmenite, and 0.8% apatite as the fractionating phases.

Calculated trace element concentrations show good agreement for Rb, Ba, Y, La, Ce, Eu, and Tb. Marginal agreement is also seen for Sr, Zr, Sm, and Yb.

5.3.2c Ne-mugearite to ne-benmoreite

The ne-mugearite to ne-benmoreite step (Table 5.6) produces 85.6% residual ne-benmoreite while fractionating 1.0% clinopyroxene, 9.2% kaersutite, 3.1% plagioclase, 0.7% magnetite, 0.2% ilmenite, and 0.2% apatite from the ne-mugearite parent. Results of the model are good except for potassium and phosphorous which have diffferences of 8.6% and -10.9% respectively, the sum of the residuals squared is 0.09. One important aspect of this model is the relatively large amount of kaersutite fractionated. Kaersutite makes up 64.16% of the fractionating mineral phases.

Trace element calculations for this model are good for Sm, Eu, Tb, Yb, and Y. The remaining elements have marginal correlations. This may be due to inaccurate partition coefficients for these elements in kaersutite. Since kaersutite is the chief fractionating phase, it would be

ne-Mugearite to ne-Benmoreite

Element	ne-Mugearite			ne-Benmoreite	+ Mineral Phases	
	calc.	obs.	diff.			
SiO2	52.40	52.51	0.11	54.08	Cpx 2	0.96%
TiO2	1.88	1.88	0.00	1.36	Kaer 2	9.22%
Al2O3	18.17	18.17	0.00	19.08	Plag 2	3.10%
FeO	8.38	8.39	0.01	7.61	Magn 3	0.68%
MnO	0.21	0.20	0.01	0.21	Ilmn 1	0.20%
MgO	3.02	3.05	0.03	1.92	Apat 3	0.36%
CaO	5.84	5.79	0.05	4.76	*	0.21%
Na2O	6.31	6.40	0.09	6.84		
K2O	3.18	2.93	0.25	3.53		
P2O5	0.61	0.68	0.07	0.60		

residuals squared = 0.09 solution= 85.63%

Trace Element Calculations

	Co (ppm)	Cl (ppm)	
		calc.	obs.
La	90	97	118
Ce	171	180	217
Sm	11.4	11.2	11.4
Eu	3.2	3.1	3.2
Tb	1.3	1.3	1.3
Yb	4.2	4.4	4.2
Rb	82	96	108
Sr	943	875	978
Ba	723	753	856
Zr	559	652	740
Y	38	44	45

TABLE 5.6 Model of ne-mugearite to ne-benmoreite and trace element calculations.
*Apatite not corrected for P difference.

expected that the middle REE would show good agreement. Also, Sun and Hanson (1976) suggest that the partition coefficients for kaersutite are strongly dependent on temperature and/or composition.

5.3.2d Ne-benmoreite to Phonolite

Two models were made for the ne-benmoreite to phonolite step. Model 1 involves a lower silica phonolite than in model 2, but both produce similiar relative amounts of fractionating minerals.

Model 1 (Table 5.7) produces 85.5% residual phonolite as a result of fractionating 2.3% clinopyroxene, 2.7% kaersutite, 7.5% plagioclase, 1.8% magnetite, abd 0.2% apatite from a ne-benmoreite. The only significant problem is a deficit (-20.5%) of phosphorous. The sum of the residuals squared is 0.20.

Trace element calculations show good agreement for all REE, Rb, Sr, and Zr, while Ba and Y have marginal agreement. Y, which shows marginal agreement, may actually have a partion coefficient similiar to the HREE which would result in a D value of approximately 0.4. This would bring the calculated value in good agreement with the observed.

Ne-Benmoreite to Phonolite 1

Element	Ne-Benmoreite			Phonolite	+ Mineral	Phases
	calc.	obs.	diff.			
SiO2	53.95	54.08	0.13	55.54	Cpx 3	2.34%
TiO2	1.42	1.36	0.06	1.02	Kaer 3	2.66%
Al2O3	19.01	19.08	0.07	19.29	Plag 3	7.47%
FeO	7.59	7.61	0.02	6.72	Magn 5	1.76%
MnO	0.20	0.21	0.01	0.21	Apat 1	0.54%
MgO	1.89	1.92	0.03	1.36	*	0.25%
CaO	4.85	4.76	0.09	3.70		
Na2O	7.21	6.84	0.37	7.83		
K2O	3.41	3.53	0.12	3.90		
P2O5	0.47	0.60	0.13	0.43		

residuals squared = 0.20 solution= 85.53%

Trace Element Calculations

	Co (ppm)	Cl (ppm)	
		calc.	obs.
La	118	122	119
Ce	217	222	217
Sm	11.5	11.3	11.4
Eu	3.2	3.0	2.8
Tb	1.3	1.3	1.3
Yb	4.2	4.4	4.4
Rb	108	126	126
Sr	978	744	750
Ba	856	866	776
Zr	740	865	832
Y	45	53	46

TABLE 5.7 Model 1 ne-benmoreite to phonolite and trace element calculations.
*Apatite not corrected for P difference.

Model 2 (Table 5.8) produces 64.5% phonolite residue with 6.1% clinopyroxene, 6.2% kaersutite, 17.7% plagioclase, 4.5% magnetite, and 0.9% apatite. Again, a phosphorous deficit (-26.7%) is the only major problem with this model.

Trace element calculations are initially very poor. After taking into account the phosphorous deficit and recalculating, values for La, Ce, Sm, and Tb show good agreement, Rb and Zr marginal agreement, and the remaining trace elements are poor.

Based on the trace element calculations, Model 1 is the most likely solution and will be the only one presented.

5.3.2e Phonolite 1 to phonolite 2

Modelling of this step (Table 5.9) using the two phonolites in the previous section produces a 75.2% residue of the higher silica phonolite, after fractionating 4.5% clinopyroxene, 4.0% kaersutite, 12.3% plagioclase, 3.2% magnetite, 0.1% ilmenite, and 0.8% apatite. Phosphorous again has a deficit (-14.1%) while potassium shows a surplus (10.9%), The sum of the residuals squared is 0.13.

Ne-Benmoreite to Phonolite 2

Element	Ne-Benmoreite			Phonolite +	Mineral Phases	
	calc.	obs.	diff.			
SiO2	53.93	54.08	0.15	59.48	Cpx 3	6.06%
TiO2	1.40	1.36	0.04	0.08	Kaer 3	6.24%
Al2O3	19.06	19.08	0.02	20.26	Plag 3	17.72%
FeO	7.59	7.61	0.02	4.56	Magn 5	4.51%
MnO	0.19	0.21	0.02	0.22	Apat 1	1.29%
MgO	1.85	1.92	0.07	0.07	*	0.93%
CaO	4.88	4.76	0.12	0.93		
Na2O	6.87	6.84	0.03	8.74		
K2O	3.78	3.53	0.25	5.61		
P2O5	0.44	0.60	0.16	0.04		

residuals squared = 0.13 solution= 64.54%

Trace Element Calculations

	Co (ppm)	Cl (ppm)	
		calc.	obs.
La	118	131	134
Ce	217	235	234
Sm	11.5	11.0	10.0
Eu	3.2	2.7	1.0
Tb	1.3	1.2	1.2
Yb	4.2	5.0	3.7
Rb	108	168	198
Sr	978	467	11.5
Ba	856	894	628
Zr	740	1146	1030
Y	45	70	47

TABLE 5.8 Model 2 ne-benmoreite to phonolite and trace element calculations.
*Apatite not corrected for P difference.

Phonolite 1 to Phonolite 2

Element	Phonolite 1			Phonolite 2 + Mineral Phases		
	calc.	obs.	diff.			
SiO2	55.52	55.54	0.02	59.48	Cpx 3	4.51%
TiO2	1.03	1.02	0.01	0.08	Kaer 3	3.99%
Al2O3	19.36	19.29	0.07	20.27	Plag 3	12.27%
FeO	6.72	6.72	0.00	4.56	Magn 5	3.17%
MnO	0.20	0.21	0.01	0.22	Ilmn 4	0.08%
MgO	1.30	1.36	0.06	0.07	Apat 1	0.90%
CaO	3.75	3.70	0.05	0.93	*	0.76%
Na2O	7.42	7.83	0.41	8.74		
K2O	4.33	3.90	0.43	5.61		
P2O5	0.37	0.43	0.06	0.04		

residuals squared = 0.36 solution= 75.22%

Trace Element Calculations

	Co (ppm)	Cl (ppm)	
		calc.	obs.
La	119	130	134
Ce	217	232	234
Sm	11.4	11.4	10.0
Eu	2.8	2.6	1.0
Tb	1.3	1.3	1.2
Yb	4.4	5.0	3.7
Rb	126	168	198
Sr	750	465	11.5
Ba	776	800	628
Zr	832	1106	1030
Y	46	61	47

TABLE 5.9 Model of phonolite 1 to phonolite 2 and trace element calculations.
*Apatite not corrected for P difference.

Trace element calculations give poor results similiar to Model 2 for the ne-benmoreite to phonolite step. This suggests that the further fractionation of the phonolite melt is more complex than the model suggests.

5.3.3 WUS

The WUS parallels the SUS from the basaltic end through mugearites. After this, the WUS shows a broad spread and many trends can be defined on major and trace element plots, especially the alkali elements and alumina. Attempts to model the steps mugearite to benmoreite, benmoreite to trachyte, trachyte to qtz-trachyte, and qtz-trachyte to comendite (Fig. 5.3) produced marginal results.

5.3.3a Mugearite to benmoreite

The mugearite to benmoreite step (Table 5.10) produces 64.0% residual benmoreite while fractionating 5.2% olivine, 0.8% clinopyroxene, 25.8% plagioclase, 1.9% magnetite, 1.1% ilmenite, and 1.2% apatite. Results of the model are not good, but with the sum of the residuals squared equal to 0.36 it is certainly acceptable. The important aspects of this model are the large amount of plagioclase, 71.6% of the fractionating phases, and the absence of kaersutite.

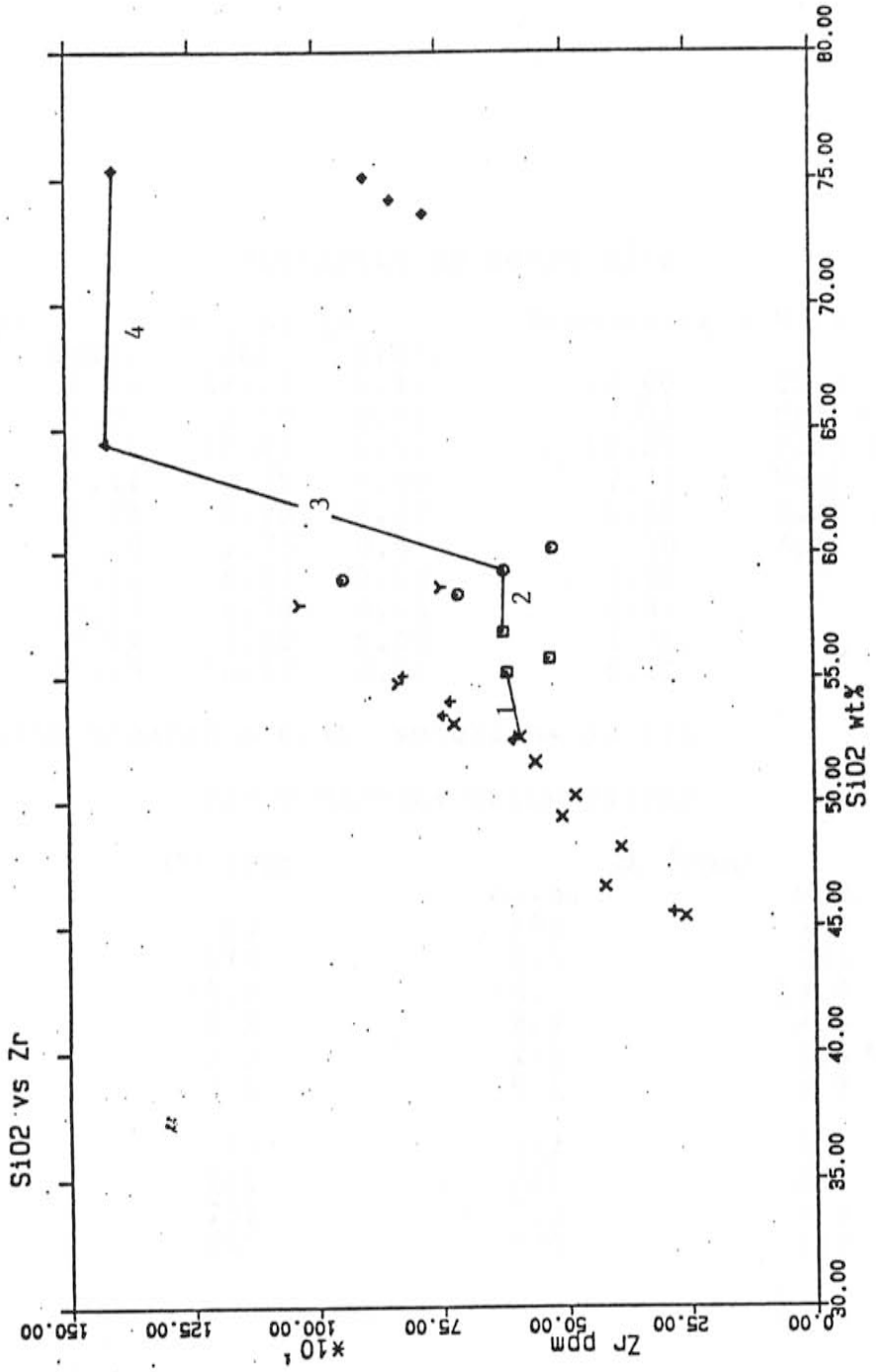

FIGURE 5.3 Variation diagram showing the steps modelled for the WUS; 1) mugearite - benmoreite, 2) benmoreite - trachyte, 3) trachyte - quartz trachyte, 4) quartz trachyte - comendite.

Mugearite to Benmoreite

Element	Mugearite			Benmoreite +	Mineral Phases	
	Calc.	obs.	diff.			
SiO2	53.41	53.04	0.37	56.80	Ol 2	5.22%
TiO2	1.81	1.80	0.01	1.21	Cpx 2	0.76%
Al2O3	18.58	18.47	0.11	18.27	Plag 5	25.79%
FeO	8.34	8.29	0.05	7.47	Magn 4	1.89%
MnO	0.22	0.20	0.02	0.23	Ilmn 2	1.13%
MgO	2.70	2.75	0.05	1.28	Apat 1	0.99%
CaO	5.31	5.37	0.06	3.46	*	1.24%
Na2O	5.94	6.39	0.45	6.55		
K2O	2.92	3.00	0.08	4.38		
P2O5	0.78	0.67	0.11	0.36		

residuals squared = 0.36 solution= 63.97%

Trace Element Calculations

	Co (ppm)	Cl (ppm)	
		calc.	obs.
La	92	108	110
Ce	174	206	214
Sm	11.2	12.9	14.4
Eu	3.2	2.9	4.6
Tb	1.3	1.5	1.6
Yb	3.8	5.1	4.2
Rb	73	114	107
Sr	948	329	661
Ba	731	712	1476
Zr	589	920	613

TABLE 5.10 Model of mugearite to benmoreite and trace element calculations. *Apatite not corrected for P difference.

Trace element calculations, after recalculating for phosphorous, are good for La, Ce, Tb, and Rb and marginal for Sm and Yb. This confirms the fractional crystallization model, but suggests that additional factors may be involved in the evolution.

5.3.3b Benmoreite to trachyte

The benmoreite to trachyte step (Table 5.11) produces very poor results. Fractionation of the benmoreite gives 85.2% residual trachyte with 1.6% clinopyroxene, 12.0% plagioclase, and 1.3% magnetite. The sum of the residuals squared is 1.26 as a result of large differences in SiO2, MgO, Na2O, and P2O5.

Trace element calculations do show good results for La, Ce, Yb, and Rb and marginal results for Tb. The overall model is weak, but gives a good first approximation as to the major fractionating phases with plagioclase again being dominant.

5.3.3c Trachyte to qtz-trachyte

This step of the sequence gives a good solution (Table 5. 12) with 12.5% residual qtz-trachyte, 6.3% clinopyroxene, 2.0% plagioclase, 73.1% anorthoclase, 5.6% magnetite, and 0.5% apatite. The sum of the residuals squared is 0.11 with significant differences only in minor

Benmoreite to Trachyte

Element	Benmoreite			Trachyte + Mineral Phases		
	calc.	obs.	diff.			
SiO2	58.31	57.46	0.85	59.64	Cpx 4	1.56%
TiO2	1.23	1.22	0.01	1.15	Plag 4	11.96%
Al2O3	18.74	18.72	0.02	18.09	Magn 2	1.26%
FeO	6.17	6.08	0.09	5.81		
MnO	0.16	0.15	0.01	0.16		
MgO	1.36	1.82	0.46	1.32		
CaO	4.17	3.98	0.19	3.18		
Na2O	6.14	6.65	0.51	6.34		
K2O	3.41	3.51	0.10	3.95		
P2O5	0.31	0.40	0.09	0.36		

residuals squared = 1.26 solution= 85.23%

Trace Element Calculations

	Co (ppm)	Cl (ppm)	
		calc.	obs.
La	110	124	128
Ce	214	242	231
Sm	14.4	16.3	13.2
Eu	4.6	4.6	2.1
Tb	1.6	1.8	1.5
Yb	4.2	4.8	5.0
Rb	107	126	140
Sr	661	416	649
Ba	1476	1680	545
Zr	613	719	618

TABLE 5.11 Model of benmoreite to trachyte and trace element calculations.

Trachyte to Qtz-Trachyte

Element	Trachyte			Qtz-Trachyte +	Mineral Phases	
	calc.	obs.	diff.			
SiO2	59.62	59.64	0.02	65.35	Cpx 3	6.27%
TiO2	1.29	1.15	0.14	0.62	Plag 4	2.03%
Al2O3	18.05	18.09	0.04	12.82	Anor 1	73.15%
FeO	5.79	5.81	0.02	8.07	Magn 5	5.55%
MnO	0.08	0.16	0.08	0.30	Apat 1	0.79%
MgO	1.17	1.32	0.15	0.16	*	0.50%
CaO	3.29	3.18	0.11	0.91		
Na2O	6.37	6.34	0.03	6.94		
K2O	4.11	3.95	0.16	4.79		
P2O5	0.23	0.36	0.13	0.05		

residuals squared = 0.11 solution= 12.50%

Trace Element Calculations

	Co (ppm)	Cl (ppm)	
		calc.	obs.
La	128	572	188
Ce	231	1076	381
Sm	13	59	27
Eu	2.1	0.6	3.2
Tb	1.5	5.9	3.6
Yb	5.0	26	10
Rb	140	1120	223
Sr	649	0.2	1.2
Ba	545	0.6	95
Zr	618	4944	1420

TABLE 5.12 Model of trachyte to qtz-trachyte and trace element calculations.
*Apatite not corrected for P difference.

elements. The trace element calculations however, show no correlation at all, thus precluding this as a possible solution.

5.3.3d Qtz-trachyte to comendite

This model (Table 5.13) also produces a good solution with the sum of the residuals squared less than 0.10. The fractionation of the qtz-trachyte produces 32.4% residual comendite, 32.7% total clinopyroxene, 19.4% anorthoclase, 46.7% sanidine, 0.7% ilmenite, and 0.1% apatite. The trace elements again show no agreement and the model is not acceptable.

5.4 Relationship of Xenoliths to the Evolutionary Trends

It is evident from the major element (Fig. 4.4) and trace element (Fig. 4.7) plots that the composition of the xenoliths closely resemble those of the volcanic rocks. Since the xenoliths fall on the major element trends, they may be used to support the idea that fractional crystallization is the chief mechanism of differentiation.

The essexites are more basic than the basanites but generally fall in line with the trends. The anorthosites resemble the hawaiites and mugearites in composition while the sodalite syenites compare closely with the trachytes.

Qtz-Trachyte to Comendite

Element	Qtz-Trachyte			Comendite +	Mineral Phases	
	calc.	obs.	diff.			
SiO2	65.54	65.35	0.19	75.18	Cpx 5	2.04%
TiO2	0.61	0.62	0.01	0.27	Aegr	20.05%
Al2O3	12.88	12.82	0.06	11.33	Anor 2	13.07%
FeO	8.11	8.07	0.04	3.54	Kspr	31.51%
MnO	0.07	0.30	0.23	0.08	Ilmn 3	0.69%
MgO	0.14	0.16	0.02	0.14	Apat 1	0.11%
CaO	0.91	0.91	0.00	0.40		
Na2O	6.91	6.94	0.03	4.31		
K2O	4.78	4.79	0.01	4.72		
P2O5	0.05	0.05	0.00	0.02		

residuals squared = 0.10 solution= 32.54%

Trace Element Calculations

	Co (ppm)	Cl (ppm)	
		calc.	obs.
La	188	462	213
Ce	381	915	418
Sm	27	57	30
Eu	3.2	1.6	1.0
Tb	3.6	7.1	3.8
Yb	10	21	10
Rb	223	685	295
Sr	1.2	0.1	0.1
Ba	95	16	123
Zr	1420	4364	1404

TABLE 5.13 Model of qtz-trachyte to comendite and trace element calculations.

If it is true that the xenoliths represent the products of crystal fractionation and settling, the mineral phases used in the computer models should be the same as those found, and the bulk chemistry should be grossly similiar. Calculations, involving the summation of major element compositions of each mineral in its respective percentage, were done on three models. However, it must be recognized that the xenoliths will not be truely representative because; a) the cumulate sample is an instant in time whereas the models are the summation of the whole process and, b) xenoliths contain intercumulus material.

The ne-hawaiite to ne-mugearite model produces a hypothetical cumulate (Table 5.14) which resembles an essexite (81473). The calculated cumulate however, has a surplus of Al2O3, CaO, and TiO2, and a deficit of MgO, Na2O, and P2O5. The surplus of Al2O3 and CaO may be a result of plagioclase not settling as fast as the other phases. The deficit of Na2O and surplus of CaO could be from slightly incorrect values of these elements in plagioclase, kaersutite, and clinopyroxene. The greater amounts of MgO and P2O5 in the real essexite may be from a high concentration of olivine and apatite in the sample . This could be a result of different settling rates and/or sample selection.

Element	Hypothetical Cumulate	Essexite 81473
SiO2	37.16	37.91
TiO2	4.34	3.92
AL2O3	17.72	13.66
FeO	16.14	16.47
MnO	0.15	0.23
MgO	6.26	7.91
CaO	14.55	13.48
Na2O	1.59	2.32
K2O	0.17	0.40
P2O5	1.90	2.89

TABLE 5.14 Comparison of observed and hypothetical cumulates for the ne-hawaiite to ne-mugearite model.

Both the ne-mugearite to ne-benmoreite (Table 5.15) and phonolite 1 to phonolite 2 (Table 5.16) models form a hypothetical cumulate, similiar to an essexite (81472), with slightly higher SiO2. The significant differences in these calculated cumulates are a deficit of Al2O3 and CaO, and a surplus of MgO and Na2O, opposite of the previous example. The differences in Al2O3, CaO, and Na2O may be explained by including a calcic intercumulus plagioclase.

The cumulate produced by the mugearite to benmoreite step of the WUS resembles an anorthosite (Table 5.17). The qtz-trachyte to comendite step produces a cumulate with a composition similiar to the sodalite syenites (Table 5.18).

Overall, the cumulates fit well with the fractional crystallization model. The phonolite trend of the SUS produces essexites throughout the entire sequence. The evolutionary trends in the WUS produce anorthosites and sodalite syenites as feldspar fractionation is the most important mechanism for production of peralkaline rocks from an alkaline parent.

Element	Hypothetical Cumulate	Essexite 81472
SiO2	42.32	42.81
TiO2	4.50	2.95
Al2O3	12.71	18.18
FeO	12.96	12.08
MnO	0.18	0.15
MgO	9.57	5.61
CaO	12.28	14.05
Na2O	3.15	1.98
K2O	1.12	0.51
P2O5	0.66	0.55

TABLE 5.15 Comparison of observed and hypothetical cumulates for the ne-mugearite to ne-benmoreite model.

Element	Hypothetical Cumulate	Essexite 81472
SiO2	43.52	42.81
TiO2	3.90	2.95
Al2O3	16.62	18.18
FeO	13.27	12.08
MnO	0.16	0.15
MgO	5.02	5.61
CaO	12.31	14.05
Na2O	3.40	1.98
K2O	0.43	0.51
P2O5	1.36	0.55

TABLE 5.16 Comparison of observed and hypothetical cumulates for the phonolite 1 to phonolite 2 model.

Element	Hypothetical Cumulate	Anorthosite 81478
SiO2	47.43	47.83
TiO2	2.87	2.47
Al2O3	19.14	17.17
FeO	11.02	10.85
MnO	0.21	0.21
MgO	5.22	4.07
CaO	8.23	8.35
Na2O	4.84	4.74
K2O	0.32	1.74
P2O5	1.22	0.80

TABLE 5.17 Comparison of observed and hypothetical cumulates for the mugearite to benmoreite model.

Element	Hypothetical Cumulate	Syenite 81480
SiO2	60.88	60.37
TiO2	0.78	0.75
Al2O3	13.62	17.36
FeO	10.32	4.85
MnO	0.07	0.18
MgO	0.14	1.22
CaO	1.16	3.42
Na2O	8.16	6.01
K2O	4.81	4.08
P2O5	0.07	0.38

TABLE 5.18 Comparison of observed and hypothetical cumulates for the qtz-trachyte to comendite model.

6 CONCLUSIONS

6.1 Summary: Evidence for Fractional Crystallization

Variations in the lavas of Mount Overlord can be explained by fractional crystallization. The sequence originated with basanites and alkali basalts which, through fractionation, developed phonolites, trachytes, and comendites. Field relationships and geochemical evidence support this idea, and least squares mass balance models produce viable solutions to each step of the fractionation sequence. The fractionation, however, is not simple and magma probably ascended and differentiated in a number of small apophyses.

Stratigraphic relationships and cognate xenoliths in the lavas support the fractional crystallization hypothesis. The caldera wall section (2.3.2) and east rim section (2.3.3) shows an increase in silica and DI as you go up in the section. The summit flow (2.3.2) contains a great number of xenoliths which may represent the eruption of a final magma-cumulate mush.

Major element, trace element, and REE plots all show continuous trends which are characteristic of fractional crystallization. The different patterns seen in major and trace elements support the fractionation of olivine, clinopyroxene, feldspar, opaque oxides, and apatite along with kaersutite and/or ilmenite. REE chondrite normalized diagrams suggest that the evolution of the SUS was dominated by kaersutite and feldspar fractionation and the evolution of the WUS by feldspar fractionation alone.

Computer modelling of the differentiation sequence proved successful. The SUS was modelled in five steps from basanite to phonolite with each producing good results. Trace element calculations, in most cases, supported the computer models. Modelling of the WUS was not as successful, but the results gave reasonable first estimates of the type of fractionation occuring. In both cases, the hypothetical cumulates produced correspond closely with xenoliths found. Fractional crystallization seems an appropriate mechanisms for the changes in chemical composition observed.

6.2 Magma Chamber Model

From the field evidence and geochemical studies, it seems apparent that the magma chamber which existed below Mount Overlord was not by any means simple (Fig. 6.1). Field evidence shows a large number of relatively small flows eminating from different portions of the cone. Geochemical evidence also supports a number of different vents with the association of magmas in a given area generally conforming to either the WUS or SUS.

The magma chamber system below Mount Overlord may have consisted of a number of small magma chambers at various depths below the surface. From this, small plumes of magma rose forming dikes and sills, or erupting onto the surface. The shallow chambers were able to evolve separately, according to their pressure and temperature conditions.

The alkali basalts, basanites, and hawaiites rose directly to the surface from the mantle, forming the various cinder cones found around the main crater. This material was also the parental material which formed the magma chambers. The rocks of the SUS and WUS, mugearites through trachytes, phonolites, and comendites evolved in these magma chambers for some time, while periodically releasing magma to the surface. The peralkaline comendites probably formed as a final residual liquid in the magma chamber and erupted

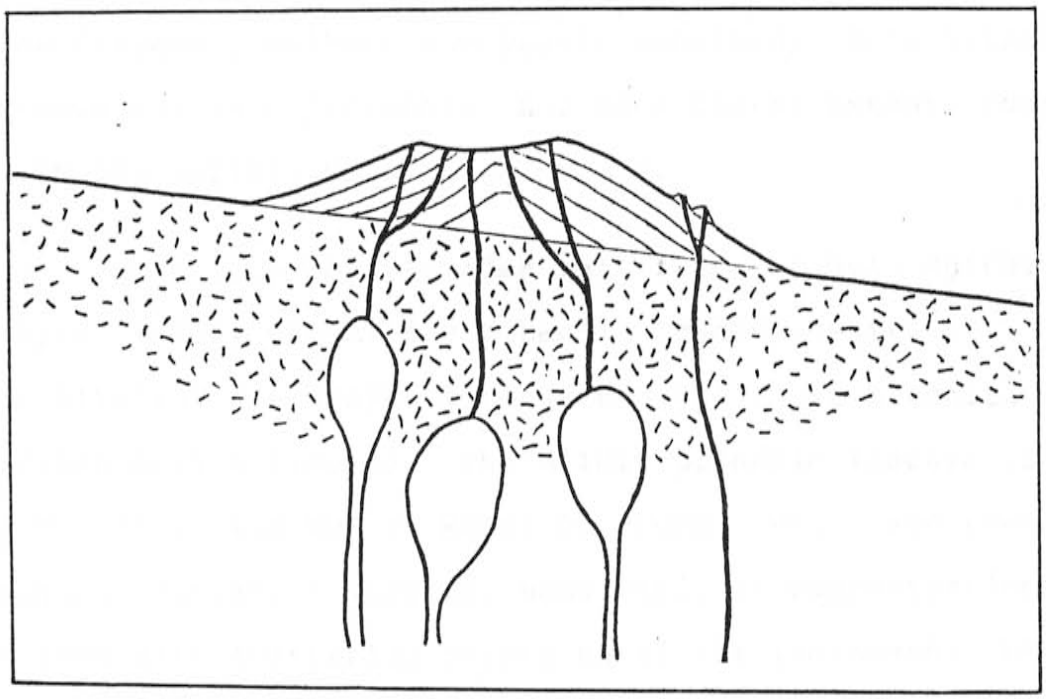

FIGURE 6.1 Diagramatic view of Mount Overlord and its magma chamber system.

during collapse of the caldera.

6.3 Comparison with other McMurdo Volcanics

In general the lavas of the McMurdo Volcanic Group are all very similiar to the SUS and WUS at Mount Overlord (Fig. 6.2). Areas which have been studied extensively are The Pleiades, Melbourne volcanic province; Ross Island, Erebus volcanic province; and to a lesser extent, rocks from the Hallett volcanic province.

Rocks from The Pleiades fall into two main suites (Kyle, 1976), the mildly potassic trachyandesite - peralkaline K-trachyte lineage and the sodic basanite - ne-benmoreite lineage. The mildly potassic lineage is similiar to the WUS at Mount Overlord. Major and trace element variation diagrams show similiar concentrations and trends with scattering points as silica increases. REE diagrams show a continuous enrichment of all REE (except Eu) through the entire sequence, and the development of a large negative Eu anomaly in the peralkaline rocks. The sodic series corresponds to the SUS at Mount Overlord but, is not as extensive as there are no phonolites at The Pleiades. Again, the major and trace element variation diagrams have similiar trends. The REE plots are also similiar with enrichment of LREE and HREE and a depletion of the MREE.

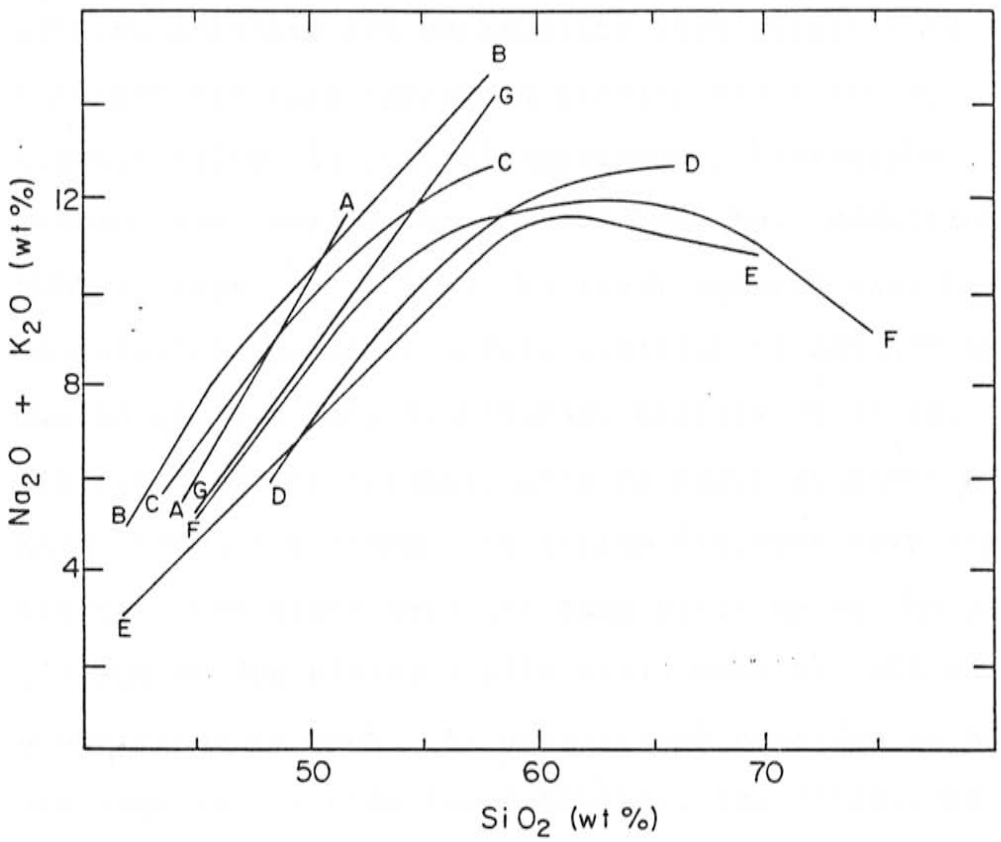

FIGURE 6.2 Total alkalis vs silica diagram showing the main lineages of the McMurdo Volcanic Group; A) Sodic lineage, The Pleaides; B) DVDP lineage; C) Erebus lineage; D) mildly potassic lineage, The Pleaides; E) Hallett volcanic province; F) WUS, Mt Overlord; G) SUS, Mt Overlord.

The Erebus volcanic province also has two main lava lineages, the DVDP lineage and the Erebus lineage. The DVDP lineage is best exemplified by the rocks found at Hut Point Peninsula and in the DVDP cores. A basanite parent produces evolved basanite and ne-hawaiite then alternating intermediate rock types and finally phonolite by fractionating olivine, clinopyroxene, kaersutite, plagioclase, opaque oxides, and apatite. Modelling of the DVDP lineage (Kyle, 1981) by least squares mass balance calculations produces models similiar to the SUS at Mount Overlord. The only significant difference is the fractionation of slightly more feldspar at Mount Overlord. Major and trace element variation diagrams have similiar trends. REE plots have the same patterns as the sodic lineage at The Pleiades with enrichment of LREE and HREE and a depletion of MREE. No significant negative Eu anomalies are seen in the DVDP lavas however, the phonolites at Mount Overlord have values of Eu/Eu* of 0.95 to 0.39. This could be a result of the greater amounts of feldspar fractionated. The Erebus lineage is similiar to the DVDP lineage but no basaltic rocks are found. An evaluation of the petrogenesis is difficult because of the strongly porphyritic nature of the rocks. The evolution of the Erebus lineage is considered to be like the DVDP lineage but without fractionating kaersutite.

Little work has been done on the petrogenesis of the rocks in the Hallett volcanic province. Analyses suggest that the rocks are similiar to the WUS at Mount Overlord. The suite found is an alkali basalt/basanite - trachyte - qtz-trachyte lineage.

6.4 Conclusions

The suites of lavas found at Mount Overlord represent the entire spectrum of rock types found within the McMurdo Volcanic Group. The development of the SUS and WUS by fractional crystallization is comparable to the evolution of other suites in the McMurdo Volcanic Group, and strongly supported by field and geochemical evidence. Fractional crystallization has been quantified by least squares mass balance models and tested using trace elemet data and the Rayleigh equation. Results of the models are good in most cases, and the fractionating mineral phases form hypothetical cumulates similiar to the xenoliths found. It is significant that all of these rock types were evolved and erupted at one site. The varying conditions neccesary to form the different suites suggests a complex magma system.

APPENDIX ONE

ANALYTICAL PROCEDURES

Major Elements

Major elements were analyzed at the New Mexico Tech X-ray lab using a Rigaku 3064 XRF spectrometer. Samples were prepared using the method of Norrish and Hutton (1969). 0.5 grams of sample are fused with spectroflux 105, a lithium borate flux, adding ammonium nitrate as an oxidizer. The machine is calibrated using a number of common standards including G2. An estimation of the precision is made by comparing triplicates of one sample (Table A1).

Major element analyses are recalculated to volitile free and CIPW norms were calculated for each rock. Tables of major element analyses and CIPW norms are presented in Appendix 2.

Trace Elements

Trace elements were determined by two means, XRF and INAA (Appendix 3). XRF analyses on pressed powders was done at New Mexico Tech for NI, Cu, Zn, Ga, Rb, Sr, Y, Zr, Nb, Pb, Th, and U. INAA was done at New Mexico Tech, using reactor facilities at Sandia National Lab, for Sc, Cr, Co, Se, Sb, Cs, Ba, La, Ce, Sm, Eu, Tb, Yb, Lu, Hf, and Ta. An estimation of the precision of the trace element analyses is done by comparing measured and accepted values of te standard G2 (Table A2).

Pressed powder pellets are made by mixing approximately 6 grams of sample with 7 drops of 1% polyvinyl alcohol. This mixture is pressed into pellets with a borax back under 10 tons of pressure.

INAA samples are prepared by placing approximately 0.25 grams of rock powder in polyurethane vials for irradiation. The irradiated samples were analyzed on a Nuclear Data 4096 channel gamma-ray spectrometer with an Ortec high purity, germanium co-axial detector.

Element	81414	81414R	81414X	Mean	S.D.	C.V.
SiO2	56.53	56.14	55.78	56.15	0.37	0.7
TiO2	1.59	1.54	1.57	1.57	0.02	1.3
Al2O3	17.81	17.68	17.89	17.79	0.10	0.6
FeO	7.08	6.50	6.77	6.78	0.29	4.3
MnO	0.16	0.16	0.16	0.16	-	-
MgO	2.32	2.22	2.25	2.26	0.05	2.2
CaO	4.77	4.62	4.64	4.68	0.08	1.7
Na2O	5.86	5.31	5.68	5.77	0.13	2.2
K2O	3.31	3.29	3.28	3.29	0.02	0.6
P2O5	0.56	0.55	0.55	0.55	0.006	1.1

TABLE A 1 Comparison of Triplicate analysis of Sample 81414. S.D. - standard deviation, C.V. - Coefficient of variation = 100 x mean/S.D.

Element	Measured	Accepted
Sc	3.58	3.5
Cr	8.4	9
Co	4.0	4.6
Ni	5.9	4.9
Cu	15.6	11
Zn	86.7	85
Ga	21.6	22
Rb	168.6	170
Sr	471.0	478
Y	10.68	11.4
Zr	300.0	300
Nb	12.2	13
Sb	0.06	0.078
Cs	1.3	1.33
Ba	1851	1880
La	87.9	86
Ce	156.7	159
Sm	7.39	7.2
Eu	1.33	1.41
Tb	0.46	0.48
Yb	0.76	0.78
Lu	0.20	0.11
Hf	7.6	7.9
Ta	0.8	0.88
Pb	30.0	31
Th	24.9	24.6
U	1.6	2.04

TABLE A2 Comparison of measured and accepted trace element concentrations for G2.

APPENDIX 2

MAJOR ELEMENT ANALYSES

AND CIPW NORMS

Rock Type	Basanite		Alkali Basalt		Hawaiite	
Sample #	81508	81510	81511	81509	81466	81500
Major Element (wt%)						
SiO_2	45.05	45.60	45.56	45.66	45.42	46.63
TiO_2	2.51	2.53	2.59	2.52	3.10	2.87
Al_2O_3	15.22	15.26	15.48	14.94	15.04	15.76
FeO *	11.06	11.48	11.22	11.39	11.86	12.59
MnO	0.20	0.20	0.20	0.20	0.20	0.22
MgO	8.70	8.34	7.64	9.66	8.07	5.41
CaO	9.85	9.65	9.72	9.52	10.52	8.12
Na_2O	3.93	3.38	3.41	2.07	3.77	3.89
K_2O	1.33	1.42	1.37	1.40	1.09	1.74
P_2O_5	0.80	0.84	0.85	0.79	0.74	0.93
LOI	0.59	-0.07	0.49	0.36	-0.42	0.28
Sum	99.24	98.63	98.53	98.51	99.39	98.44
CIPW Norms (wt%)**						
Q	-	-	-	-	-	-
Or	7.86	8.39	8.10	8.27	6.44	10.28
Ab	15.11	18.46	19.75	17.52	16.55	26.18
An	19.96	22.27	22.88	27.34	20.90	20.40
Ne	9.83	5.49	4.93	-	8.32	3.65
Ac	-	-	-	-	-	-
Ns	-	-	-	-	-	-
Di-wo	9.89	8.40	8.26	6.15	11.05	5.76
Di-fs	3.25	2.96	2.99	2.08	3.93	2.85
Di-en	6.08	5.00	4.86	3.74	6.56	2.81
Wo	-	-	-	-	-	-
Hy-fs	-	-	-	1.87	-	-
Hy-en	-	-	-	3.37	-	-
Fo	10.93	11.05	9.93	11.88	9.49	7.47
Fa	6.44	7.20	6.73	7.28	6.26	8.35
Mt	2.90	2.90	2.90	2.18	2.90	2.90
Hm	-	-	-	-	-	-
Il	4.77	4.80	4.92	4.79	5.89	5.45
Ap	1.95	1.95	1.97	1.83	1.72	2.16
DI	32.80	32.35	32.78	25.79	31.31	40.11
AN #	56.91	54.67	53.68	60.95	55.80	43.79
Mg #	62.61	60.60	59.15	63.20	58.89	47.40
Agpaitic Index	0.52	0.46	0.46	0.33	0.49	0.53

* Total Fe As FeO

** Calculated using Fe_2O_3 = 1.50 when Alkalies < 4.0
= 2.00 4.0 < Alkalies < 7.0
= 2.50 7.0 < Alkalies

Rock Type	Mugeareite					
Sample #	81461	81465	81459	81424	81420	81422
Major Element(wt%)						
SiO_2	48.20	49.43	50.27	51.62	52.50	52.60
TiO_2	2.32	2.28	2.37	1.85	1.74	1.78
Al_2O_3	18.29	17.98	17.61	17.86	17.94	18.31
FeO *	9.95	9.56	9.77	8.25	8.12	8.22
MnO	0.20	0.22	0.21	0.20	0.20	0.20
MgO	3.93	3.32	3.64	3.00	2.78	2.73
CaO	8.24	7.09	6.79	5.69	5.23	5.32
Na_2O	4.86	6.12	5.41	6.29	5.67	6.33
K_2O	2.19	2.65	2.35	2.88	2.95	2.97
P_2O_5	0.87	0.92	0.92	0.67	0.66	0.66
LOI	-0.04	-0.61	0.15	0.27	0.77	0.73
Sum	99.01	98.96	99.49	98.58	98.56	99.85
CIPW Norms (wt%) **						
Q	-	-	-	-	-	-
Or	12.94	15.66	13.89	17.02	17.43	17.55
Ab	25.69	26.62	33.62	34.30	39.57	36.98
An	21.62	13.76	16.82	11.99	14.79	12.78
Ne	8.36	13.64	6.56	10.25	4.56	8.98
Ac	-	-	-	-	-	-
Ns	-	-	-	-	-	-
Di-wo	5.67	6.43	4.53	4.95	2.86	3.89
Di-fs	2.94	3.20	2.32	2.19	1.47	1.96
Di-en	2.58	3.09	2.10	2.61	1.31	1.83
Wo	-	-	-	-	-	-
Hy-fs	-	-	-	-	-	-
Hy-en	-	-	-	-	-	-
Fo	4.80	3.55	4.73	3.40	3.82	3.59
Fa	4.65	3.77	4.71	3.14	3.75	3.75
Mt	3.62	3.62	3.62	3.62	3.62	3.62
Hm	-	-	-	-	-	-
Il	4.41	4.33	4.50	3.51	3.30	3.38
Ap	2.02	2.13	2.13	1.55	1.53	1.53
DI	46.99	55.91	54.11	61.57	61.56	63.52
AN#	45.70	34.08	33.33	25.90	27.20	25.67
Mg#	47.66	44.78	46.37	47.15	45.86	44.96
Agpaitic Index	0.57	0.72	0.65	0.75	0.70	0.74

* Total Fe As FeO

** Calculated using Fe_2O_3 = 1.50 when Alkalies $\leq$ 4.0
= 2.00 4.0 < Alkalies< 7.0
= 2.50 7.0 < Alkalies

Rock Type	Ne-benmoreite					
Sample #	81433	81431	81418	81432	81434	81427
Major Element (wt%)						
SiO_2	53.43	52.49	53.50	54.06	54.06	54.07
TiO_2	1.26	1.74	1.35	1.25	1.23	1.06
Al_2O_3	18.64	17.97	18.88	18.95	18.89	19.04
FeO *	6.77	8.13	7.53	7.11	6.88	6.72
MnO	0.19	0.20	0.21	0.20	0.19	0.21
MgO	1.82	2.84	1.90	1.85	1.81	1.48
CaO	4.63	5.31	4.71	4.50	4.31	3.85
Na_2O	6.06	6.94	6.77	7.55	6.95	7.19
K_2O	3.49	2.99	3.49	3.62	3.57	3.78
P_2O_5	0.55	0.66	0.59	0.56	0.55	0.46
LOI	2.10	-0.14	0.55	0.20	0.65	0.55
Sum	99.67	99.13	99.48	99.85	99.09	98.41
CIPW Norms (wt%) **						
Q	-	-	-	-	-	-
Or	20.62	17.67	20.62	21.39	21.10	22.34
Ab	39.76	34.80	36.65	35.35	38.56	37.84
An	13.35	9.05	10.82	7.12	9.80	8.51
Ne	6.24	12.96	11.18	15.46	10.97	12.46
Ac	-	-	-	-	-	-
Ns	-	-	-	-	-	-
Di-wo	2.52	5.42	3.63	4.82	3.34	3.16
Di-fs	1.23	2.46	1.98	2.52	1.68	1.78
Di-en	1.24	2.81	1.63	2.25	1.60	1.38
Wo	-	-	-	-	-	-
Hy-fs	-	-	-	-	-	-
Hy-en	-	-	-	-	-	-
Fo	2.31	2.99	2.18	1.65	2.04	1.68
Fa	2.53	2.89	2.93	2.03	2.37	2.31
Mt	3.62	3.62	3.62	3.62	3.62	3.62
Hm	-	-	-	-	-	-
Il	2.39	3.30	2.56	2.37	2.34	2.01
Ap	1.27	1.53	1.37	1.30	1.27	1.07
DI	66.62	65.43	68.45	72.20	70.62	72.64
An #	25.14	20.64	22.79	16.77	20.27	18.37
Mg #	41.78	46.32	39.11	40.47	41.09	37.15
Agpaitic Index	0.74	0.82	0.79	0.86	0.81	0.84

* Total Fe As FeO

** Calculated using Fe_2O_3= 1.50 when Alkalies < 4.0
= 2.00 4.0 < Alkalies < 7.0
= 2-50 7.0 < Alkalies

Rock Type	Benmoreite					
Sample #	81430	81429	82077	81414 X	81414 R	81414
Major Element(wt%)						
SiO_2	55.08	54.66	55.22	55.78	56.14	56.53
TiO_2	0.94	1.17	1.18	1.57	1.54	1.59
Al_2O_3	19.42	19.12	17.76	17.89	17.68	17.81
FeO *	6.46	6.83	7.26	6.77	6.50	7.08
MnO	0.21	0.19	0.22	0.16	0.16	0.16
MgO	1.33	1.58	1.24	2.25	2.22	2.32
CaO	3.38	4.09	3.36	4.64	4.62	4.77
Na_2O	7.16	6.60	6.37	5.68	5.31	5.86
K_2O	3.85	3.60	4.26	3.28	3.29	3.31
P_2O_5	0.38	0.51	0.35	0.55	0.55	0.56
LOI	1.11	0.85	2.24	0.75	0.75	0.75
Sum	99.52	99.20	99.96	99.32	98.76	100.74
CIPW Norms (wt%) **						
Q	-	-	-	-		
Or	22.75	21.27	25.17	19.38		
Ab	40.37	41.56	41.30	47.75		
An	9.48	11.91	7.28	13.63		
Ne	10.95	7.74	6.83	0.17		
Ac	-	-	-	-		
Ns	-	-	-	-		
Di-wo	2.42	2.12	2.96	2.42		
Di-fs	1.41	1.47	1.95	0.95		
Di-en	1.02	0.95	1.08	1.36		
Wo	-	-	-	-		
Hy-fs	-	-	-	-		
Hy-en	-	-	-	-		
Fo	1.56	2.09	1.41	2.97		
Fa	2.38	2.78	2.81	2.97		
Mt	3.62	3.62	3.62	3.62		
Hm	-	-	-	-		
Il	1.78	2.22	2.24	2.98		
Ap	0.88	1.18	0.81	1.27		
DI	74.07	70.58	73.30	67.30		
AN #	10.02	22.28	14.99	22.21		
Mg #	35.54	38.12	30.64	47.08		
Agpaitic Index	0.82	0.77	0.85	0.72		

* Total Fe As FeO

** Calculated using Fe_2O_3 = 1.50 when Alkalies < 4.0
= 2.00 4.0 < Alkalies < 7.0
= 2.50 7.0 < Alkalies

Rock Type	Phonolite				Trachyte	
Sample #	81444	81428	82072	81464	81439	81436
Major Element (wt%)						
SiO_2	56.86	54.78	57.96	58.66	58.37	58.38
TiO_2	1.21	1.01	0.08	0.56	0.90	0.53
Al_2O_3	18.52	19.03	19.75	18.65	18.81	18.98
FeO *	6.02	6.63	4.44	4.74	5.12	4.74
MnO	0.15	0.21	0.21	0.15	0.13	0.16
MgO	1.80	1.34	0.07	0.85	1.18	0.72
CaO	3.94	3.65	0.91	2.12	3.09	1.91
Na_2O	6.58	7.72	8.52	7.75	6.61	6.34
K_2O	3.47	3.85	5.47	5.16	4.05	5.04
P_2O_5	0.40	0.42	0.04	0.17	0.30	0.18
LOI	0.32	0.52	1.19	0.62	0.30	1.97
Sum	99.27	99.16	98.64	99.38	98.56	98.95
CIPW Norms (wt%) **						
Q	-	-	-	-	-	-
Or	20.51	22.75	32.32	30.49	23.93	29.78
Ab	48.28	37.96	39.93	42.97	50.96	48.53
An	10.75	5.90	-	0.86	9.69	8.30
Ne	4.01	14.82	16.90	12.25	2.69	2.77
Ac	-	-	-	-	-	-
Ns	-	-	-	-	-	-
Di-wo	2.58	3.95	1.78	3.57	1.54	-
Di-fs	1.02	2.32	1.84	1.62	0.58	-
Di-en	1.46	1.65	0.13	1.85	0.88	-
Wo	-	-	-	-	-	-
Hy-fs	-	-	-	-	-	-
Hy-en	-	-	-	-	-	-
Fo	2.12	1.18	0.03	0.18	1.44	1.26
Fa	1.63	1.83	0.47	0.18	1.05	1.48
Mt	3.62	3.62	3.20	3.62	3.62	3.62
Hm	-	-	-	-	-	-
Il	2.30	1.92	0.15	1.06	1.71	1.01
Ap	0.93	0.97	0.09	0.39	0.70	0.42
DI	72.79	75.54	89.16	85.71	77.59	81.09
An #	18.21	13.45	0.00	1.96	15.98	14.60
Mg #	46.03	35.32	5.40	37.89	42.36	34.07
Agpaitic Index	0.79	0.89	1.01	0.98	0.81	0.84

* Total Fe As FeO

** Calculated using Fe_2O_3 = 1.50 when Alkalies < 4.0
= 2.00 4.0 < Alkalies < 7.0
= 2.50 7.0 < Alkalies

Rock Type						Q-Trac
Sample #	81425	81442	81446	81426	82069	81075
Major Element (wt%)						
SiO_2	58.48	58.96	59.15	59.31	60.19	64.45
TiO_2	1.04	0.68	0.68	1.14	0.54	0.61
Al_2O_3	17.80	18.24	18.21	17.99	18.54	12.64
FeO *	5.30	5.27	5.18	5.78	4.50	7.96
MnO	0.15	0.17	0.17	0.16	0.17	0.30
MgO	1.21	0.81	0.74	1.31	0.60	0.16
CaO	3.24	2.21	1.94	3.16	1.69	0.90
Na_2O	6.20	6.70	7.13	6.31	5.92	6.84
K_2O	3.93	4.98	4.89	3.93	5.66	4.72
P_2O_5	0.33	0.22	0.19	0.36	0.16	0.05
LOI	1.32	0.91	0.59	0.31	1.19	0.48
Sum	98.96	99.15	98.87	99.76	99.16	99.11
CIPW Norms (wt%) **						
Q	-	-	-	-	-	9.04
Or	23.22	29.43	28.90	23.22	33.45	27.89
Ab	52.46	48.17	48.94	53.39	50.09	38.74
An	9.13	4.99	3.24	9.17	7.30	-
Ne	-	4.62	6.17	-	-	-
Ac	-	-	-	-	-	7.23
Ns	-	-	-	-	-	2.54
Di-wo	2.00	1.90	2.15	1.74	0.02	1.73
Di-fs	0.78	1.08	1.24	0.78	0.01	1.86
Di-en	1.13	0.82	0.91	0.91	0.01	0.07
Wo	-	-	-	-	-	-
Hy-fs	0.77	-	-	1.12	0.27	8.16
Hy-en	1.11	-	-	1.30	0.27	0.32
Fo	0.54	0.84	0.65	0.74	0.85	-
Fa	0.41	1.22	0.97	0.70	0.94	-
Mt	3.62	3.62	3.62	3.62	3.62	-
Hm	-	-	-	-	-	-
Il	1.98	1.29	1.29	2.16	1.03	1.16
Ap	0.76	0.51	0.44	0.83	0.37	0.12
DI	75.69	82.22	84.01	76.62	83.54	75.67
An #	14.82	9.38	6.21	14.64	12.72	0.00
Mg #	41.49	32.38	31.08	39.89	32.22	4.76
Agpaitic Index	0.81	0.90	0.94	0.81	0.86	1.29

* Total Fe As FeO

** Calculated using Fe_2O_3 = 1.50 when Alkalies < 4.0
= 2.00 4.0 < Alkalies < 7.0
= 2.50 7.0 < Alkalies

Rock Type	Comendites					
Sample #	82059	82061	82065	82060	82062	81416
Major Element(wt%)						
SiO_2	68.64	68.70	69.00	69.20	73.24	73.64
TiO_2	0.26	0.26	0.25	0.25	0.16	0.28
Al_2O_3	14.55	14.60	14.38	14.33	12.52	11.71
FeO *	3.51	3.50	3.57	3.09	2.40	3.44
MnO	0.09	0.11	0.10	0.09	0.06	0.08
MgO	0.06	0.03	0.01	0.01	0.01	0.08
CaO	1.05	0.90	0.79	0.70	0.40	0.46
Na_2O	5.23	5.42	5.61	5.33	5.06	4.11
K_2O	5.24	5.27	5.11	5.20	4.61	4.76
P_2O_5	0.03	0.02	0.02	0.01	0.01	0.02
LOI	0.39	0.59	0.74	1.36	1.23	0.69
Sum	99.05	99.40	99.58	99.57	99.70	99.27
CIPW Norms (wt%) **						
Q	16.83	16.03	16.16	17.62	26.69	31.14
Or	30.96	31.14	30.20	30.73	27.24	28.13
Ab	44.26	45.76	45.52	44.76	38.73	33.73
An	0.75	-	-	-	-	-
Ne	-	-	-	-	-	-
Ac	-	0.09	1.72	0.30	3.60	0.92
Ns	-	-	-	-	-	-
Di-wo	0.17	0.12	0.55	0.03	-	0.29
Di-fs	-	0.03	0.62	-	-	0.06
Di-en	0.15	0.08	-	0.03	-	0.20
Wo	1.61	1.70	1.03	1.39	0.78	0.61
Hy-fs	-	-	-	-	-	-
Hy-en	-	-	-	-	-	-
Fo	-	-	-	-	-	-
Fa	-	-	-	-	-	-
Mt	3.60	3.58	2.76	2.28	0.22	3.16
Hm	0.02	-	-	0.82	1.11	-
Il	0.49	0.49	0.48	0.48	0.30	0.53
Ap	0.07	0.05	0.05	0.02	0.02	0.05
DI	92.05	92.93	91.87	93.11	92.67	93.00
An #	1.66	0.00	0.00	0.00	0.00	0.00
Mg #	7.82	4.10	0.14	2.08	1.17	10.72
Agpaitic Index	0,98	1.00	1.03	1.00	1.06	1.02

* Total Fe As FeO

** Calculated using Fe_2O_3 = 1.50 when Alkalies < 4.0
= 2.00 4.0 < Alkalies < 7.0
= 2.50 7.0 < Alkalies

Rock Type				
Sample #	81417	81435 B	81435 A	82078
Major Element(wt%)				
SiO_2	73.95	74.21	75.09	75.38
TiO_2	0.26	0.26	0.27	0.28
Al_2O_3	11.20	11.57	11.31	10.36
FeO *	3.27	3.28	3.21	4.13
MnO	0.08	0.08	0.08	0.08
MgO	0.08	0.02	0.06	0.41
CaO	0.44	0.48	0.38	0.29
Na_2O	4.60	4.44	5.00	3.58
K_2O	4.64	4.76	4.71	4.51
P_2O_5	0.02	0.02	0.02	0.01
LOI	0.71	0.42	0.22	0.31
Sum	99.25	99.54	100.35	99.34
CIPW Norms (wt%) **				
Q	29.91	30.38	29.96	36.15
Or	27.42	28.13	27.83	26.65
Ab	31.78	33.01	31.95	28.18
An	-	-	-	-
Ne	-	-	-	-
Ac	6.30	4.02	7.23	1.86
Ns	-	-	0.50	-
Di-wo	0.86	0.66	0.73	0.57
Di-fs	0.81	0.68	0.73	0.35
Di-en	0.12	0.05	0.08	0.23
Wo	-	0.28	-	-
Hy-fs	0.51	-	0.72	1.24
Hy-en	0.08	-	0.07	0.79
Fo	-	-	-	-
Fa	-	-	-	-
Mt	0.47	1.61	-	2.69
Hm	-	-	-	-
Il	0.49	0.49	0.51	0.53
Ap	0.05	0.05	0.05	0.02
DI	89.11	91.52	89.73	90.98
An #	0.00	0.00	0.00	0.00
Mg #	12.30	3.36	10.08	28.08
Agpaitic Index	1.12	1.08	1.18	1.04

* Total Fe As FeO

** Calculated using Fe_2O_3= 1.50 when Alkalies < 4.0
= 2.00 4.0 < Alkalies < 7.0
= 2.50 7.0 < Alkalies

Rock Type	Essexite					Anorthosite
Sample #	81471	81469	81473	81472	81478	81492
Major Element (wt%)						
SiO_2	35.21	35.65	37.91	42.81	47.83	49.03
TiO_2	6.15	5.51	3.92	2.95	2.47	2.18
Al_2O_3	14.90	11.76	13.66	18.18	17.17	14.49
FeO *	14.33	20.60	16.98	12.08	10.85	12.35
MnO	0.15	0.32	0.23	0.15	0.21	0.34
MgO	9.24	5.92	7.91	5.61	4.07	4.97
CaO	13.80	13.28	13.48	14.05	8.35	6.54
Na_2O	2.13	2.33	2.32	1.98	4.74	5.01
K_2O	0.59	0.29	0.40	0.51	1.74	2.68
P_2O_5	2.34	2.28	2.89	0.55	0.80	0.75
LOI	-0.04	-0.51	-0.55	0.87	0.64	0.50
Sum	98.80	97.43	99.15	99.74	98.87	98.84
CIPW Norms (wt%)**						
Q	-	-	-	-	-	-
Or	-	1.83	2.36	3.01	10.28	15.84
Ab	-	1.40	6.56	8.80	23.85	26.99
An	29.35	20.00	25.68	39.21	20.43	9.13
Ne	12.50 t	9.51	7.08	4.31	8.81	8.34
Ac	-	-	-	-	-	-
Ns	-	-	-	-	-	-
Di-wo	8.79	12.61	9.32	11.23	8.55	7.69
Di-fs	2.95	8.32	4.67	5.48	4.44	3.96
Di-en	5.35	4.57	4.50	5.53	4.00	3.63
Wo	-	-	-	-	-	-
Hy-fs	-	-	-	-	-	-
Hy-en	-	-	-	-	-	-
Fo	12.38	6.85	10.65	5.91	4.30	6.13
Fa	7.52	13.76	12.19	6.46	5.26	7.37
Mt	2.18	2.18	2.18	2.18	2.90	3.62
Hm	-	-	-	-	-	-
Il	11.68	10.16	7.44	5.60	4.69	4.14
Ap	5.42	6.00	6.70	1.27	0.18	1.74

* Total Fe As FeO

t includes 2.73 wt% Leucite

** Calculated using Fe_2O_3 = 1.50 when Alkalies < 4.0
= 2.00 4.0 < Alkalies < 7.0
= 2.50 7.0 < Alkalies

Rock Type			Sodalite Syenite		
Sample #	81479	81485	81476	81484	81480
Major Element(wt%)					
SiO_2	50.39	50.46	50.50	56.91	60.37
TiO_2	2.00	1.72	1.86	1.17	0.75
Al_2O_3	18.89	17.52	17.76	18.16	17.36
FeO *	8.11	8.22	8.70	6.64	4.85
MnO	0.17	0.21	0.22	0.19	0.18
MgO	2.24	2.56	2.85	1.69	1.22
CaO	7.42	5.61	6.12	3.47	3.42
Na_2O	5.80	6.30	6.27	6.32	6.01
K_2O	2.14	2.75	2.64	4.03	4.08
P_2O_5	0.74	0.71	0.77	0.36	0.38
LOI	1.84	2.31	0.88	0.65	0.27
Sum	99.74	98.37	98.57	99.59	98.89
CIPW Norms(wt%)**					
Q	-	-	-	-	-
Or	12.65	16.25	15.60	23.81	24.11
Ab	33.95	34.04	32.60	46.16	50.86
An	19.19	11.40	12.52	9.28	8.34
Ne	8.20	10.44	11.08	3.96	-
Ac	-	-	-	-	-
Ns	-	-	-	-	-
Di-wo	5.34	4.92	5.35	2.33	2.56
Di-fs	2.65	2.43	2.63	1.17	0.90
Di-en	2.60	2.40	2.63	1.12	1.53
Wo	-	-	-	-	-
Hy-fs	-	-	-	-	0.89
Hy-en	-	-	-	-	1.51
Fo	2.09	2.78	3.14	2.16	-
Fa	2.35	3.10	3.46	2.49	-
Mt	3.62	3.62	3.62	3.62	3.62
Hm	-	-	-	-	-
Il	3.80	3.27	3.53	2.22	1.42
Ap	1.72	1.64	1.78	0.83	0.88

* Total Fe As FeO

** Calculated using Fe_2O_3 = 1.50 when Alkalies < 4.0
= 2.00 4.0 < Alkalies < 7.0
= 2.50 7.0 < Alkalies

APPENDIX 3

TRACE ELEMENT ANALYSES

Rock Type	Basanite			Hawaiite		
Sample #	81510	81466	81500	81461	81465	81459
Sc	22	26	17	12	9.24	12
Cr	392	359	55	32	8	20
Co	46	48	38	28	22	26
Ni	160	126	47	22	15	17
Cu	50	55	35	24	19	24
Zn	112	102	134	115	122	108
Ga	20	23	21	23	23	23
Se	0.8	0.7	0.9	1.1	1.3	1.0
Rb	40	37	46	61	80	64
Sr	887	867	1015	1074	1084	968
Y	29	28	36	32	34	33
Zr	294	259	421	389	507	480
Nb	93	75	101	128	153	119
Sb	0.1	0.1	0.2	0.32	0.2	0.3
Cs	0.5	0.3	0.4	0.7	1.1	0.8
Ba	524	446	590	656	767	613
La	63	50	73	86	99	80
Ce	125	106	147	164	183	157
Sm	8.8	8.9	12	10	12	10
Eu	2.9	3.0	3.8	3.2	3.4	3.2
Tb	1.2	1.1	1.3	1.2	1.2	1.2
Yb	2.3	2.2	2.7	2.9	3.2	2.9
Lu	0.3	0.4	0.4	0.6	0.5	0.4
Hf	5.81	5.56	8.73	7.32	9.54	9.50
Ta	5.50	4.54	6.19	7.78	9.61	7.76
Pb	<2	<2	-	2	2	2
Th	7	6	9	13	14	10
U	1	2	2	2	3	2

Rock Type	Mugearite			Ne-benmoreite		
Sample #	81424	81422	81433	81431	81418	81434
Sc	10	8.54	-	8.78	4.30	4.51
Cr	40	25	-	30	4	5
Co	18	16	-	16	13	11
Ni	17	15	<10	13	12	<10
Cu	11	13	12	12	12	<10
Zn	114	121	126	130	126	125
Ga	25	25	25	22	28	27
Se	1.2	1.2	-	1.2	1.6	1.5
Rb	82	73	108	85	109	111
Sr	943	948	1013	928	978	999
Y	38	37	42	39	45	42
Zr	559	589	720	601	741	727
Nb	128	133	176	135	175	176
Sb	0.2	0.2	-	0.2	0.4	0.4
Cs	1.4	1.2	-	1.2	1.3	1.8
Ba	723	731	-	747	856	887
La	90	92	-	92	118	114
Ce	171	174	-	176	217	211
Sm	11	11	-	11	-	11
Eu	3.2	3.2	-	3.2	3.2	3.1
Tb	1.3	1.3	-	1.3	1.4	1.3
Yb	3.8	3.8	-	3.5	4.2	4.4
Lu	0.5	0.5	-	0.5	0.7	0.6
Hf	11	11	-	11	14	13
Ta	8.55	8.88	-	8.82	12	11
Pb	2	9	10	6	9	11
Th	16	18	26	18	27	28
U	3	4	4	5	6	5

Rock Type			Benmoreite		Phonolite	
Sample #	81430	82077	81414X	81444	81428	82072
Sc	2.34	4.20	8.22	5.49	3.72	1.42
Cr	3	3	19	24	3	2
Co	8	4	13	10	8	0.8
Ni	<10	<10	<10	14	<10	<10
Cu	<10	<10	10	<10	<10	<10
Zn	136	136	126	87	132	178
Ga	29	24	25	25	27	34
Se	1.6	1.7	1.3	1.4	1.7	2.1
Rb	127	107	110	123	126	198
Sr	769	661	905	831	750	12
Y	44	48	44	38	46	47
Zr	822	613	529	620	832	1030
Nb	182	189	151	153	186	207
Sb	0.5	0.3	0.2	0.3	0.4	0.5
Cs	2.0	1.5	2.4	2.3	2.0	3.1
Ba	830	1476	972	1020	776	90
La	118	110	93	97	119	134
Ce	211	215	182	183	217	234
Sm	11	14	12	11	11	10
Eu	2.8	4.37	3.2	3.0	2.8	1.0
Tb	1.3	1.6	1.5	1.3	1.3	1.2
Yb	4.6	4.2	3.7	3.8	4.4	4.0
Lu	0.7	0.6	0.6	0.5	0.7	0.6
Hf	15	13	11	13	15	19
Ta	12	12	10	10	12	15
Pb	13	5	13	11	14	17
Th	31	19	19	22	31	37
U	5	4	3	5	6	7

Rock Type				Trachyte		Qtz-Trachyte
Sample #	81464	81439	81442	81426	82069	82075
Sc	1.94	4.34	4.43	-	2.11	2.30
Cr	6	5	8	-	2	5
Co	4	7	4	-	3	0.4
Ni	<10	<10	<10	<10	<10	<10
Cu	<10	<10	<10	<10	<10	<10
Zn	100	77	141	115	90	322
Ga	25	24	28	28	24	42
Se	1.8	1.4	2.0	-	1.3	2.9
Rb	142	141	159	140	141	223
Sr	261	811	229	649	199	1.20
Y	38	36	54	49	30	121
Zr	744	710	943	618	522	1420
Nb	200	150	238	172	140	323
Sb	0.3	0.2	0.3	-	0.2	0.5
Cs	2.7	2.8	3.0	-	1.9	6.5
Ba	628	112	545	-	835	95
La	104	99	128	-	86	188
Ce	190	175	231	-	159	381
Sm	9.6	9.5	13	-	8.5	27
Eu	1.9	2.6	2.1	-	2.0	3.2
Tb	1.1	1.1	1.5	-	0.9	3.6
Yb	3.7	3.3	5.0	-	2.7	10
Lu	0.6	0.5	0.7	-	0.4	1.4
Hf	15	15	19	-	10	32
Ta	13	11	15	-	9.37	9.16
Pb	14	13	17	12	12	29
Th	30	25	32	24	22	46
U	5	4	6	4	3	8

Rock Type	Comendite			
Sample #	81416	81435B	81435A	82078
Sc	0.88	0.77	-	0.34
Cr	2	4	-	3
Co	0.3	0.4	-	0.1
Ni	<10	<10	<10	<10
Cu	<10	<10	<10	<10
Zn	158	166	168	224
Ga	30	31	30	38
Se	1.3	1.4	-	2.5
Rb	220	240	247	295
Sr	2.59	5.92	3.40	0.08
Y	94	88	89	126
Zr	775	842	896	1404
Nb	147	159	166	259
Sb	0.3	0.4	-	0.4
Cs	7.8	8.9	-	3.4
Ba	76	68	-	123
La	104	109	-	213
Ce	218	230	-	418
Sm	18	19	-	30
Eu	0.4	0.4	-	1.0
Tb	2.6	2.6	-	3.8
Yb	7.9	8.1	-	10
Lu	1.1	1.2	-	-
Hf	19	21	-	34
Ta	10	11	-	18
Pb	26	29	32	32
Th	31	33	37	61
U	5	6	7	14

Rock Type	Essexite				Anorthosite	
Sample #	81471	81469	81473	81472	81478	81492
Sc	31	-	19	24	16	19
Cr	17	-	81	55	18	146
Co	52	-	54	37	32	26
Ni	>10	21	28	33	-	46
Cu	33	65	60	65	-	21
Zn	66	132	112	65	-	172
Ga	16	21	19	18	-	24
Se	0.4	-	0.3	0.4	1.1	2.6
Rb	5.66	5.42	9.23	13	42	114
Sr	1752	1550	1658	1589	998	697
Y	42	62	38	17	36	68
Zr	76	128	105	126	316	595
Nb	41	62	33	36	90	223
Sb	0.1	-	-	0.1	0.1	0.1
Cs	0.1	-	1.7	0.2	0.5	2.2
Ba	379	-	241	244	580	954
La	43	-	65	30	71	139
Ce	131	-	159	64	144	282
Sm	18	-	16	6.3	11	19
Eu	6.3	-	4.9	2.6	3.5	4.5
Tb	1.8	-	1.7	0.8	1.3	2.3
Yb	2.0	-	2.0	1.3	3.0	6.7
Lu	0.2	-	0.3	0.2	0.4	1.0
Hf	2.68	-	16	3.20	7.21	17
Ta	2.27	-	13	2.03	6.32	14
Pb	-	-	-	-	2	15
Th	-	1	-	-	7	17
U	2	-	1	-	1	2

Rock Type			Sodalite	Syenite
Sample #	81479	81476	81484	81480
Sc	10	11	12	5
Cr	8	20	15	6
Co	19	20	10	4
Ni	-	-	-	-
Cu	-	-	-	-
Zn	-	-	-	-
Ga	-	-	-	-
Se	1.3	1.8	2.3	1.4
Rb	55	71	100	127
Sr	1081	1139	573	444
Y	38	43	45	51
Zr	347	450	710	393
Nb	100	147	200	120
Sb	0.2	0.2	0.1	0.2
Cs	0.8	1.0	1.7	1.6
Ba	720	1056	1059	1348
La	85	109	115	119
Ce	174	209	211	231
Sm	12	14	13	14
Eu	3.9	3.9	2.9	2.6
Tb	1.4	1.5	1.4	1.6
Yb	3.1	4.3	4.2	4.3
Lu	0.5	0.5	0.6	0.6
Hf	8.20	9.48	16	8.87
Ta	7.62	10	13	7.74
Pb	<2	5	8	14
Th	12	14	17	28
U	2	4	3	4

REFERENCES

Armstrong, R.L., 1978. K/Ar dating: McMurdo volcanics and Dry Valley glacial history, Victoria Land, Antarctica. N. Z. J. Geol. Geophys., 21, 683-698.

Bailey, D.K., 1974. Experimental petrology relating to oversaturated peralkaline volcanics: A review: Bull. Volcan., 38, special issue.

Bailey, D.K., and Schairer, J.F., 1964. Feldspar-liquid equilibria in perlakaline liquids - the orthoclase effect. Amer. J. Sci., 262, 1198-1206.

Bowen, N.L., 1945. Phase equilibria bearing on the origin and differentiation of the alkaline rocks. Amer. J. Sci., 75-89.

Carmichael, I.S.E., 1964. Natural liquids and the phonolitic minimum. Geol. J., 4, 55-60.

Carmichael, I.S.E., 1967. The iron-titanium oxides of salic volcanic rocks and their associated ferromagnesian silicates. Contr. Miner. Petrology, 14, 36-64.

Carmichael, I.S.E., Turner, F.J., and Verhoogen, J., 1974. Igneous Petrology. McGraw Hill, N.Y.

Collinson, J.W., and Kemp, N.R., 1983. Permian-Triassic sequence in Northern Victoria Land, Antarctica, in Oliver, R.L., James, P.R., and Jago, J.B., Antarctic Earth Science. Australian Academy of Science, Canberra.

Coombs, D.S., 1963. Trends and affinities of basaltic magmas and pyroxenes as illustrated on the diopside-olivine-silica diagram. Min. Soc. Am. Spec. Pap. 1, 227-50.

Coombs, D.S., and Wilkinson, J.F.G., 1969. Lineages and fractionation trends in undersaturated volcanic rocks from the East Otago Volcanic Province (N.Z.) and related rocks. J. Petrol. 10, 440-501.

Coryell, C.D., Chase, J.W., and Winchester, J.W., 1963. A procedure for geochemical interpretation of terrestrial rare-earth abundance patterns. J. Geophys. Res. 68, 559.

Cox, K.G., Bell, J.D., and Pankhurst, R.J., 1980. The Interpretation of the Igneous Rocks. London: Allen and Unwin, 450 p.

Deer, W.A., Howie, R.A., and Zussman, J., 1963. Rock-Forming Minerals, Vol. 4 Framework Silicates. Longman, London.

Frey, F.A., Green, D.H., and Roy, S.D., 1978. Integrated models of basalt petrogenesis: a study of quartz tholeiites to divine melilitites from south eastern Australia utilizing geochemical and experimental petrological data. J. Petrology, 19, 463-513.

Gair, H.S., 1967. The geology from the upper Rennick Glacier to the coast, northern Victoria Land, Antarctica. N. Z. J. Geol. Geophys. 10, 309-344.

Grindley, G.W., and Warren, G., 1964. Stratigraphic nomenclature and correlation in the western Ross Sea region. Antarctic Geology. 314-333. North Holland, Amsterdam.

Gunn, B.M., and Warren, G., 1962. The geology of Victoria Land between the Mawson and Mulock Glaciers, Ross Dependency, Antarctica. Bull. Geol. Surv. N. Z. n.s. 71.

Harker, A., 1909. The Natural History of Igneous Rocks. New York: Macmillan.

Harrington, H.J., 1958. Nomenclature of Rock Units in the Ross Sea Region, Antarctica. Nature 192, 290.

Harrington, H.J., Wood, B.L., McKellar, I.C., and Lensen, G.S., 1967. Topography and geology of the Cape Hallett District, Victoria Land, Antarctica. Bull. Geol. Sur. N. Z. 80.

Hayes, D.E., and Conolly, J.R., 1972. Morphology of the southeast Indian Ocean. In Antarctica Oceanology 2: Australia - New Zealand Sector. Antarctic Research Series, 19. Ed. D.E. Hayes. Amer. Geophys. Union, Washington D.C., p. 125-145.

Irvine, T.N., 1982. Terminology for Layered Intrusions. J. Petrology, 23, 127-162.

Irvine, T.N., and Baragar, W.R.A., 1971. A guide to the chemical classification of the common volcanic rocks. Canad. J. Earth Sci. 8, 523- 548.

Jones, L.M., and Walker, R.L. (1972). Geochemistry of the McMurdo Volcanics, Victoria Land Part 1: Strontium isotope composition. Antarctic Journal of the U.S. 7 142-144.

Kay R.W., and Gast, P.W., 1973. The Rare Earth Content and origin of alkali basalts. J. Geol. 81, 653-682.

Kyle, P.R., 1976. Geology, Mineralogy, and Geochemistry of the Late Cenozoic McMurdo Volcanic Group, Victoria Land, Antarctica. Ph.D. thesis, Victoria University of Wellington.

Kyle, P.R., 1981. Mineralogy and geochemistry of a basanite to phonolite sequence at Hut Point Peninsula, Antarctica, based on core from Dry Valley Drilling Project Drillholes 1, 2, and 3. J. Petrology, 22, 451-500.

Kyle, P.R., and Cole, J.W., 1974. Structural control of volcanism in the McMurdo Volcanic Group, Antarctica. Bull. Volcanologique 38, 16-25.

Luth, W.C., and Tuttle, O.F., 1966. The alkali feldspar solvus in the system Na2O-K2O-Al2O3-SiO2-H2O. Am. Miner., 51, 1359-73.

Macdonald, G.A., 1960. Dissimilarity of continental and oceanic rock types. J. Petrol. 1, 172-177.

Macdonald, G.A., and Katsura, T., 1964. Chemical composition of Hawaiian lavas. J. Petrol. 5, 82-133.

Macdonald, R., 1974. Nomenclature and petrochemistry of the peralkaline oversaturated extrusive rocks: Bull. Volcan., 38.

Masuda, A., 1962. Regularities in variation of relative abundances of lanthanide elements and an attempt to analyze separation-index patterns of some minerals. J. Earth Sci., Nagoya Univ. 10, p. 173.

Moorhouse, W.W., 1959. The Study of Rocks in Thin Section. Harper and Row, N.Y.

Nathan, S., 1971. Geology and petrology of the Campbell-Aviator Divide, Northern Victoria Land, Antarctica. N. Z. J. of Geol. and Geop. 14, 564-596.

Nathan, S., and Schultz, F.J., 1968. The geology and petrology of the area between the Campbell and Aviation Glaciers. N. Z. J. Geol. Geophys. 11, 940-975.

Norrish, K., and Hutton, J.T., 1969. An accurate x-ray spectrographic method for the analysis of a wide range of geologic samples. Geoch. et. Cosmo. Acta 33, 431-453.

Ricker, J., 1964. Oute of the geology beteween the Mawson and Priestley Glaciers, Victoria Land, Proc. 1st Int. symp. on Antarctic Geol. North Holland Amsterdam.

Riddols, B.W., and Hancox, G.T., 1968. The geology of the upper Mariner Glacier region, north Victoria Land, Antarctica. N. Z. J. Geol. Geophys. 11, 881-899.

Saggerson, E.P., and Williams, L.A.J., 1964. Ngurumanite from Southern Kenya and its bearing on the origin of rocks in the northern Tanganyika alkaline district. J. Petrology 5, 40-81.

Schairer, J.F., d Yoder, H.S., 1960. The nature of residual liquids from crystallization, with data on the system nepheline-diopside-silica. Am. J. Sci., 258A, 273-83.

Schwarzer, R.R., d Rogers, J.J.W., 1974. A Worldwide Comparison of Alkali Olivine Basalts and their Differentiation Trends. EPSL, 23, 286-296.

Sorensen, H., 1974. Chap VI, Petrogenesis, in The Alkaline Rocks. H. Sorensen, ed., John Wiley and Sons, London.

Sun, S.S., and Hanson, G.N., 1975. Origin of Ross Island basanitoid and limitations upon the heterogeniety of mantle sources for alkali basalts and nephelinities. Contrib. Mineral. Petrol. 52, 77-106.

Thornton, C.P., and Tuttle, O.F., 1960. Chemistry of igneous rocks. I. Differentiation index. Amer. J. Sci. 258, 664-684.

Wager, L.R., and Brown, G.M., 1967. Layered igneous rocks. Oliver and Boyd, Edinburgh, London. 588 p.

Walker, B.C., 1983. The Beacon Supergroup of Northern Victoria Land, Antarctica. in Oliver, R.L., James, P.R., and Jago, J.B., Antarctic Earth Science. Australian Academy of Science, Canberra.

Wilkinson, J.F.G., 1966. Residual glasses from some alkali basaltic lavas from New South Wales. Mineralog. Mag. 35, 847-860.

Willians, H., Turner, F., and Gilbert, C.M., 1954. Petrography, An Introduction to the Study of Rocks in Thin Section. Wm. H. Freeman and Co. San Francisco.

Wright, J.B., 1963. A note on possible differentiation trends in Tertiary to Recent Lavas of Kenya. Geol. Mag. 100, 164-180.

Wright, T.L., 1974. Presentation and interpretation of chemical data for igneous rocks. Contr. Mineral. and Petrol. 48, 233-248.

Wright, T.L., and Doherty, P.C., 1970. A linear programming and least squares computer method for solving petrologic mixing problems. Geol. Soc. Amer. Bull. 81, 1995-2008.

Wyllie, P.S., 1979. Magmas and volatile components. Am. Miner. 64, 469-500.

Yoder, H.S., and Tilley, C.E., 1962. Origin of basalt magmas: An experimental study of natural and synthetic rock systems. J. Petrology 3, 342-532.